Title	Plasma Enhanced Chemical Vapor Deposition and Electrical Characterization of Diamond-Like Carbon Thin Films
Author(s)	Md. Kamrul, Hassan
Citation	高知工科大学，博士論文.
Date of issue	2007-09
URL	http://hdl.handle.net/10173/493
Rights	
Text version	author

Ph.D. Thesis

Plasma Enhanced Chemical Vapor Deposition and Electrical Characterization of Diamond-Like Carbon Thin Films

Md. Kamrul Hassan

Department of Electronic and Photonic Systems Engineering

Graduate School of Engineering

Kochi University of Technology

Kochi, Japan

Ph.D. Thesis

Plasma Enhanced Chemical Vapor Deposition and Electrical Characterization of Diamond-Like Carbon Thin Films

Md. Kamrul Hassan

Dissertation Supervisor: Prof. Akimitsu Hatta

A dissertation submitted to
Kochi University of Technology
in partial fulfillment of the requirements
for the degree of
Doctor of Engineering

Department of Electronic and Photonic Systems Engineering
Graduate School of Engineering
Kochi University of Technology
Kochi, Japan

September, 2007

ACKNOWLEDGEMENTS

I would like to express my profound gratitude to my supervisor, Prof. Akimitsu Hatta, for giving me the opportunity to join in his group. I would also like to express my sincere appreciation to him for meticulous guidance, constant help and encouragement throughout the course of this work. I am indebted to him for giving me the financial support during my study in KUT. I also like to thank him for providing the necessary support to join several international and domestic conferences to gather knowledge for conducting this research work.

I would like to express my appreciation to my committee members Professor Tadashi Narusawa, Professor Takashi Katoda, Professor Takashi Hirao and Associate Professor Michio Watamori for their helpful discussion and valuable suggestion.

I would like to thank my colleagues and all the members of the Hatta group for their assistance, co-operation and friendship throughout the study. I would also like to appreciate the help of other colleagues and friends.

I am grateful to Japan Student Service Organization (JASSO) for awarding me the GAKUSHU SHOREI-HI scholarship and the International Relation Centre (IRC) of KUT for recommending me for this scholarship.

I would also like to express my gratitude to Dr. Mirza Shamim for his cooperation and encouragement.

I would like to express my appreciation and gratitude towards my mother-in-law, sister-in-law, brother-in-laws, brothers, sisters and other relatives for their support and encouragement.

I am grateful to my wife Mirza Sultana, whose co-operation, encouragement and support has been a constant source of inspiration during my stay and study in Kochi, Japan.

Md. Kamrul Hassan
September, 2007

TABLE OF CONTENTS

LIST OF FIGURES

LIST OF TABLES

Abbreviations

DLC	Diamond-like carbon
a-C	Amorphous carbon
a-C: H	Hydrogenated amorphous carbon
RF-PECVD	Radio-frequency plasma-enhanced chemical vapor deposition
TAC	Tetrahedral amorphous carbon
RCN	Random covalent network
NEA	Negative electron affinity
PLCH	Polymer-like hydrogenated amorphous carbon
GAC	Graphite-like amorphous carbon
OES	Optical emission spectroscopy
CVD	Chemical vapor deposition
PVD	Physical vapor deposition
MSIBD	Mass-slected ion beam deposition
ECR	Electron cyclotron resonance
MBE	Molecular beam epitaxy
APCVD	Atmospheric pressure chemical vapor deposition
LPCVD	Low-pressure chemical vapor deposition
UHVCVD	Ultrahigh vacuum chemical vapor deposition
AACVD	Aerosol assisted chemical vapor deposition
DLICVD	Direct liquid injection chemical vapor deposition
ALCVD	Atomic layer chemical vapor deposition
HWCVD	Hot wire chemical vapor deposition
MOCVD	Metal organic chemical vapor deposition
RTCVD	Rapid thermal chemical vapor deposition
RPECVD	Remote plasma-enhanced chemical vapor deposition
VPE	Vapor phase epitaxy
HF	Hydrofluoric acid
SEM	Scanning electron microscopy
CRT	Cathode-ray tube

DC	Direct current
MIS	Metal-insulator-semiconductor
FET	Field effect transistor
MIM	Metal-insulator-metal
SOS	Semiconductor-oxide-semiconductor
MOS	Metal-oxide-semiconductor
PF	Poole Frenkel
SCL	Space charge limited
TFL	Trap-filled-limited

Abstract

Deposition of diamond-like carbon (DLC) films and the study of their electrical properties have drawn increasing interest for research owing to its potential applications. These include application in magnetic head device as reader gap insulation layer, DLC metal-insulator-metal (MSM) switches for active matrix display, interconnect dielectric in high performance ultra-large scale integrated device, high efficiency and low cost solar cell applications and memory and antifuse devices. Insulating DLC's are required for the above applications.

This research reports the fabrication and electrical characterization of diamond-like amorphous carbon films (DLC) deposited by using radio-frequency plasma-enhanced chemical vapor deposition (RF-PECVD) technique. The major advantages of this technique are large-area processing and ability to fabricate films ranging from insulating diamond to metallic graphite. The properties DLC are influenced by the deposition condition and the precursors used. The optimization technique may be improved to correlate the film electrical characterization by applying appropriate deposition condition.

A systematic investigation concerning the deposition and the electrical characterization of the diamond like carbon films synthesized in different experimental conditions and from two different two different saturated and unsaturated hydrocarbon source gases such as CH_4 and C_2H_2 is to be presented. Apart from the carbon containing precursors Ar gas were added to dilute the precursor gases to investigate the effects of Ar dilution on the film electrical properties.

Electrical characterization DLC has been performed using I-V, C-V, C-F and the resistivity measurements. Experimental results concerning the electrical conduction mechanism are also presented and discussed.

The following chapters of the thesis cover the whole research work.

Chapter 1. Introduction

This chapter comprises of the history of synthesis, various types of a-C:H films, physical properties, present and perspective of future application, problems, objective

and scope of the research. The purpose and significance of this research are clearly pointed out.

Chapter 2 Synthesis of DLC films using RF plasma CVD method

The history of synthesis of DLC films and the different techniques of synthesis of is introduced. Synthesis of DLC films by RF-PECVD using CH_4 and C_2H_2 and the admixture of CH_4-Ar and C_2H_2-Ar gases are described. The deposition of DLC was performed by varying the plasma deposition conditions. This chapter also covers the details of substrate preparation and cleaning, RF-PECVD principle, experimental apparatus, deposition conditions and thickness measurement technique. During the deposition process optical emission spectroscopy is applied to investigate the plasma. The correlation between plasma chemistry and film growth rate is also discussed. It is observed that the growth rate of the C_2H_2-based films were more than three times than that of the CH_4-based films. Highest deposition rates were obtained for the films deposited at highest RF power, lowest flow rate or lowest deposition pressure. It has been found that the deposition rate drops due to the pronounced etching effect of Ar ion sputtering.

Chapter 3 Electrical characterization of DLC films

For the electrical characterization top gold electrodes of were fabricated on the DLC films using a vacuum evaporator. The bottom of the silicon wafer was coated with gold using a DC sputtering apparatus. The current-voltage (I-V) characteristics of the Au/DLC/n-Si/Au structure at room temperature were investigated and compared. The temperature dependence of the I-V characteristics were investigated over the temperature range of 296-358 K. The overall features of the I-V characteristics of the DLC films were similar. It is also observed that these I-V characteristics were symmetrical and nonlinear for both the current directions.

The C-V-F measurements were carried out by a ZM2355 LCR meter in parallel circuit mode with frequencies ranging from 100 Hz to 200 KHz. C-V-F measurement confirmed that the measured capacitance is bias and frequency dependent.

Electrical resistivities were calculated from the current density, voltage and the film thickness plotted against the applied electric field. The resistivities the

resistivities of the DLC films strongly depend on electric field strength. The electrical resistivities of the DLC films were found to be dependent on the substrate bias and the precursors used. The effect of Ar gas dilution CH_4 and C_2H_2 on the electrical properties and the possible explanations have been discussed.

Chapter 4 Conduction Mechanism

In this chapter the conduction mechanism of the DLC films over a wide range of applied electric field of up to 10^6 V/cm were investigated. The dominant conduction in DLC has been identified as Poole-Frenkel type of conduction. Critical analysis of the conduction mechanism of DLC films was analyzed.

Chapter 5 Conclusions

In the light of experimental investigations and their analysis the major results of this research are summarized.

1.1 Introduction

Diamond-like carbon (DLC) films have attracted increasing interest because of their many unique properties such as chemical inertness, thermal stability, optical transparency, high breakdown voltage, tunable band gap, low friction coefficient, high electrical resistivity and low dielectric constant, biocompatibility, low water vapor and oxygen permeability and low electron affinity. These properties of DLC films make them ideal for a variety of microelectronic, technical and industrial applications. At the beginning, DLC films found their way into many industrial wear resistant, antireflections, corrosion resistance coating for biomedical application due to their excellent tribological behavior. Apart from the industrial wear application, DLC films have gradually moved to novel research material for electronic application. At the beginning, most of the academic research was concerned on their electrical properties. DLC shows different electrical properties ranging from insulating diamond to metallic graphite. It can behave as a semiconductor and is able to accept dopants. Different attempts at n-type doping with nitrogen [1], phosphorus [2] and p-type doping with boron [3] have been made by many researchers. Anita *et al.* found that nitrogen incorporation reduced the electrical resistivity of the DLC films obtained from different precursors [4]. Hayashi *et al*. incorporated nitrogen for n-type doping of amorphous carbon films [1] and also doped a-C:H films for p-type with boron for solar cell application [3], but the efficiency was very low[1, 3]. The work on DLC was carried out by a number of possible electronic applications such as electron field emitter, DLC MSM switch for active matrix display, photovoltaic solar cell, ultra-large-scale integrated (ULSI) device, electro-luminescence device and antifuse applications.

Radio-frequency plasma-enhanced chemical vapor deposition (RF-PECVD is one of the most popular techniques for the synthesis of DLC films. DLC can be deposited from a variety of precursors such as CH_4, C_6H_6, C_6H_{12}, C_2H_4 and C_2H_2 as well as mixture of these gases with Ar or H_2.

In this research, RF-PECVD was used for the synthesis of DLC films at a frequency of 13.56 MHz using CH_4 (methane) and C_2H_2 (acetylene) for three purposes: (a) optimization of deposition condition from CH_4, (b) comparison of

source gases CH_4 (maximum hydrogen concentration) or C_2H_2 (minimum hydrogen concentration) and (c) the influence of Ar-dilution with CH_4 and C_2H_2 on the electrical properties.

In this study, we compared the growth rate and electrical resistivity of diamond-like hydrogenated amorphous carbon (a-C:H) films deposited from CH_4 and C_2H_2 by varying the RF power, flow rate, pressure. The effect of Ar (argon) gas addition into CH_4 and C_2H_2 were also investigated.

1.2 History and Perspective of DLC Films

Diamond-like carbon or DLC is an amorphous hard carbon, since 1969‘s it has been produced for a variety of practical applications. Studies of DLC has been performed extensively since 1971, when Aisenberg and Chabot first prepared such carbonaceous films by ion beam deposition that showed the properties of that resembled diamond as opposed to graphite [5]. The transparency of the films indicated the absence of free electrons and the current-voltage measurement showed the high resistivity [6]. It was found that these carbon films had many of the properties similar to diamond but the films were predominantly amorphous in nature and not single crystal. Thus the name “diamond like carbon” (DLC) material was introduced [5, 7]. Sputtering techniques such as RF bias and magnetron sputtering are also used to produce diamond like carbon films. Different forms of sputtering techniques were used to produce DLC films by many researchers [8-10]. Besides sputtering techniques and ion-beam deposition, a-C:H is most often prepared by plasma enhanced chemical vapor deposition (PECVD) from hydrocarbon source gases. Holland and Ojha produced hydrogenated DLC (or DAC:H) films by using RF-PECVD in 1976 [11]. These films showed some of the excellent mechanical and optical properties as observed by Aisenberg and Chabot. In early research, Aksenov *et al.* produced highly tetrahedral sp^3 DAC films by using a cathodic arc, which was hydrogen free, and these films are known as tetrahedral amorphous carbon (TAC) films [12].

1.2.1 Structure of DLC Films

DLC films are metastable form of amorphous carbon (a-C) or hydrogenated amorphous carbon (a-C:H) in which carbon atoms bonded in mainly sp^3 and sp^2 hybridization. Carbon can form bonds with three different hybridizations, namely tetrahedral sp^3 (like in diamond), trigonal sp^2 (like in graphite) or linear sp^1 bond (like in acetylene). DLC films form with a mixture of any of these three bonds with other carbon atoms or impurities. This enables DLC to form different bonding structure. The possible example of a-C:H structure is shown in Fig. 1.1 [13]. Their properties are intermediate between that of diamond, graphite and polymer hydrocarbons. DLC contains a good portion of sp^2 bonding sometimes upto 60% and sp^3 contents of 40-60% [14]. The properties of DLC films are determined by the bonding hybridization of carbon atoms and the relative concentration of the different bonds, ie sp^2, $sp^3$and sp^1 as well as hydrogen distribution among the different types of bonds. Fig.1.2 shows the structure-composition of diamond like carbon in ternary phase diagram in terms of sp^2, sp^3 and H concentrations which is given by Robertson [15]. The exact position of the diamond like material in the phase diagram is determined by the precursor and the deposition parameter [16]. The three corners represents to diamond, graphite and the hydrocarbons, respectively. There is a region of high H contents, where films can not form. The glassy carbon and evaporated a-C lie in the sp^2 corner. In the hydrogenated DLC films, some of the carbon atoms are terminated by hydrogen. Fig. 1.3 [17] also shows that the diamond-like carbon films, comprising sp^2, sp^3 and even sp^1 carbon bonds, have ranges of properties delimited by the properties of diamond, graphite and polymers.

The detailed chemical bonding and structure of DLC is not clearly understood. Different models have been put forward by different workers. Robertson [18] modeled the structure of DLC as a random network of covalently bonded carbon atoms in the different hybridization, with a substantial degree of medium range order on the 1 nm scale. Angus and Jahnsen [19] have described the structure of hydrogenated DLC by random covalent network (RCN) model. According to RCN model, the structure of a-C:H can be regarded as a three-dimensional array of mostly six membered rings, which is able to contain 17-61% of bound hydrogen.

1.2.2 Physical Properties of DLC Films

The physical properties of the DLC films depend on the concentration of the carbon atoms in the sp^2 and sp^3 configurations in the film and the amount of hydrogenation. The attractive properties of the DLC have made it a special candidate for large amount of research on their deposition and characterization, and on the development of specific applications. Diamond like carbon possesses many unique properties and makes this material ideal for a large variety of applications. DLC films are characterized by chemical inertness, high hardness, high breakdown voltage, high electrical resistivity, high thermal conductivity, high infrared transparency [20, 21], neno level smoothness [22] wear and corrosion resistance, low friction co-efficient, biocompatibility, low water vapor and oxygen permeability [23], low dielectric constant [24, 25, 26], optical transparency [27] and negative electron affinity (NEA) [28]. DLC is a low mobility semiconductor with a band gap of 1-4 eV. Hydrogenated amorphous carbon in general has hardness value in the region of 20-40 GPa. Typical physical properties for different forms of a-C:H is shown in Table 1.1 [29].

1.2.3 Hydrogenated and Hydrogen-Free DLC Films

The term "diamond-like" is often referred to many kinds of non-crystalline or amorphous carbonaceous films. Depending on the hydrogen content, DLC films can be mainly classified into two categories: hydrogenated (a-C:H) and non-hydrogenated (a-C). Hydrogenated DLC films may contain up to 20-50% hydrogen and are quite different from the hydrogen free DLC films [30]. The hydrogen content of a-C is less than 1%. Both hydrogenated and hydrogen-free diamond-like carbons are metastable materials deposited using a variety of deposition method under the influence of energetic particle bombardment [31].

The PECVD method is the most frequently used technique to deposit diamond films, polycrystalline diamond films and diamond-like carbon films (hydrogenated and non-hydrogenated). But for the hydrogenated DLC films, RF-PECVD is the most commonly used technique. On the other hand, non-hydrogenated DLC films can be deposited either by a cathodic arc [32, 33], filtered cathode arc [34-36], using an ion beam [37, 38], mass selected ion beam [39-41] and laser ablation [42, 43].

All the diamond-like carbon contains significant fraction of C-C sp^3 bonds. The a-C:H films contains sp^3 fraction smaller than 50%, on the other hand a-C films may contain up to 85% or more sp^3 type of bonds [44]. Hydrogenated amorphous carbon can be classified into following classes [45]:

(1) Polymer-like a-C:H (PLCH): This type of films have the highest hydrogen content of above 40%. The sp^3 content may be up to 60%. Hydrogen prefers to bond in a sp^3 configuration. These films are soft and most of the sp^3 bonds are terminated by hydrogen.

(2) Diamond-like a-C:H (DLCH): a-C:H film with intermediate hydrogen contents between 20-40% and sp^3 content of 40-60% are known as diamond-like a-C:H (DLCH). They have higher C-C sp^3 bond than that of PLCH.

(3) Tetrahedral amorphous carbon (TAC or ta-C:H): This class of a-C is characterized with highest C-C sp^3 content up to 60-85% and hydrogen content close to 25%. TAC films may be hydrogenated or hydrogen free. TAC films have closest resemblance to the microstructure of the diamond films due to high sp^3 content.

(4) Graphite-like amorphous carbon (GAC): These types of amorphous carbon have low hydrogen content (less than 20%). They have high sp^2 content and sp^2 clustering. The band gap is less than 1(0-0.6 eV) eV [46]. The conductivity of graphite-like amorphous carbon is very high close to that of graphite.

1.3 Present Application and Market Potential

Owing to the excellent properties of DLC films, together with the possibility of adjusting the properties by varying the appropriate deposition condition make them suitable for a variety of application. Diamond like carbon at present very significant on a worldwide in commercial use contributes immensely in many areas of scratch and corrosion resistant coatings. DLC are also suitable for many diffusion-barrier applications because of their relative high density (2.0-3.2 gm/cm^3) [47]. DLC films are being considered as passivation layers for inside plastic bottles for beverages. TAC has successfully used as ultra thin protective overcoats for hard disk heads [47, 48] and razor blades [44, 47]. The negative electron affinity (NEA) of hydrogenated diamond surface plays a vital role [49], and different surface terminating species can

greatly affect the emission properties [50]. The electron emission from diamond and DLC films is increasing much interest due to potential applications in cold cathode device [28].

DLC are also important for electronic switching, memory applications, optical window, heart devices, dialysis, membranes, orthopedic pins, medical instruments and many other passive applications. A brief summary of properties and application of hydrogenated and non-hydrogenated DLC is shown in Table 1.2 [51].

1.4 Perspective of Electronic Application

At the beginning, most of the academic research on DLC's was concerned on their electronic properties. Intensive work and investigation on DLC was carried out for a number of possible electronic applications. It was thought that DLC would be a good electron field emitter for field emission display. But it was found that the emission was largely extrinsic. Similarly, a-C:H with a large and gap possesses strong room temperature photoluminescence, which could be utilized in a display, however no electro-luminance device have been produced [52]. Hydrogenated amorphous carbon and tetrahedral amorphous carbon thin films may be a possible alternative of silicon based dielectric in antifuse devices but limited for commercial application due to the degradation of the device characteristics that occurs after many write-erase cycles [53]. Although DLC has been disappointing from an electronic perspectives, but DLC still have potential for electronic applications. So there is still a vast amount of research to be done to optimize the properties of DLC films for electronic applications.

In the recent research amorphous DLC shows properties ranging from insulating diamond to metallic graphite. It can behave as a semiconductor and is able to accept dopants. It has a tunable band-gap (ranging from1eV to 4.5 eV) which can be controlled by varying the plasma deposition conditions. However its electronic properties are quite restrictive for application. It includes a large density of midgap states, wide band tail, low carrier mobility and poor doping response [52]. The problems are due to the complex sp^2/sp^3 mixed structure and the difficulties in

controlling the conduction type, carrier concentration and control over optical band gap energy [54].

1.5 Scope and Objective of the Thesis

A systematic investigation on the results concerning the deposition and the electrical characterization of the diamond like carbon films synthesized in different experimental conditions and from two different saturated and unsaturated hydrocarbon source gases are presented. The aim of this research is to study the possibility of adjusting the properties using two different carbon sources with additional Ar gas by RF-PECVD. The control of the properties of DLC has been studied by changing the growth condition. Two main points of this work are focused on: (1) synthesis of DLC films and (2) electrical characterization.

The main objectives of this research are;

1) synthesis of DLC films and to improve their insulating properties,
2) identification and control of the parameters that determine the properties of DLC films prepared by using RF-PECVD system using two different precursor gases CH_4 and C_2H_2, and the admixture with Ar,
3) comparative study on the CVD of DLC films from CH_4 and C_2H_2 using the RF plasma ,
4) study the correlation between plasma monitored by optical emission spectroscopy (OES) with the growth kinetics and film properties,
5) electrical characterization, I-V, C-V and C-F of the films under different deposition conditions,
6) study on the dominant conduction mechanism of the DLC films was also presented.

It is intended to develop an understanding on the electrical characterization of the DLC coatings that will allow their optimization and design for a number of advance engineering applications.

The organization of the thesis is shown in Fig. 1.4.

In this research work chapter 2 deals with: synthesis of DLC films, substrate preparation and cleaning, RF-PECVD principle, experimental apparatus and thickness measurement techniques.

Electrical characterization are presented in chapter 3 which includes the fabrication principles and methods of deposition of electrical contacts, experimental circuit diagram and experimental apparatus for data acquisition for I-V and C-F-V measurements and electrical resistivities of the DLC films. The experimental results are presented in this chapter. The interpretation and discussions of all the experimental results are also presented.

Chapter 4 covers the dominant conduction mechanism of the diamond-like carbon films, which reviews the various models of conduction in thin insulating films.

In chapter 5, experimental results and their analysis are summarized.

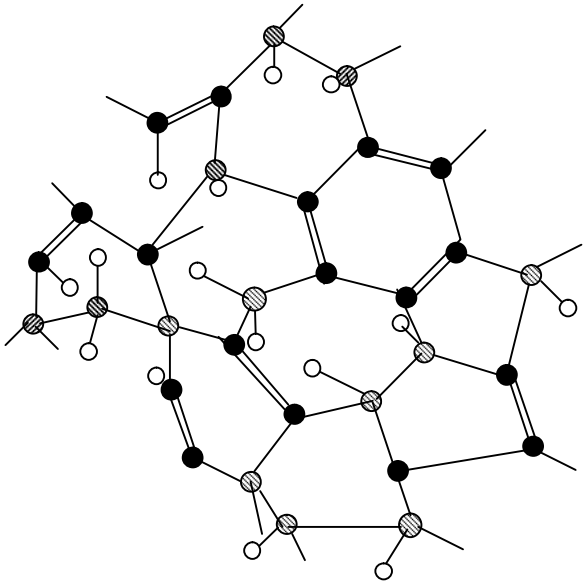

● sp^2 carbon atom; ◍ sp^3 carbon atom; ○ hydrogen atom

Fig. 1.1 A two dimensional representation of diamond-like carbon film structure [13].

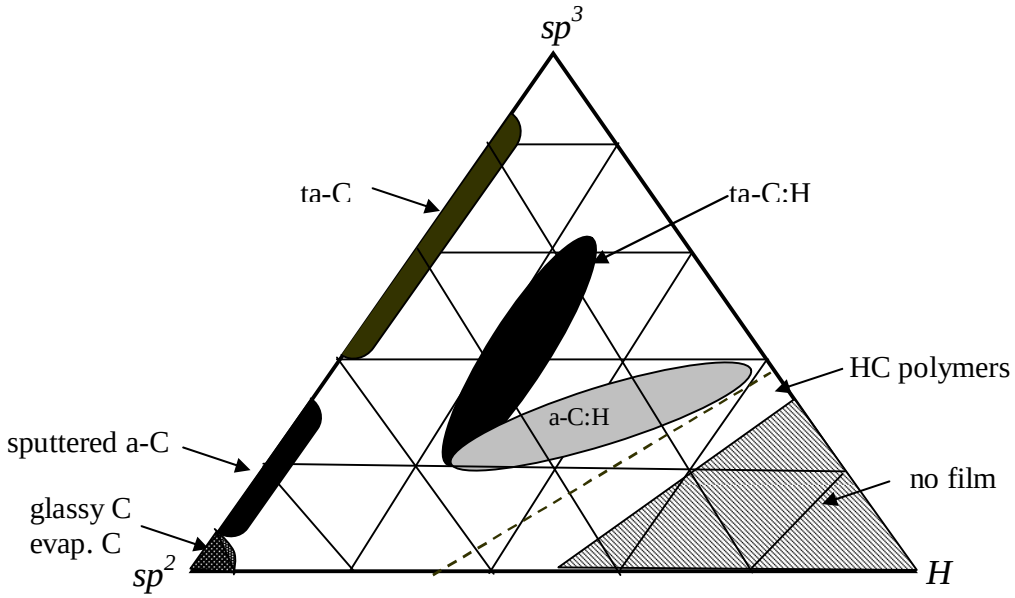

Fig. 1.2 Phase diagram of diamond-like carbon materials [15].

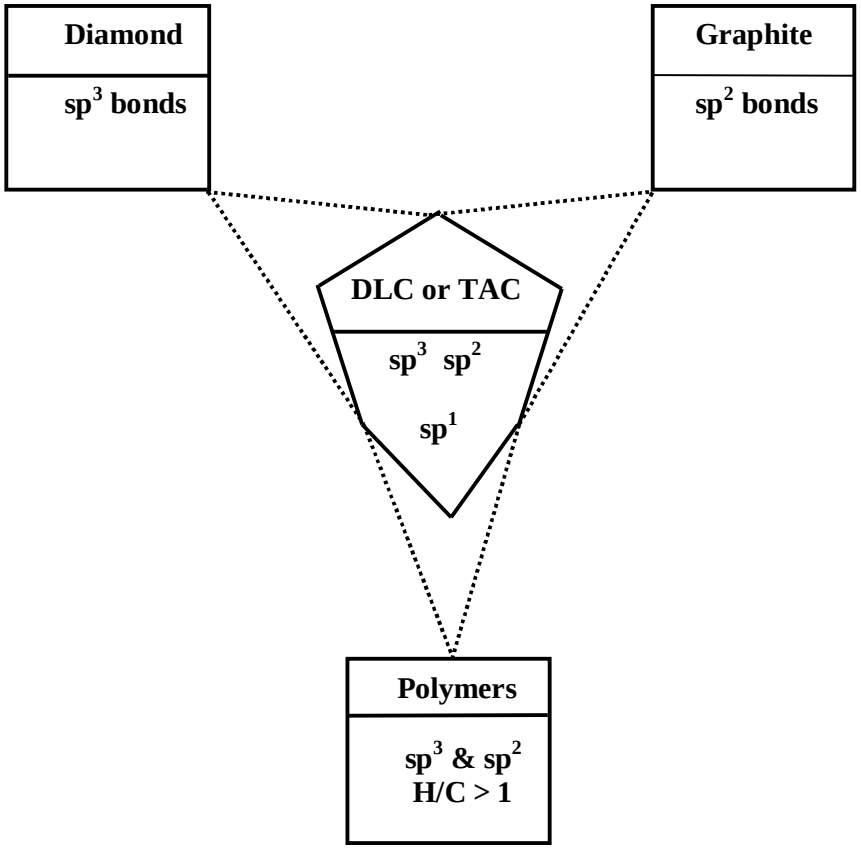

Fig. 1.3 Delimitation of properties of diamond-like carbon films [17].

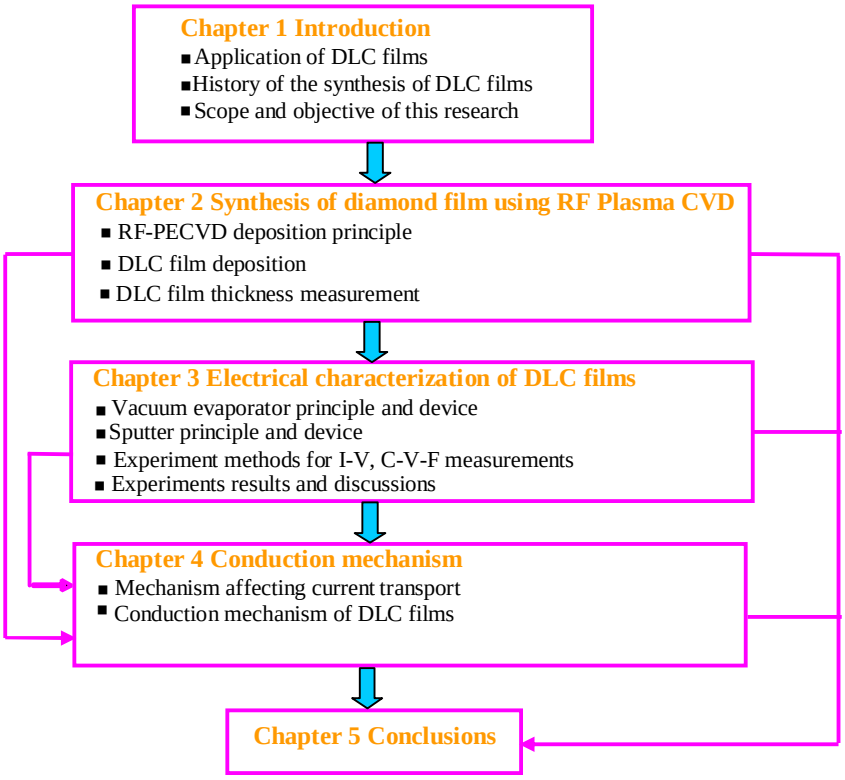

Fig. 1.4 Organization flow chart of the thesis.

Table 1.1 Typical physical properties of different forms of amorphous carbon thin films [29].

Category	Hardness (GPa)	sp^3 (%)	Optical bandgap (eV)	Density (g cm^{-3})	H (at. %)
DAC	20 - 40	40 - 60	0.8 - 4.0	1.8 - 3.0	20 - 40
TAC	40 - 65	65 - 90	1.6 - 2.6	2.5 -3.5	0 - 30
PAC	Soft	60 - 80	2.0 -5.0	0.6 - 1.5	40 - 65
GAC	Soft	0 -30	0.0 - 0.6	1.2 -2.0	0 - 40
NAC	20 - 40	30 - 80	0.8 - 2.6	2.0 - 3.2	0 -30

Table 1.2 Summary of properties and applications of diamond-like carbon films. Text in the parentheses indicates potential applications [51].

Property	**Type of use**	**Application**
Transparency in Vis and IR; optical band = 1.0-4.0 eV	Optical coatings	Antireflection and wear-resistant coating for IR optics
Chemical inertness to acids, alkalis and organic solvents	Chemically passivating coatings	Corrosion protection of magnetic media, bimedical
High hardness; H=5-80 GPa; low friction coefficient. <0.01-0.7	Tribological, wear-resistant coatings	Magnetic hard drives, magnetic tapes, razor blades (bearing gear)
Nanosmooth	Very thin coatings <5 nm	Magnetic media
Wide range of electrical resistivities = 10^2 - 10^{16} Ω/cm	Insulating coatings	Insulating films
Low dielectric constant <4	Low-k dielectrics Field emission	(Interconnect dielectrics) (Field emission flat panel displays)

References

[1] Y. Hayashi, T. Kamino, T. Soga, K. Kaneko and T. Jimbo, Diam. Relat. Mater., **14** (2005) 970.

[2] M. T. Kuo, P. W. May, A. Gunn, M. N. R. Ashfold and R. K. Wild, Diam. Relat. Mater., **9** (2000) 1222.

[3] Y. Hayashi, S. Ishikawa, T. Soga, M. Umeno and T. Jimbo, Diam. Relat. Mater., **12** (2003) 687.

[4] V. Anita, T. Butuda, T. Maeda, K. Takizawa, N. Saito and O. Takai, Diam. Relat. Mater., **13** (2004) 1993.

[5] S. Aisenberg and R. Chabot, J. Appl. Phys. **42** (1971) 2953.

[6] J. J. Pouch and S. A. Alterovitz, Properties and Characterization of Amorphous Carbon Films, Material Science Forum, Vols. **52** & **53**, Trans Tech Publications, Aedermannsdorf, 1990, p. 3.

[7] S. Aisenberg and R. Chabot, Proceedings of the 17th National Vacuum Symposi--um, Washington, D. C. (Oct. 20-23, 1970).

[8] R. Kleber, Diam. Relat. Mater., **2**(1991) 246.

[9] B. Andre, F. Rossi, H. Dunlop, Diam. Relat. Mater., **1** (1992) 307.

[10] J.-U. Oh, K.-R. Lee, K. Y. Eun, Thin Solid Films, **270** (1995) 173.

[11] L. Holland, S. M. Ojha, Thin Solid Films, **38** (1976) 17.

[12] I. I. Aksenov, V. A. Belous, V. G. Padalka and V. M. Khoroshikh, Sov. J. of Plasma Phys. (USA), **4** (1978) 425.

[13] E. Staryga, G. W. Bak, Diam. Relat. Mater., **14** (2005) 25.

[14] S. R. P. Silva, Properties of Amorphous Carbon (INSPEC, London, 2003) Emis Data Reviews Series No. **29**, Chap. 1, p. 5.

[15] J. Robertson, Philos. Mag. B Phys. Condens. Matter Stat. Mech. Electron, Opt. Magn. Prop. UK, **76** (1997) 335.

[16] A. Grill, Diam. Relat. Mater., **8** (1999) 433.

[17] P. Koidl, C. Wild, R. Locher, R. E. Sah in: R. E. Clausing, L. L.Horton, J. C. Angus, P. Koidl (Eds), Diamond and Diamond-Like Film and Coatings, NATO--ASI Series B: Physics, Plenum, New York, 1991, p. 243.

[18] J. Robertson, Adv. Phys., **35** (1986) 317.

[19] J. C. Angus, F. Jansen, J.Vac. Sci. Technol., **A6** (1998) 1778.

[20] M. Rusop, A. M. M. Omer, S. Adhikari, S. Adhikary, H. Uchida, T. Soga, T. Jimbo and M. Umeno, Diam. Relat. Mater., **14** (2005) 975.

[21] A. M. M. Omer, S. Adhikari, S. Adhikary, H. Uchida and M. Umeno, Diam. Relat. Mater., **13** (2004) 2136.

[22] J. Kim and C. Lee, J. Korean Phy. Soci., **42** (2003) S956.

[23] V. Anita, T. Butuda, T. Maeda, K. Takizawa, N. Saito and O. Takai, Diam. Relat. Mater., **13** (2004) 1993.

[24] S. R. P. Silva, Properties of Amorphous Carbon (INSPEC, London, 2003) Emis Data Reviews Series No. **29**, Chap. 10, p. 326.

[25] A. Grill, Diam. Relat. Mater., **10** (2001) 234.

[26] S. P. Louh, I. C. Leu and M. H. Hon, Diam. Relat. Mater., **14** (2005) 1005.

[27] E. Amanatides and D. Mataras, Diam. Relat. Mater., **14** (2005) 292.

[28] P.W. May, M.-T. Kuo and M.N.R. Ashfold, Diam. Relat. Mater., **8** (1999) 1490.

[29] S. R. P. Silva, Properties of Amorphous Carbon (INSPEC, London, 2003) Emis Data Reviews Series No. **29**, Chap. 1, p. 4.

[30] Y. Lifshitz, Diam. Relat. Mater., **8** (1999) 1659.

[31] J. J. Pouch and S. A. Alterovitz, Properties and Characterization of Amorphous Carbon Films, Material Science Forum, Vols. **52** & **53**, Trans Tech Publications, Aedermannsdorf, 1990, p. 5.

[32] J. J. Pouch and S. A. Alterovitz, Properties and Characterization of Amorphous Carbon Films, Material Science Forum, Vols. **52** & **53**, Trans Tech Publications, Aedermannsdorf, 1990, p. 212.

[33] H. J. Scheibe, B. Schultrich, Thin Solid Films, **246** (1994) 92.

[34] A. Anders, S. Anders and I.G. Brown, J. Appl. Phys., **75** (1994) 4900.

[35] S. Falabella and D. M. Sanders, J. Vac. Sci. Technol., **10** (1992) 394.

[36] J.-K. Shin, C. Lee, K.-R. Lee and K. Y. Eun, Appl. Phys. Lett., **27** (2001) 63.

[37] S. Aisenberg and R. Chabot, J. Appl. Phys., **42** (1971) 2953.

[38] J. J. Pouch and S. A. Alterovitz, Properties and Characterization of Amorphous Carbon Films, Material Science Forum Vols. **52** & **53**, Trans Tech Publications, Aedermannsdorf, 1990, p. 1.

[39] Y. Lifshitz, Diam. Relat. Mater., **2** (1993) 285.

[40] Y. Lifshitz, G. D. Lempert, S. Rotter, I. Avigal, C. Uzansaguy and R. Kalish, Diam. Relat. Mater., **3**-**5** (1996) 1611.

[41] H. Hofsass, H. Binder, T. Klumpp, E. Recknagel, Diam. Relat. Mater., **3** (1994) 137.

[42] D. T. Peeler and P. T. Murray, Diam. Relat. Mater., **3** (1994) 1124.

[43] D. L. Pappas, K. L. Saenger, J, Bruley, W. Krakow, J. J. Cuomo, T. Gu and R. W. Collins, J. Appl. Phys. **71** (1992) 5675.

[44] A. Grill, Diam. Relat. Mater., **8** (1999) 428.

[45] C. Casiraghi, F. Piazza, A. C. Ferrari, D. Grambole and J. Robertson, Diam. Relat. Mater., **14** (2005) 1098.

[46] S. R. P. Silva, Properties of Amorphous Carbon (INSPEC, London, 2003) Emis Data Reviews Series No. **29**, Chap. 1, p. 10.

[47] S. R. P. Silva, Properties of Amorphous Carbon (INSPEC, London, 2003) Emis Data Reviews Series No. **29**, Chap. 10, p. 312.

[48] M. Schlatter, Diam. Relat. Mater., **11** (2002) 1781.

[49] C. Bandis and B.B. Pate, Appl. Phys. Lett. **69** (1996) 366.

[50] P. W. May, J. C. Stone, M. N. R. Ashfold, K. R. Hallam, W, N. Wang and N. A. Fox, Diam. Relat. Mater., **7** (1998) 671.

[51] A. Grill, Diam. Relat. Mater., **8** (1999) 433.

[52] J. Robertson, Diam. Relat. Mater. **12** (2003) 79.

[53] S. R. P. Silva, Properties of Amorphous Carbon (INSPEC, London, 2003) Emis Data Reviews Series No. **29**, Chap. 10, p. 322.

[54] Y. Hayashi, S. Ishikawa, T. Soga, M. Umeno and T. Jimbo, Diam. Relat. Mater., **12** (2003) 687.

Chapter 2 Synthesis of DLC Films by Using RF Plasma CVD

2.1 Introduction

Diamond-like carbon films are suitable for a variety of applications by choosing the right deposition technique and deposition parameters. DLC can be grown as a thin film on different substrates and comprises of the properties of both the diamond and graphite. Besides the sputtering technique and ion beam deposition a-C:H are most often prepared by plasma enhanced chemical vapor deposition from hydrocarbon source gases. In these plasmas, the hydrocarbon molecules are dissociated and ionized and the radicals as well as the ions impinging on the substrates lead to the growth of the DLC films. Different forms of the PECVD leads to the main methods for depositing hydrogenated DLC films. This chapter mainly deals with the RF-PECVD method and plasma reactors used in the present study and the experimental details.

In this chapter, deposition of DLC films by RF-PECVD using CH_4 and C_2H_2 and the admixture of CH_4-Ar and C_2H_2-Ar under different experimental conditions are described. This chapter deals with the details of substrate preparation and cleaning, RF-PECVD principle, experimental apparatus, deposition condition and thickness measurement technique. During deposition optical emission spectroscopy was used to monitor the plasma. The correlation between the plasma chemistry and the film properties is also discussed.

2.2 Synthesis Techniques of DLC Films

Aisenberg and Chabot in 1971 [1] first deposited the diamond like carbon films by ion beam deposition and showed some of the material and physical properties close to diamond. They used a beam of carbon ions produced by sputtering carbon electrodes in Ar plasma to form an a-C layer. Spencer *et al.* further demonstrated that these DLC films are reproducible using the same technique [2]. Holland and Ojha in 1976 used an RF-PECVD system to produce hydrogenated DLC films [3] which showed some of the mechanical and optical properties as observed by Aisenberg and Chabot [1]. Sputtering may also be used to deposit DLC films with and without hydrogen. RF bias sputtering and magnetron sputtering are the two main techniques to deposit DLC

films. Common deposition techniques include deposition from hydrocarbon plasmas, ion beam deposition and carbon sputtering within hydrogen atmosphere.

The two broad categories for the deposition of the DLC films are CVD (chemical vapor deposition) and physical vapor deposition (PVD). The CVD process utilizes hydrocarbon gases and the later uses the solid carbon in the form of graphite target sources as the precursor material.

Thin a-C or hydrogen-free DLCs with very high sp^3 content can be deposited by the filtered cathodic vacuum arc [4, 5, 6], mass slected ion beam deposition (MSIBD) [7, 8], pulsed laser deposition [9,10], magnetron sputtering[11].

Hydrogenated amorphous carbon (a-C:H) can be deposited by a wide range of techniques such as dc plasma deposition [12], RF-plasma deposition [13-17] and microwave electron cyclotron resonance (ECR) plasma deposition [18-22]. Hydrogenated amorphous carbon is usually made by ion beam method, plasma enhanced chemical vapor deposition (PECVD) or reactive sputtering.

Radio frequency plasma enhanced chemical vapor deposition (RF-PECVD) is one of the most popular technique for the deposition of DLC films using hydrocarbon source gases becauses the plasma enhanced ion bombardment during deposition improves the quality of the film. The advantage of PECVD are low temperature deposition, high deposition rate and good control over the stoichiometry, cleanliness and low particulate levels [23].

Different types of deposition technique is shown in the flow diagram as shown in Fig. 2.1 [24].

Generally, there are two types of depositions:

1) Physical Vapor Deposition:
   Vacuum evaporation
   Sputter deposition
   Molecular beam epitaxy (MBE)
2) Chemical Process
   Solgel
   Plating
   CVD

2.2.1 Chemical Vapor Deposition

Chemical vapor deposition (CVD) is the process of chemically reacting volatile compound of a material to be deposited with other gases to produce a non volatile solid that deposit atomistically on a suitable placed substrates. CVD is a chemical process which transforms gaseous molecules, called the precursors into a solid material in the form of thin film or powder, on the surface of substrates.

CVD is a chemical process often used in the semiconductor industry for the deposition of thin films of various materials. In a typical CVD process the substrate is exposed to one or more volatile precursors, which react and/or decompose on the substrate surface to produce the desired deposit. Frequently, volatile byproducts are also produced, which are removed by gas flow through the reaction chamber. The block diagram of the CVD process is shown in Fig. 2.2.

CVD is widely used in the semiconductor industry, as part of the semiconductor device fabrication process, to deposit various films including: polycrystalline, amorphous, and epitaxial silicon, carbon fiber, filaments, carbon nanotubes, SiO_2, silicon-germanium, tungsten, silicon nitride, silicon oxynitride, titanium nitride, and various high-k dielectrics. The CVD process is also used to produce synthetic diamonds and diamond-like carbon films.

A number of CVD are widely used and are frequently referenced in the literature. These processes are classified on the basis by which chemical reactions are initiated (e.g., activation process) and process conditions.

Plasma-enhanced CVD (PECVD) - CVD processes that utilize plasma to enhance chemical reaction rates of the precursors. PECVD processing allows deposition at lower temperatures, which is often critical in the manufacture of semiconductors.

Atmospheric pressure CVD (APCVD) - CVD processes at atmospheric pressure. Low-pressure CVD (LPCVD) - CVD processes at sub atmospheric pressures. Ultrahigh vacuum CVD (UHVCVD) - CVD processes at a very low pressure, typically below 10^{-6} Pa (~ 10^{-8} torr). Aerosol assisted CVD (AACVD) - A CVD process in which the precursors are transported to the substrate by means of a liquid/gas aerosol, which can be generated ultrasonically. This technique is suitable for use with involatile precursors. Direct liquid injection CVD (DLICVD) - A CVD

process in which the precursors are in liquid form (liquid or solid dissolved in a convenient solvent). Liquid solutions mainly metal-organic precursors are used.

Atomic layer CVD (ALCVD) (also referred to as atomic layer epitaxy and atomic layer deposition (ALD)) - A CVD process in which two complementary precursors (e.g. Al $(CH_3)_3$ and H_2O) are alternatively introduced into the reaction chamber.

Hot wire CVD (HWCVD) - Also known as catalytic CVD (Cat-CVD) or hot filament CVD (HFCVD) which utilizes the hot filament to decompose the precursors.

Metal organic CVD (MOCVD) - CVD processes based on metal-organic precursors.

Microwave plasma-assisted CVD (MPCVD) - CVD process utilizes microwave power to decompose the precursor to sustain plasma.

Rapid thermal CVD (RTCVD) - CVD processes that use heating lamps or other methods to rapidly heat the wafer substrate. Heating only the substrate rather than the gas or chamber walls helps reduce unwanted gas phase reactions that can lead to particle formation.

Remote plasma-enhanced CVD (RPECVD) - Similar to PECVD except that the wafer substrate is not directly in the plasma discharge region which allows the processing temperature down to the room temperature.

Vapor phase epitaxy (VPE) - Growth from the vapor phase is categorized based on the sources used.

2.2.2 Principle of RF-PECVD

For the deposition of diamond like carbon film several techniques are appropriate and the common preparation technique includes deposition from hydrocarbon plasma.

A common feature for the techniques are-

1) A plasma is used as a source of reactive species
2) The substrate is subjected around the room temperature
3) Exposure of the growing film to a flux of energetic ions, due to ion bombardment, the growth of the a-C:H occurs under non-equilibrium condition.

In our research we will concentrate on the RF excited hydrocarbon plasma onto negatively self-biased substrates, a widely used technique which was pioneered by

Holland and coworkers [3]. The substrate was placed on a 6 cm dia and 0.5cm thick Al electrode (cathode) which was capacitively connected to 13.56 MHz rf-generator. The power is coupled to the RF generator through the applied electric field. A large parallel plate counter electrode serves as the anode situated inside the plasma chamber. The RF power is coupled to two parallel plates in a vacuum chamber.

Due to the different mobilities of ions and electrons in the plasma, a high potential drop is formed across the cathode dark space [25]. This leads to the increase in ion bombardment of the electrode and the substrate. The electron current through the plasma sheath during the positive phase of the electric field is much higher than the corresponding ion current during the negative phase. Due to the capacitor in the external circuit this leads to a collection of negative charges on the electrodes. A sheath voltage develops, that retards electrons such that the net current during full period of the RF cycle becomes zero [26]. As a result, the surface takes on a negative potential with respect to the plasma that is of the same order of magnitude as the RF peak voltage. This negative voltage is the self bias.

The time average value of this sheath potential is given by the sum of the negative self bias voltage of the cathode and the plasma potential $Vs = V_B+V_P$ [25]. In this asymmetric discharge with small capacitively coupled cathode and large grounded anode, the plasma potential reduces to a small fraction of the RF amplitude. The bias voltage is measured by a voltmeter through a low pass filter. Fig. 2.3 shows the spatial and temporal potential distribution in a capacitively coupled RF discharge with asymmetric electrodes [27]. The RF glow discharge sustained in a hydrocarbon atmosphere. The hydro-carbon ions generated in the glow space are accelerated across the ion sheath towards the cathode. Condensations of these energetic particles takes place on the substrate and generate thin films.

2.2.3 General System Requirements for RF-PECVD

A CVD apparatus generally consists of the following basic components:

1) Gas and vapor delivery lines - For the supply of precursors to the reactor chamber.
2) Reactor main chamber - Chamber within which film deposition takes place.

3) Materials of construction / geometry.
4) Substrate loading/unloading assembly - A system for introducing and removing the substrates.
5) Energy source(s) - Provide the energy/heat to decompose/react the precursor gases. Common energy sources are RF and radiant heating, plasma, photo-irradiation.
6) Vacuum systems (LPCVD) - System for removing all other gaseous species other than those took part for chemical reaction or deposition.
7) Exhaust system - System for removal of volatile byproducts from the deposition chamber.
8) Exhaust treatment system - In some cases, exhaust may not be suitable for release directly to the atmosphere and require treatment before releasing into the air.
9) Process control and measurement gauges - Gauges, controllers etc. to monitor and control the process parameters such as gas flow rate, pressure, temperature and time.
10) Safety equipments - Hazardous vapor phase reactants and products are frequently encountered; ventilation, sensors, alarms are needed for protection.

2.2.4 Experimental Apparatus Used for DLC Deposition

A chemical vapor deposition system with plane cathode was utilized for the deposition of DLC thin films. Because DLC thin films are characterized by high resistivity, we have employed a parallel plate radio-frequency plasma-enhanced chemical vapor deposition (RF-PECVD) reactor, using capacitively coupled parallel plate, operating at a frequency of 13.56 MHz and 50-1000 W RF power generator was used to deposit diamond-like DLC films from CH_4, C_2H_2, CH_4-Ar and C_2H_2-Ar mixtures on n-type single crystal Si (100). A RF-PECVD system used in this work for DLC deposition is shown in Fig. 2.4 (a) and the schematic is shown in Fig. 2.4 (b). The main deposition chamber was a 6 inch-diameter stainless-steel tube equipped with a turbo molecular pump and an oil rotary pump. The pressure was monitored by an apparent value using an ionization gauge without calibration for each gas (Schulz

gauge, Anelva, LG-11S). The flow rate was maintained using a mass-flow controller calibrated for CH_4. For C_2H_2, a conversion factor of 0.7 was used for calibration. The substrate holder was an Al plate of 6 cm diameter and 6 mm thick, working as a powered electrode. The RF power was supplied to the electrode through coaxial tubes from a matching box. The reflection should be minimum usually less than 1% to make the best use of power. The matching network consists of 2 large adjustable gang capacitors. The tuning is done by varying the capacitance of these capacitors. The substrate holder was cooled using flowing water in the central conductor of the coaxial tube. The self-bias voltage of the substrate holder was monitored using a digital multimeter through a low-pass filter.

2.3 DLC Film Deposition

2.3.1 Preparation of the Substrate

The preparation and cleanliness of the substrates surface exerts a decisive influence on the film growth and adhesion. A thoroughly cleaned surface is a pre-requisite for the preparation of the films with reproducible properties. In this study mirror-polished low-resistivity (<0.02 ohm-cm) n-type silicon (100) wafer was used for the substrate. An ultrasonic bath (Yamoto 3210) is used for the cleaning of the substrates.

The following procedure was adopted for preparation and cleaning of the substrates as shown in Fig. 2.5.

1. Wafer cut: n-type silicon wafer of size 100mmΦx0.5mm thick were cut into1.8x1.8cm^2 size pieces with a diamond-head ball point to use as substrate.
2. The silicon wafers were taken in separate sample box to avoid scratching.
3. The substrates were first cleaned with ultrasonic agitation with acetone for 5 minutes and then rinsed by ultra-pure distilled water and dried with N_2.
4. Cleaned with ultrasonic agitation by methanol for 5 minutes to remove acetone and then rinsed by ultra-pure distilled water and dried with N_2.
5. Removal of native oxide layer: Then, the substrates were etched by using dilute hydrofluoric (HF) acid solution (H_2O:HF=10:1) for 2 minutes to remove any native oxide layer on the surface and were dried with N_2.

2.3.2 Deposition Process

For the deposition, two or three process parameters were kept constant and the remaining one was varied step by step. Each step is considered as a single deposition experiment; so the total knowledge of the dependence of the specific properties need many deposition run.

DLC films were deposited on mirror-polished low-resistivity <0.02 ohm-cm n-type silicon (100) substrates using a capacitively coupled RF-PECVD system at 13.56 MHz and CH_4 and C_2H_2 gas. These substrates were subjected to properly cleaning before loading into the chamber. Thin films are deposited on the silicon substrates positioned on the surface of the cathode. The substrate holder was cooled using flowing water in the central conductor of the coaxial tube. To obtain vacuum in the process chamber, it utilized a system with oil rotary pump and turbo molecular pump. The chamber pressure was monitored before and the plasma was applied. The basic vacuum pressure was pumped down to $6x10^{-3}$ Pa by using turbo molecular pump. The matching network was utilized between the power supply and cathode in view to increase the maximum power dissipation in the discharge. The reflected power was adjusted almost zero. During the time of deposition the self-bias voltage was monitored in order to obtain information about the energy of ions involved in the thin film growth. DLC thin films are deposited by varying the plasma deposition conditions such as RF power (50-500 W), flow rate (10- 100 sccm) and pressure by changing the cross sectional area of the pumping line. During the deposition process, the plasma was monitored by optical emission spectroscopy (OES).

2.3.3 Deposition from Different Precursors

DLC can be deposited from a variety of precursors such as CH_4, C_6H_6, C_6H_{12}, C_6H_{14} and C_2H_2. In other words the source gases used may be saturated hydrocarbons and the unsaturated hydrocarbons as well as a mixture of these gases with hydrogen or Ar. CH_4 is a popular source gas because it is safe to use and is the main component of natural gas. On the other hand, C_2H_2 is not safe to use but it has two carbon atoms per molecules instead of the one of methane.

In this research, two types of hydrocarbon precursors were used such as CH_4 and C_2H_2 with higher and lower number of hydrogen atoms per molecule respectively. The small fragments, such as C, C_2 or CH may be regarded as the actual precursors for a-C:H growth. Plasma chemistry in the glow space which leads to strongly gas-dependent for the properties of hard a-C:H layer. In this study, two sets of diamond-like hydrogenated amorphous carbon (a-C:H) films are deposited from pure CH_4 and C_2H_2 by varying the plasma deposition conditions such as RF power, flow rate and the deposition pressure. Another two sets of films have been deposited using CH_4-Ar and C_2H_2- Ar gas mixtures with various RF power.

2.3.4 Deposition Conditions

The parameters which have strong influence on the film properties are the RF power, flow rate, deposition pressure and the substrate temperature. The unique properties of DLC films and their modifications, together with the possibility of adjusting the properties by varying the appropriate deposition parameter make them suitable for a variety of application.

In order to reduce the contamination of the films, before deposition carried out the chamber was thoroughly cleaned by etching with O_2 plasma for few hours to remove the carbon particle as CO_2 and CO. The etching conditions for cleaning the chamber is shown in Table 2.1.

Before each deposition, the chamber and the substrate holder was thoroughly cleaned with Kim wiper wetted with methanol to remove any loosely attached flakes of previously deposited materials repeatedly. Then the chamber was cleaned by dry Kim wiper.

Different deposition condition of DLC films are employed for the following purposes-

I) optimization of DLC films from CH_4,

II) comparison of the source gases from CH_4 and C_2H_2,

CH_4 - with maximum hydrogen concentration,

C_2H_2 - with minimum hydrogen concentration,

III) to investigate the effect of deposition pressure from CH_4 and C_2H_2,

III) and the influence of Ar dilution with CH_4 and C_2H_2 on the electrical properties.

I) Optimization of DLC films from CH_4

For optimization of DLC from CH_4 two sets of films were deposited. The experimental parameters for DLC film deposition are listed in Tables 2.2 and 2.3. For the first set, the RF power was varied between 50 to 250 W, and the flow rate of CH_4 was kept constant at 100 sccm. For the second set, the flow rate was varied between 10-100 sccm, keeping the RF power constant at 100 W. The deposition time was 30 min. for all the samples in both cases.

II) Comparison of the source gases CH_4 and C_2H_2

For the comparison of the DLC films from source gases CH_4 and C_2H_2, two sets of films were fabricated and the deposition conditions are shown in Tables 2.4 and 2.5, (a) and (b). In the first set, the RF power was varied from 50 to 250 W. In the second case, the RF power was varied from 50 to 500 W. The flow rate of CH_4 or C_2H_2 in both cases was maintained constant at 70 sccm. The deposition time was 30 min. for CH_4 samples, but it was 10 min. for C_2H_2 samples to fabricate films of almost the same thickness for the same RF power.

III) To investigate pressure dependence of the DLC films the deposition pressure was manipulating by the turbo-molecular pump delivery valve at full open, intermediate and almost close position. The RF power was 250 W and the flow rate was 70 sccm for both CH_4 and C_2H_2 samples. The experimental parameters for the pressure run are shown in Table 2.6 (a) and (b).

IV) Effect of Ar dilution with CH_4 and C_2H_2:

In case of CH_4-Ar and C_2H_2-Ar based films the RF power was varied from 50 to 250 W. The flow rate of CH_4 or C_2H_2 in both cases was maintained constant at 70 sccm and that of Ar was 20 sccm. The deposition time was 30 min. for CH_4-Ar samples, but it was 10 min. for C_2H_2-Ar samples to fabricate films of almost the same thickness for the same RF power. The experimental parameters for DLC film deposition are listed in Table 2.7 (a) and (b).

2. 3.5 Effect of RF Power on the Pressure during Deposition

The effect of RF power on the deposition pressure in case of CH_4 and C_2H_2 without any admixture at different flow rate is shown in Fig. 2.6 and the effect of RF power on the deposition the deposition gas pressure CH_4-Ar and C_2H_2-Ar mixture is shown in Fig. 2.7. It can be shown from Fig. 2.6 that, in case of C_2H_2, the tendency of the chamber pressure was slightly decreasing while in case of CH_4 first it was slightly decreasing then it was slightly increasing with RF power at different flow rates. Fig. 2.7 shows that, in case of CH_4-Ar the tendency of the pressure was first increasing then decreasing and again slightly increasing with RF power. On the other hand the tendency of the deposition pressure in case of C_2H_2-Ar mixture is always decreasing with RF power. In general, the pressure after applying the plasma was lower than that of before igniting the plasma. The pressure drop depends on the precursor gas used and is largest in acetylene in both cases.

2.3.6 Plasma Monitoring by OES

Optical emission spectroscopy (OES) is the powerful tool to investigate the active species present in glow discharge plasma. A number of studies reported the spectroscopic studies of the process of RF deposited amorphous carbon films involving OES on CH_4, C_2H_2, and CH_4-Ar plasma. C. Barholm-Hansen *et al.* investigate the OES during the growth of the DLC films from the methane plasma and the influence of flow rate [28]. V. Barbarossa *et al.* also reported the RF deposited amorphous carbon films from hydrogen-rich methane mixture and the relationship among the plasma characteristics, deposition rate and the material properties [29]. G. Cicala *et al.* used the OES for diagnostics of the CH_4-Ar plasma to study how the plasma influence on the a-C:H deposition [30]. J. C Cubertafon *et al.* performed the emission spectroscopy diagnostics on a DC plasma jet Ar, H_2, CH_4 chemical vapor deposition reactor in the large spectral range of 250 to 850 nm [31]. Y. Liao *et al.* utilize the OES to understand the effect of growth parameter during diamond film growth in hot filament CVD [32].

In this research, OES was used to investigate the plasma chemistry, growth mechanism of a-C:H film and the influence on the plasma on the film properties. OES

was found to be useful for investigation of the decomposition process of CH_4, C_2H_2, CH_4-Ar and C_2H_2-Ar mixtures. The emissions of the excited species for both the CH_4, C_2H_2, CH_4-Ar and C_2H_2-Ar plasmas in the spectral range of 200-850 nm were monitored using a fiber-coupling spectrometer (Ocean Optics, USB 2000, 50 μm slit and #14 UV grating) through a quartz vacuum feedthrough (Ocean Optics, VFT-400-UV-40) mounted on the top flange of the chamber as shown in Fig. 2.4 (b). The Ocean Optics spectrometer, USB 2000 was used in the experiment. The OES system was controlled by computer. Fig 2.8 (a) (b) to 2.13 (a) (b) show the optical emission spectra of the CH_4 and C_2H_2, CH_4-Ar and C_2H_2-Ar plasmas for 50, 100, 200 W RF discharges. As can be observed in these Figs., the predominant emission lines of the CH_4, C_2H_2, CH_4-Ar and C_2H_2-Ar plasmas are the atomic hydrogen lines of the Balmer series (H_α at 656.57 nm, H_β at 486.44 nm, H_γ at 434.29 nm and H_δ at 410.65 nm) and CH systems ($A^2\Delta$ - $X^2\Pi$ at 431.26 nm and $B^2\Sigma$ - $X^2\Pi$ at 390.28 nm). In the CH_4 and CH_4-Ar plasma, H_2 emission bands are also observed. On the other hand, in the C_2H_2 and C_2H_2-Ar plasma, C_2 spectra belonging to the Swan system ($A^3\Pi g$ - $X^3\Pi u$) band head at 516.51 and 468.81 nm are observed. In both cases, the intensities of the CH radicals are almost equal, but the intensity of H_α in the C_2H_2 and C_2H_2-Ar plasma is almost one-half that in the CH_4 and CH_4-Ar plasma. The intensity ratio of the CH radicals to H_α in the C_2H_2 and C_2H_2-Ar plasma is approximately 3:1, but in the CH_4 and CH_4-Ar plasma, the ratio is approximately 3:2. The broad band emission observed in the case of C_2H_2 and C_2H_2-Ar is also much more predominant than that observed in the case of CH_4 and CH_4-Ar.

The emission lines due to Ar were observed in the CH_4-Ar and C_2H_2-Ar systems. The most intense spectra of Ar are observed in 650-850 nm regions. The main lines observed are for wavelength of 675.9, 687.66, 697.91, 703.97, 707.04, 721.38, 727.76, 738.65, 750.98, 763.83, 772.74, 795.14, 801.86 and 811.75 nm. All these lines are attributed to ArI (neutral argon).

The intensity of the H_2 emission bands observed in the case of CH_4-Ar plasma is much more predominant than that observed in the case of pure CH_4 plasma for the RF powers of 50 and 100 W.

2.4 Measurement of Film Thickness

2.4.1 Techniques of Measurement Film Thickness

The thickness of a film is one of the most important characteristics feature and the thickness measurements are one of the vital importance of the thin film investigation. The reason is that thin-film electrical and optical properties and behavior depends on the thickness. In some applications such as decorative, metallurgical, and protective films and coatings, the actual film thickness is not so significant. One the other hand, in microelectronic application, precise and reproducible film thickness is required. There are various techniques for measurement of film thickness as given below

a. Optical Methods for Measuring Film Thickness:

Optical method for film thickness measurement is the widely used method for thickness measurement. Both opaque and transparent films thickness can be measured with high accuracy by this method. Moreover measurement can be performed quickly, nondestructive and utilize relatively cheaper equipments are required. The basic principle of this method is the interference of two or more beams of light whose optical path difference is related to the film thickness.

Interferometry is considered as a standard technique for determining the surface features [33]. The major advantage of this method is that no contact is required. Light is reflected from the surface and interferes with light from an optically flat reference surface. Deviation in the fringe pattern produced due to the interferences is related to the differences in the surface features (such as step height or film thickness).

b. Mechanical Techniques for Measuring Film Thickness

1. Stylus-method profilometers use the movement of a diamond or other hard stylus over the sample surface [34, 35]. Typically the radius of curvature of the stylus is 1-10 μm which serves as the electromagnetic pickup. The force of the stylus on the surface can be adjusted to optimize the load of the sample surface. The range of the force can be adjusted in the range of 1-50 mg. The signal is digitized and stored. The instrument possesses microscope/camera for locating the exact region for analysis. By scanning over the stylus over the edge of the film the thickness can be measured.

Several factors such as stylus penetration and scratching of film, substrate roughness and vibration of the equipment limit the resolution of stylus measurements [35].

c. Weight Measurement

Measurement of the weight of the film deposit appears, to be an easy direct way to determine film thickness *d*. Knowing the film mass *m*, the deposit area *A*, and film density ρ_f we have

$$d = \frac{m}{A\rho_f} \tag{2.1}$$

The values of d so obtained are not precise because the film density is not known correctly.

d. Cross-sectional scanning electron microscopy (SEM):

SEM is one of most widely used equipment to measure the thickness of the films with sub-micron size. It operates by scanning a focused electron beam over a surface and sensing the secondary electron emitted from the surface. The beam size determines the resolution. The intensity of the secondary electron emission depends on the local surface geometric relief because of the asymmetric location of the detector. The sample surface topography is magnified into an image on the CRT (cathode-ray tube). DLC films grown on Si can be directly observed by SEM without any conducting coating being deposited on the surface. With this equipment the thickness of the film can be measured with an accuracy of ±10 nm.

2.4.2 Thickness Measurement by SEM

In this work the thickness of the film was measured by cross-sectional scanning electron microscope (SEM) HITACHI, Model S-3000N. This method comprises of two steps.

1) Mask deposition for thickness measurement

First DLC films are partly coated and partly uncoated on the same type Si substrate by RF-PECVD using the same deposition condition of the respective films by placing suitable thin Al mask before deposition. A very thin Al foil with sharp edge was used

as a mask. If correctly positioned, a sharp edge from the DLC is formed on the Si substrate, which makes taking SEM measurement relatively easy.

2) Measurement of the film thickness by SEM

The partly coated DLC films were put on the SEM stage and the stage was tilted 90°. Then the sample was focused at the sharp edge with high magnification to get the film thickness.

Thus the film thickness was measured by SEM using the cross-sectional method and consequently the deposition rate was calculated.

2.4.3 Deposition Rate

Deposition rate and bias voltage of DLC films as function of RF input power for CH_4 at different RF power and flow rate is shown in Fig. 2.14 (a) and (b) respectively. Fig. 2.15 (a) and (b) shows deposition rate and bias voltage of DLC films as a function of RF input power for CH_4 and C_2H_2 constant flow rate (70 sccm). The deposition rate as a function of deposition pressure for both CH_4 and C_2H_2 is plotted in Fig. 2.16. Deposition rate and bias voltage of DLC films as function of RF input power for CH_4 and CH_4-Ar, C_2H_2 and C_2H_2-Ar mixtures at different RF power is shown in Fig. 2.17 (a) and (b) respectively.

2.5 Results and Discussions

Figs. 2.6 (a) and (b) shows the deposition pressure vs. RF power curve for both CH_4 and C_2H_2. Figs. 2.7 (a) and (b) shows the deposition pressure vs. RF power curve for both CH_4-Ar and C_2H_2-Ar, respectively. As can be seen from Figs. 2.6 (a) and (b) that, in case of C_2H_2, the tendency of the chamber pressure was slightly decreasing while in case of CH_4 first it was slightly decreasing then it was slightly increasing with RF power at different flow rates. On the other hand, Fig. 2.7 shows that, in case of CH_4-Ar, the tendency of the pressure was first increasing then decreasing and again slightly increasing with RF power. But the tendency of the deposition pressure in case of C_2H_2-Ar mixture was always decreasing with RF power. It can be explained in terms of simple dissociation reaction of CH_4 and C_2H_2,

$$CH_4 \longrightarrow C + 2H_2, \text{ and}$$

$$C_2H_2 \longrightarrow 2C + H_2.$$

When CH_4 dissociates it gives two hydrogen molecules of H_2, but in case of C_2H_2 one molecule of hydrogen evolves. Due to the low sensitivity of the ion gauge to hydrogen, the tendency of the pressure in case of C_2H_2 is always decreasing and in case of methane it is increasing.

The sensitivity of ion gauge to Ar gas is much higher. In case of CH_4-Ar at low power intensity of H_2 emission band are much predominant than pure CH_4. So Ar addition in CH_4 increases the pressure at low power. Probably due to the combined effect of sensitivity of H_2 and Ar to ion gauge, the change of pressure occurs in CH_4-Ar and C_2H_2-Ar.

Deposition rate and bias voltage of DLC films as a function of RF input power for CH_4 at different RF powers and flow rate are shown in Figure 2.14 (a) and (b), respectively. Figure 2.14 shows that, during the deposition of the DLC films, the dc negative bias voltages are found to increase with the increase of RF power for a constant flow rate of 100 sccm. The growth rate of the films increases almost linearly with RF power and bias. On the other hand, the negative self bias voltages are found to decrease with the increase of flow rate for a constant RF power of 100 W, as shown in Fig. 2.14 (b). The growth rate of the films decreases almost linearly with the flow rate and bias.

The average impact energy has been controlled by the bias voltage (V_b). The behavior of ions and electrons in an RF discharge depends on the plasma frequency equation [36],

$$f_{p\,i,e} = \frac{1}{2\pi}\left(\frac{n_{i,e}e}{m_{i,e}\varepsilon_o}\right)^{\frac{1}{2}} \tag{2.2}$$

where $n_{i,e}$ and $m_{i,e}$ are respectively are respectively the ion and the electron density and mass. Assuming that in hydrocarbon plasmas $n_i = n_e = 10^{10}$ cm^{-3}. Thus in 13.56 MHz discharge, the RF field frequency is sufficiently high that the ions require many RF cycles to cross the sheath while electrons are able to follow the RF field. The RF electrode is capacitively coupled; the steady state DC current must be zero. Since the powered electrode area is smaller than the grounded part of the system, it develops a negative self bias voltage V_b relative to the ground.

For a non collision sheath, the mean ion energy is thus given by equation [36],

$$E_i = e\left(\bar{V}_p - V_b\right) = e|V_b|. \tag{2.3}$$

It is also found that V_b is a linear function of the square root of the ratio of the RF power over the discharge pressure,

$$V_b \sim \left(\frac{W}{P}\right)^{1/2}. \tag{2.4}$$

Bubenzer et *al*. [37] demonstrated that the ion energy depends on both bias potential and pressure,

$$E_i \sim V_b P^{-1/2}. \tag{2.5}$$

Combining equations (2.4 and 2.5) we get

$$E_i \sim \frac{W^{1/2}}{P}. \tag{2.6}$$

Equation 2.6 gives the relation between ion energy and the discharge parameter i.e. power and pressure, which is deduced by Zarowin [38]. Thus the key variables which controls the energy of the ions impinging on the substrate are the self bias voltage (or the power) and the discharge pressure.

In an RF-PECVD system, the impact energy of the films forming the hydrocarbon ions is determined by the bias voltage and the inelastic collisions in the ion sheath. It is found that the impact energy of the forming hydrocarbons is the most important deposition parameter. The electron thermal velocity $(eT_e/m)^{1/2}$ is at least 100 times the ion thermal velocity $(eT_i/M)^{1/2}$ because $m/M << 1$ and $T_e > T_i$ [39]. With the increase of power, the ion energy increases and the electron density (Ne) increases, and consequently the bias also increases, sufficient dissociation of the gas molecules occurs, hence the growth rate increases. With the increase of flow rate, deposition pressure increases and consequently the electron energy (Te) decreases. As a result bias decreases and insufficient dissociation occurs. So the growth rate decreases.

The deposition rate and bias voltage of DLC films deposited from CH_4 and C_2H_2 at constant flow rate of 70 sccm are shown as a function of RF input power from 50-250 W and from 50-500 W in Fig. 2.15 (a) and (b) respectively. In these figures, it is

observed that self-bias voltage increases with applied power and a similar trend is observed in both cases. It is also observed that the growth rate of C_2H_2-based films is more than three times than that of CH_4-based films for all the RF powers considered, although the self-bias voltages of both films are similar. The number of carbon atoms in C_2H_2 is two times larger than that in CH_4 at the same flow rate. Possibly because of the difference in the amount of hydrogen, however, the ratio of the deposition rate was more than two.

The higher growth of the C_2H_2 based films than the CH_4 based films can also be explained in terms of optical emission spectroscopy (OES). From the OES we observed in both cases, the intensities of the CH radicals are almost equal, but the intensity of H_α in the C_2H_2 plasma is almost one-half that in the CH_4 plasma. The intensity ratio of the CH radicals to H_α in the C_2H_2 plasma is approximately 3:1, but in the CH_4 plasma, the ratio is approximately 3:2. In the case of C_2H_2, C_2 emission lines are also observed. C_2, CH radicals and atomic H, namely CH and H_α, cause the growth of the a-C:H (DLC) layer [40, 41]. CH radicals are favorable for the formation of the DLC layer [41, 42]. On the other hand, H atoms enhance chemical etching with respect to growth [41, 42, 43]. Thus, the net deposition rate is determined from the concentrations of CH radicals and H_α in the plasma. Thus, the CH/H_α intensity ratio is used as a monitor for the deposition rate of DLC's. Because the intensity ratio of CH radicals to H_α in the C_2H_2 plasma is higher than that in CH_4 plasma, the deposition rate of C_2H_2 films is higher than that of CH_4 films. In the C_2H_2 plasma, the large amount of C_2 molecules also contributes to the higher growth rate.

Fig. 2.16 shows the deposition rate and bias voltage of the DLC films as a function of deposition pressure for both CH_4 and C_2H_2. As can be seen, the negative-self bias voltage and the deposition rate decreases with the increase of deposition pressure for both the precursors considered. The decrease of deposition rate with the increase of pressure associated with the decrease of the electron energy (Te).

The deposition rate and bias voltage of DLC films grown from CH_4 and CH_4-Ar mixture are shown as a function of RF input power in Fig. 2.17 (a). In this figure, it is observed that self-bias voltage increases with applied power and a similar trend is observed in both cases. It is also observed that the growth rate of CH_4-Ar based films

is lower than that of pure CH_4-based films for all the RF powers considered, although the self-bias voltages of both films are similar.

In the CH_4-Ar plasma, both Ar ions and H atoms enhances the sputter-etching process with respect to growth. It is well known that the deposition rate of the films depends on the plasma density and the ion energy, and may be considered to be a resulting effect of the balance between the deposition and etching. The decrease of the growth in the CH_4-Ar based film is due to the increase of the sputter-etching rate based on the interplay of H_α and Ar species.

The decrease of the growth rate with Ar addition can also be explained with the relation (Equation 2.6) between ion energy and discharge parameters such as power and pressure.

Ar addition increases the deposition pressure and consequently the ion energy decreases and hence the growth rate also decreases.

The deposition rate and bias voltage of DLC films grown from C_2H_2 and C_2H_2-Ar mixture are shown as a function of RF input power in Fig. 2.17 (b). In this figure, it is observed that self-bias voltage increases with applied power and a similar trend is observed in both cases. It is also observed that the growth rate of C_2H_2-Ar based films is lower than that of pure C_2H_2-based films for all the RF powers considered, although the self-bias voltages of both films are similar.

In the similar manner to CH_4-Ar mixture films, it can be explained that the decrease of the growth in the C_2H_2- Ar based film is due to the increase of the sputter-etching rate based on the interplay of H_α and Ar species.

The decrease of the growth rate with Ar addition can also be explained with the relation between ion energy and discharge parameters such as power and pressure i.e. equation 2.6. Ar addition increases the deposition pressure and consequently the ion energy decreases and hence the growth rate also decreases.

2.6 Summary

DLC thin films were prepared by RF-PECVD using CH_4, C_2H_2 and the admixture of CH_4-Ar and C_2H_2-Ar gases. The dc negative bias voltages were found to increase

with the increase of RF power. On the other hand, the negative self bias voltages were found to decrease with the increase of flow rate and deposition pressure.

DLC thin films were prepared by RF-PECVD using CH_4 and C_2H_2 at different RF powers. In both cases, the intensities of the CH radicals were similar, but the intensity of H_α in the C_2H_2 plasma was about one-half that in the CH_4 plasma. Similar trend were also observed in case of CH_4-Ar and C_2H_2-Ar plasmas.

With the increase of RF power, the growth rate increased at a constant flow rate. On the other hand, growth rate decreased with the increase of deposition pressure and flow rate. Highest deposition rates were obtained for the films deposited at highest RF power, lowest flow rate or lowest deposition pressure.

With the increase of power, the electron density (Ne) increases and the bias also increases, sufficient dissociation of the gas molecules occurs, hence the growth rate increases. With the increase of flow rate and deposition pressure the electron density (Ne) decreases. As a result bias decreases and insufficient dissociation occurs. So the growth rate decreases.

The growth rate of DLC films prepared using the C_2H_2 plasma was more than three times higher than that of the CH_4-plasma-prepared DLC films. The number of carbon atoms in C_2H_2 is two times larger than that in CH_4 at the same flow rate. Possibly because of the difference in the amount of hydrogen, however, the ratio of the deposition rate was more than two.

Because the intensity ratio of CH radicals to H_α in the C_2H_2 plasma is higher than that in CH_4 plasma, the deposition rate of C_2H_2 films is higher than that of CH_4 films. In the C_2H_2 plasma, the large amount of C_2 molecules also contributes to the higher growth rate. OES analysis showed that the higher the H_α and Ar intensities, the lower the deposition rate of DLC films.

Addition of Ar decreased the growth rate due to the sputtering effect of Ar ions. Ar addition increases the deposition pressure and consequently the ion energy decreases and hence the growth rate also decreases.

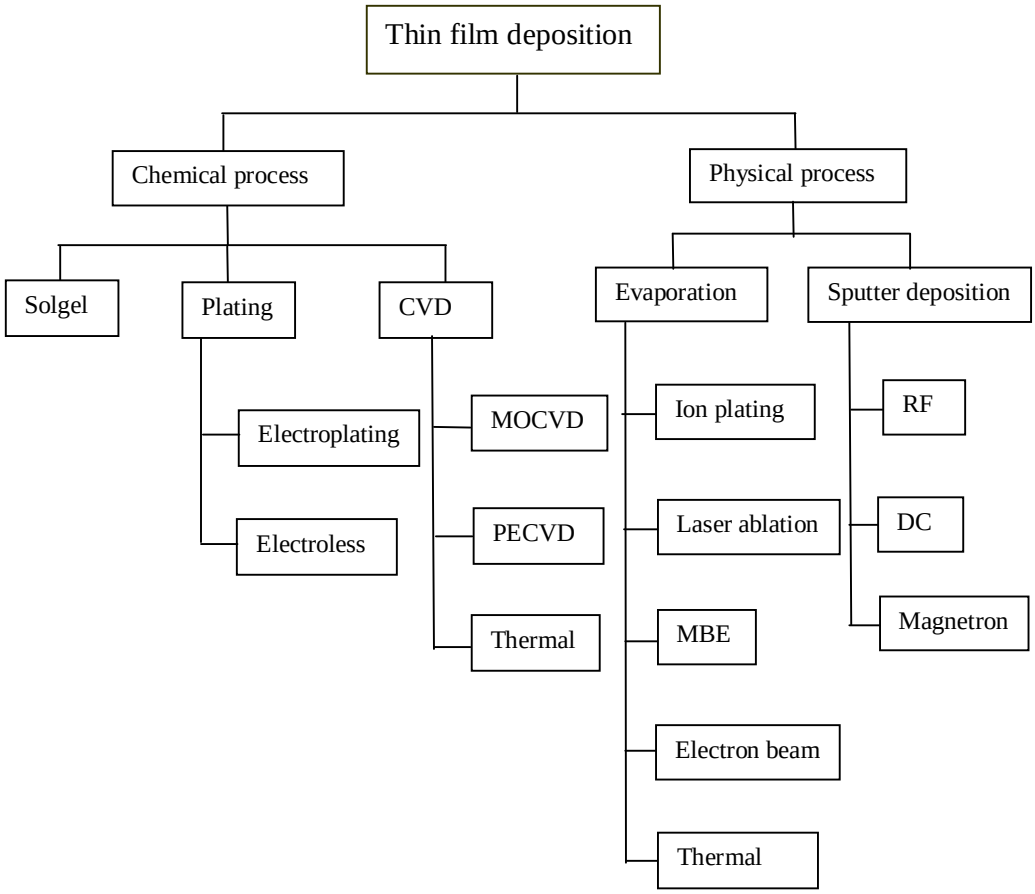

Fig. 2.1 Classification of the most common deposition processes [24].

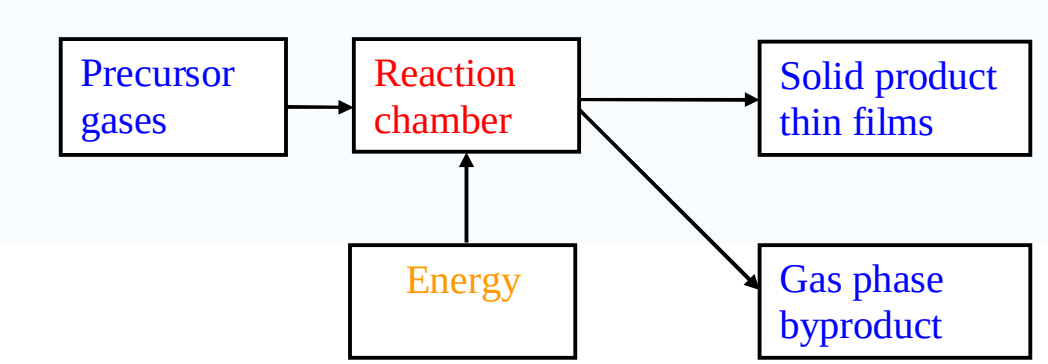

Fig. 2.2 Block diagram of the CVD process.

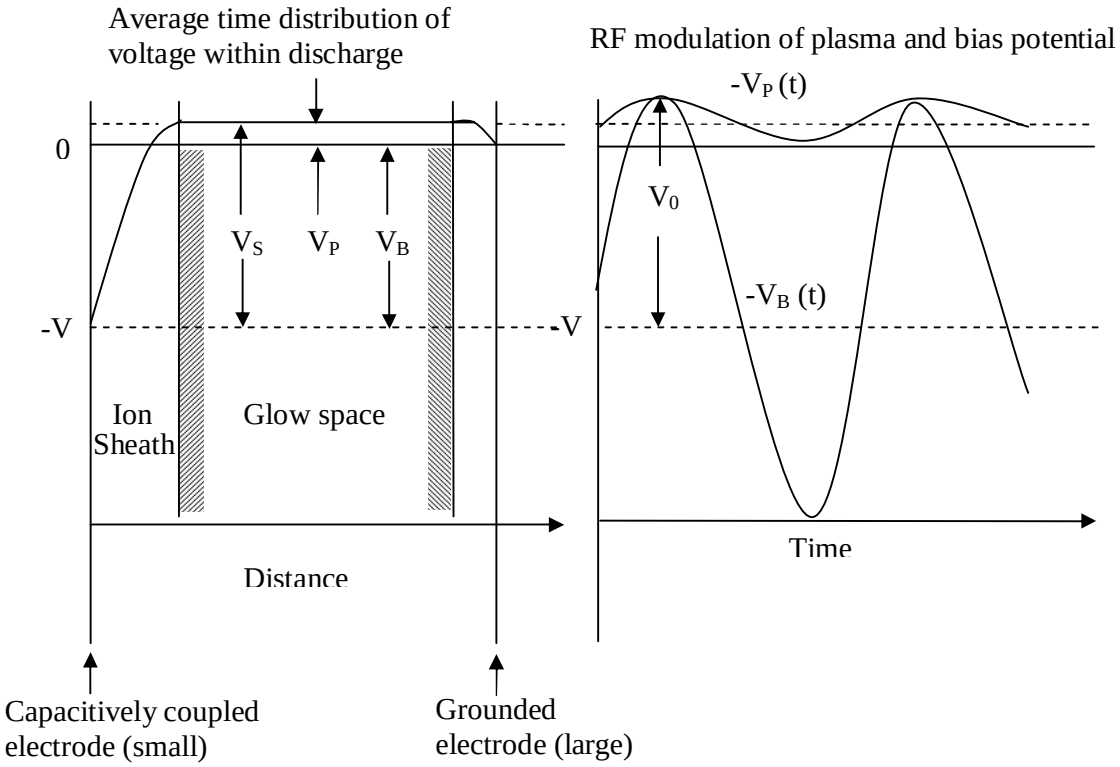

Fig. 2.3 The spatial and temporal potential distribution in a capacitively coupled RF discharge with asymmetric electrodes [27].

Fig. 2.4 (a) RF-PECVD apparatus used for DLC deposition.

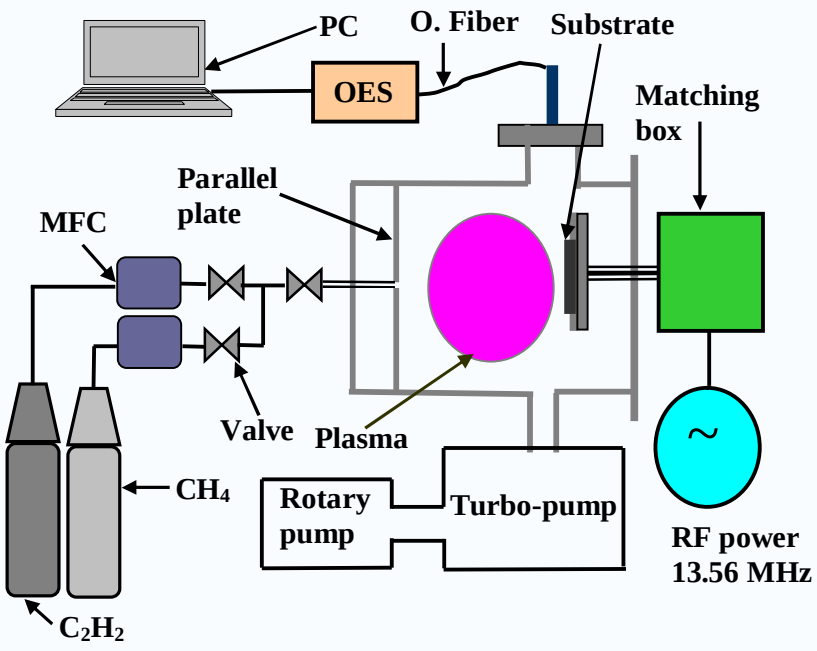

Fig. 2.4 (b) Schematic diagram of RF-PECVD system used for DLC deposition.

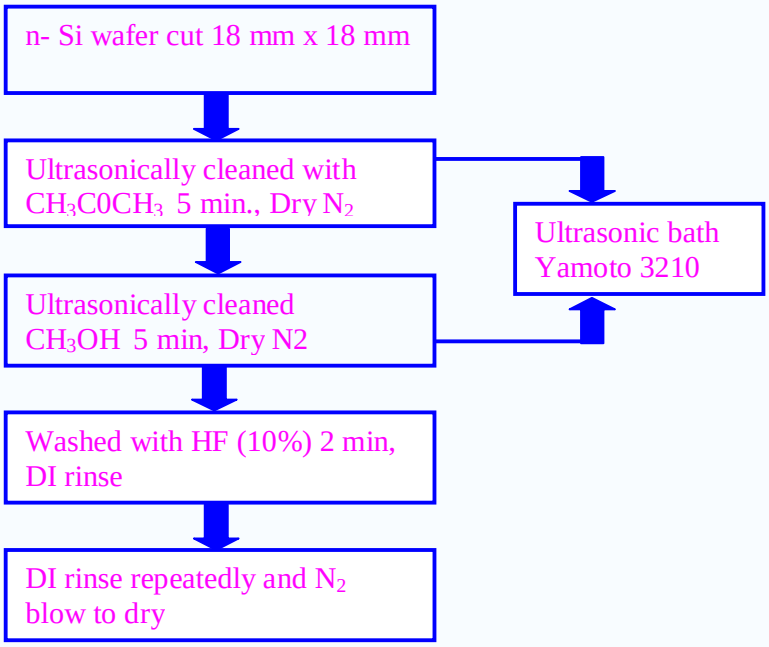

Figure 2.5 Block diagram of the substrate preparation and cleaning.

Table 2.1 Etching conditions for cleaning the deposition chamber with O_2 plasma.

`

RF power (W)	O_2 flow rate (sccm)	Etching pressure (Pa)	Bias voltage (V)	Etching time (hour)
100~150	100	3~4.8	500~570	6 ~ 14

Table 2.2 Experimental parameter for the DLC deposition from CH_4 at constant flow rate.

Sample no.	R.F. power (W)	CH_4 flow rate (sccm)	Deposition pressure (Pa)	Negative bias voltage (V)	Deposition time (min)	Thickness (nm)
1	50		16	267		330
2	100		20	372		675
3	150	100	22	440	30	1175
4	200		24	483		1500
5	250		26	526		1800

Table 2.3 Experimental parameters for the DLC deposition from CH_4 at constant RF power.

Sample no.	CH_4 flow rate (sccm)	RF power (W)	Deposition pressure (Pa)	Negative bias voltage (V)	Deposition time (min)	Thickness (nm)
1	10		0.85	593		1300
2	25		1.4	567		1175
3	50	100	2.4	556	30	1050
4	75		3.4	488		825
5	100		20	372		675

Table 2.4 (a) Experimental parameters for the DLC deposition from CH_4 at constant flow rate and RF power ranging from 50 to 250 W.

Sample no.	R.F. power (W)	CH_4 flow rate (sccm)	Deposition pressure (Pa)	Negative bias voltage (V)	Deposition time (min)	Thickness (nm)
1	50	70	4.65	319	30	425
2	100		4.6	512		650
3	150		4.7	564		1100
4	200		4.7	635		1475
5	250		4.85	691		1750

Table 2.4 (b) Experimental parameters for the DLC deposition from C_2H_2 at constant flow rate and RF power ranging from 50 to 250 W.

Sample No.	R.F. power (W)	C_2H_2 flow rate (sccm)	Deposition pressure (Pa)	Negative bias voltage (V)	Deposition time (min)	Thickness (nm)
1	50	70	4.45	351	10	525
2	100		4.3	537		1100
3	150		4.2	613		1450
4	200		4.1	696		1600
5	250		4	744		1950

Table 2.5 (a) Experimental parameters for the DLC deposition from CH_4 at constant flow rate and RF power ranging from 50 to 500 W.

Sample no.	R.F. power (W)	CH_4 flow rate (sccm)	Deposition pressure (Pa)	Negative bias voltage (V)	Deposition time (min)	Thickness (nm)
1	50		4.65	319		425
2	100		4.65	512		650
3	200	70	4.6	467	30	1475
4	300		4.7	755		1800
5	400		5.3	840		2000
6	500		5.4	937		2275

Table 2.5 (b) Experimental parameters for the DLC deposition from C_2H_2 at constant flow rate and RF power ranging from 50 to 500 W.

Sample no.	R.F. power (W)	C_2H_2 flow rate (sccm)	Deposition pressure (Pa)	Negative bias voltage (V)	Deposition time (min)	Thickness (nm)
1	50		4.45	351		525
2	100		4.3	537		1100
3	200	70	4.3	696	10	1600
4	300		4.5	836		2050
5	400		4.3	953		2150
6	500		4.2	994		2400

Table 2.6 (a) Experimental parameters for the DLC deposition from CH_4 by varying the deposition pressure.

Sample no.	R.F. power (W)	CH_4 flow rate (sccm)	Deposition pressure (Pa)	Negative bias voltage (V)	Deposition time (min)	Thickness (nm)
Full open			3.7	728		1825
Inter. pos.	250	70	4.85	704	30	1750
Almost close			7.8	651		1625

Table 2.6 (b) Experimental parameters for the DLC deposition from C_2H_2 by varying the deposition pressure.

Sample no.	R.F. power (W)	C_2H_2 flow rate (sccm)	Deposition pressure (Pa)	Negative bias voltage (V)	Deposition time (min)	Thickness (nm)
Full open			3.6	810		2000
Inter. pos.	250	70	4	779	10	1950
Almost close			6.5	773		1875

Table 2.7 (a) Experimental parameter for the DLC deposition from CH_4-Ar at constant flow rate.

Sample no.	R.F. power (W)	Flow rate (sccm)		Deposition pressure (Pa)	Negative bias voltage (V)	Deposition time (min)	Thickness (nm)
		CH_4	Ar				
1	50			5.5	355		375
2	100			5	493		525
3	150	70	20	4.8	571	30	675
4	200			5.3	640		950
5	250			5.5	704		1275

Table 2.7 (b) Experimental parameters for the DLC deposition from C_2H_2-Ar at constant flow rate

Sample no.	R.F. power (W)	Flow rate (sccm)		Deposition pressure (Pa)	Negative bias voltage (V)	Deposition time (min)	Thickness (nm)
		C_2H_2	Ar				
1	50			6	340		400
2	100			6.3	497		890
3	150	70	20	6.2	602	10	975
4	200			6	687		1200
5	250			5.6	754		1450

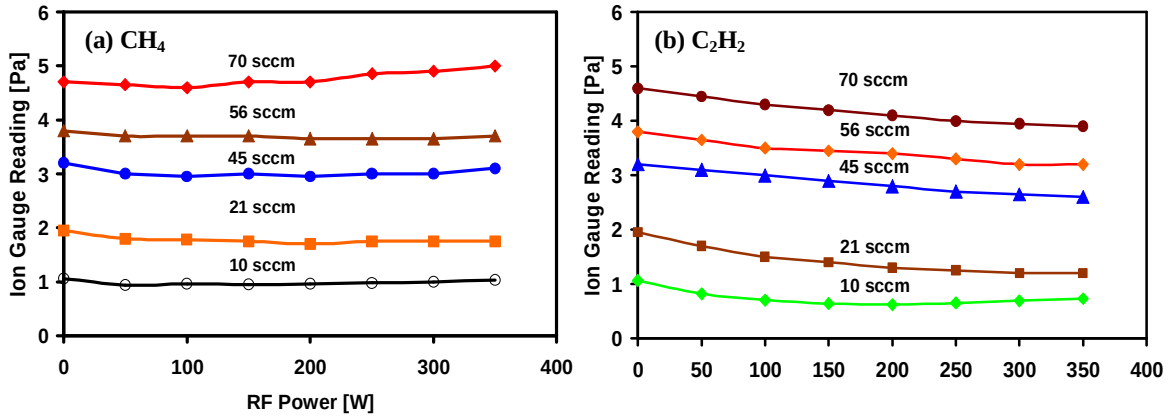

Fig. 2.6 Deposition pressure vs. RF power at different flow rate (a) CH_4 and (b) C_2H_2.

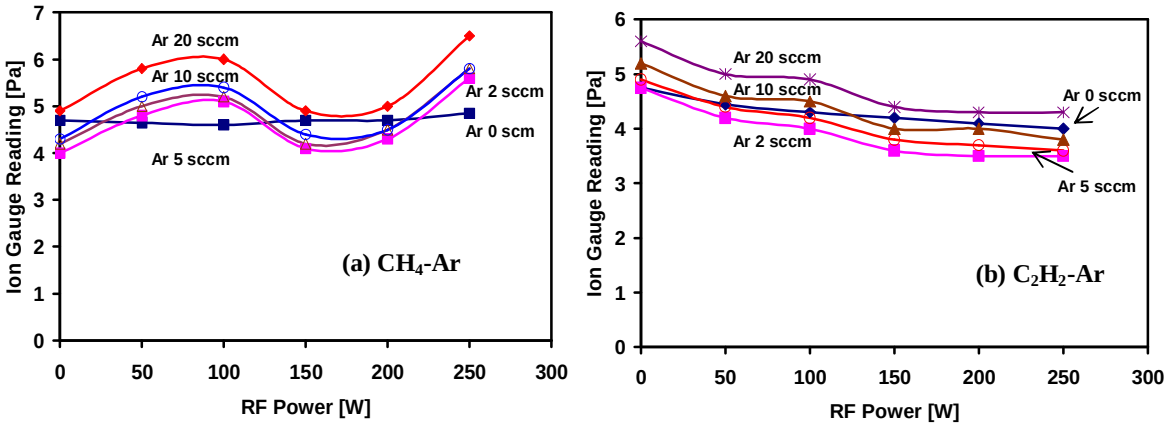

Fig. 2.7 Deposition pressure vs. RF power at different flow rate (a) CH_4-Ar and (b) C_2H_2-Ar.

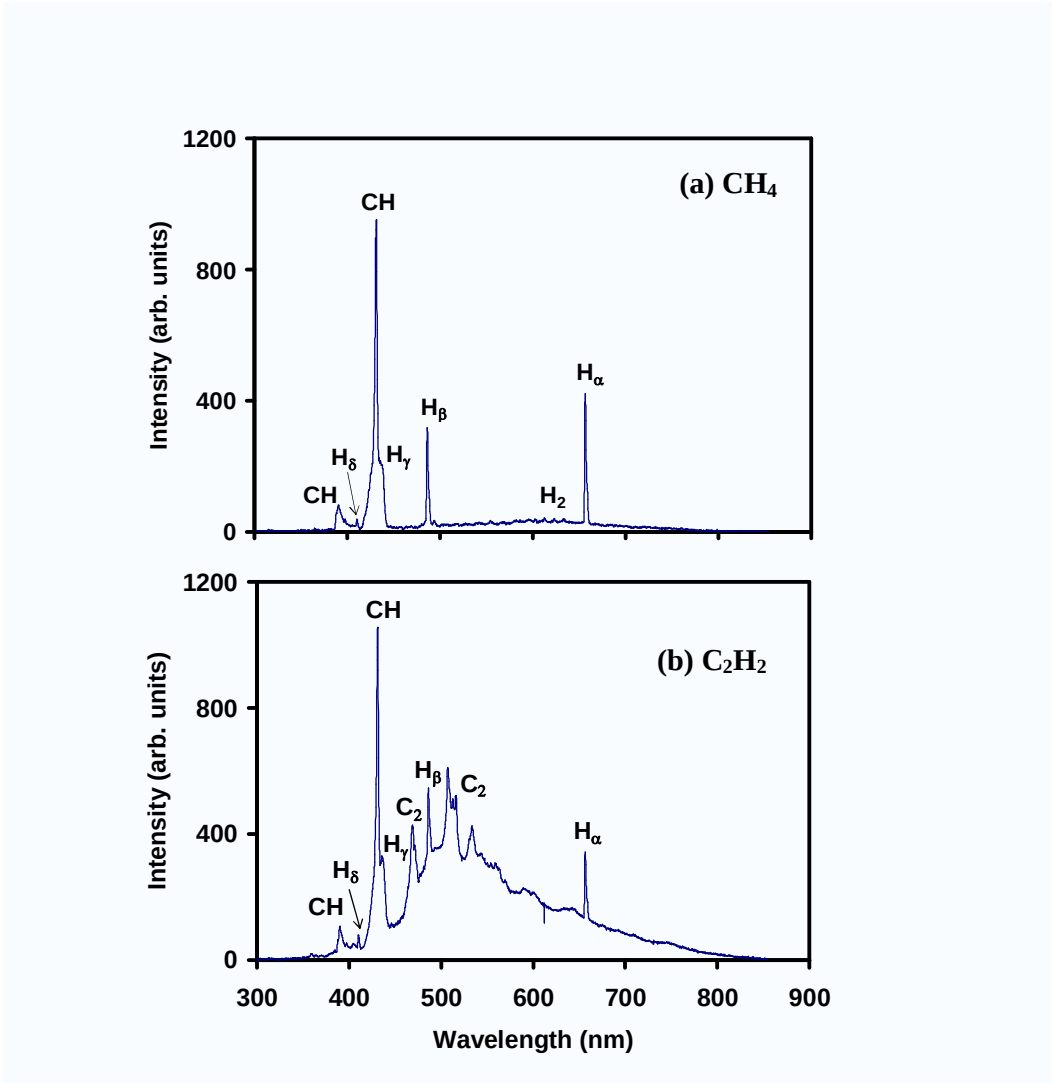

Fig. 2.8 Typical optical emission spectra of CH_4 and C_2H_2 plasmas produced at RF power of 50 W and flow rate of 70 sccm (a) CH_4 and (b) C_2H_2.

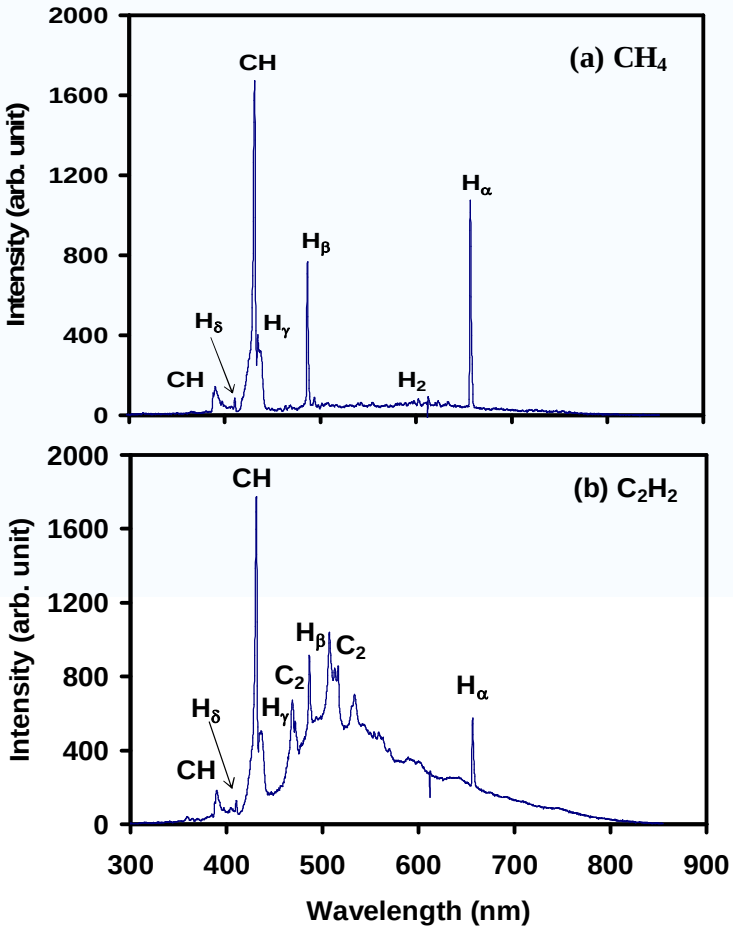

Fig. 2.9 Typical optical emission spectra of CH_4 and C_2H_2 plasmas produced at RF power of 100 W and flow rate of 70 sccm (a) CH_4 and (b) C_2H_2.

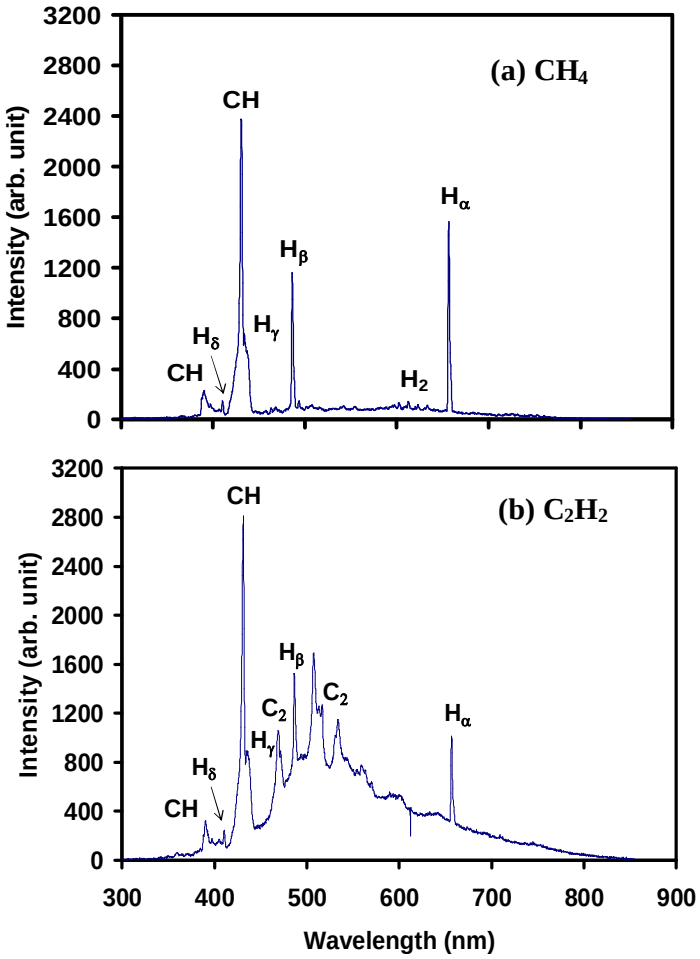

Fig. 2.10 Typical optical emission spectra of CH_4 and C_2H_2 plasmas produced at RF power of 200 W and flow rate of 70 sccm (a) CH_4 and (b) C_2H_2.

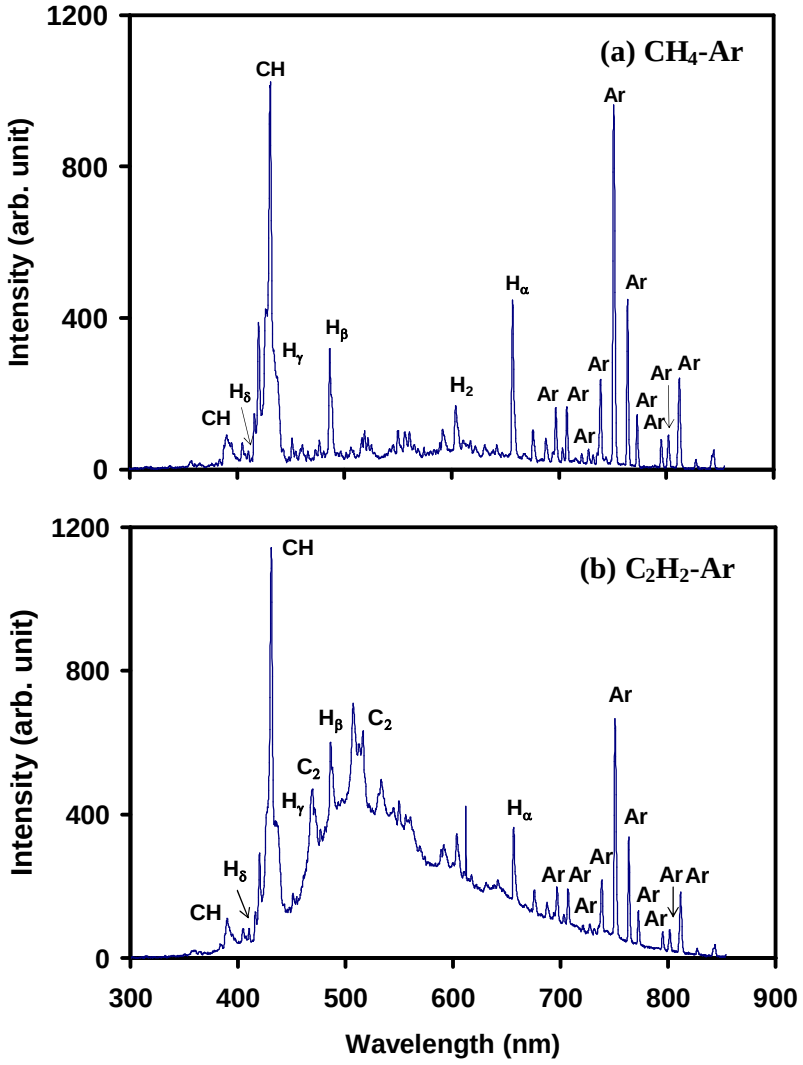

Fig. 2.11 Typical optical emission spectra of CH_4-Ar and C_2H_2-Ar plasmas produced at RF power of 50 W and flow rate of CH_4/C_2H_2 70 sccm and Ar 20 sccm (a) CH_4-Ar and (b) C_2H_2-Ar.

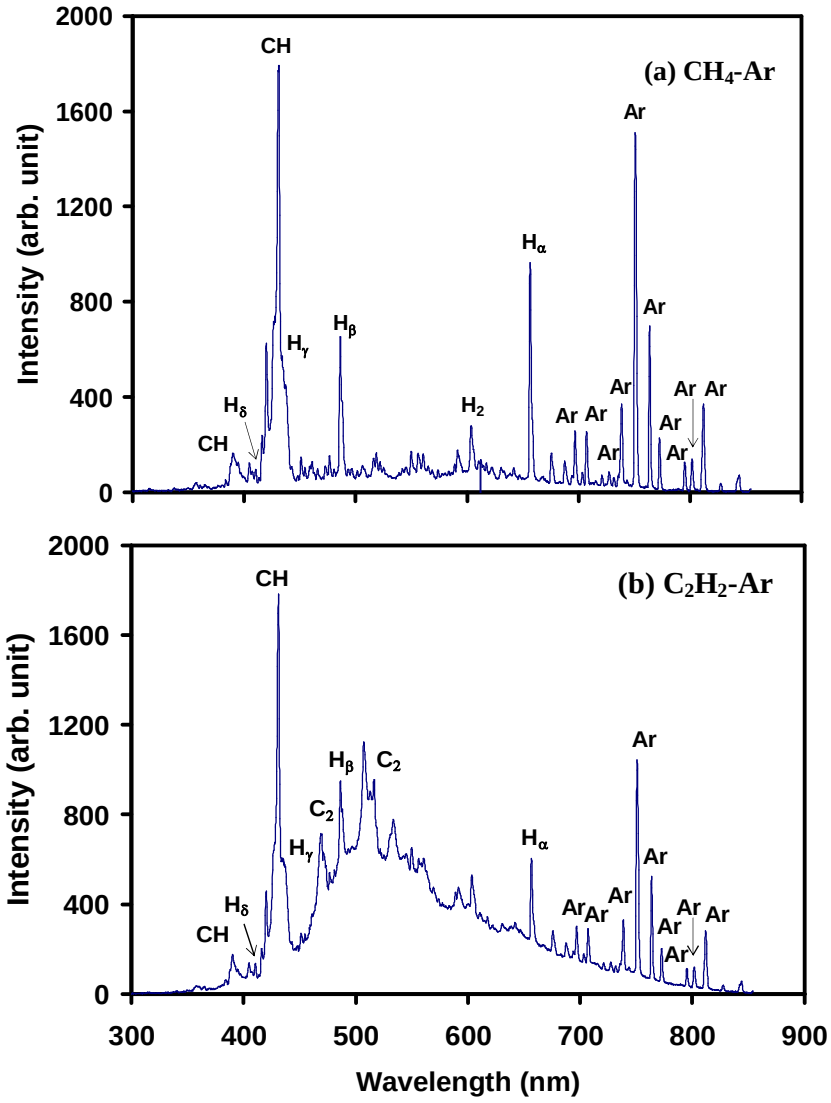

Fig. 2.12 Typical optical emission spectra of CH_4-Ar and C_2H_2-Ar plasmas produced at RF power of 100 W and flow rate of CH_4/C_2H_2 70 sccm and Ar 20 sccm (a) CH_4-Ar and (b) C_2H_2-Ar.

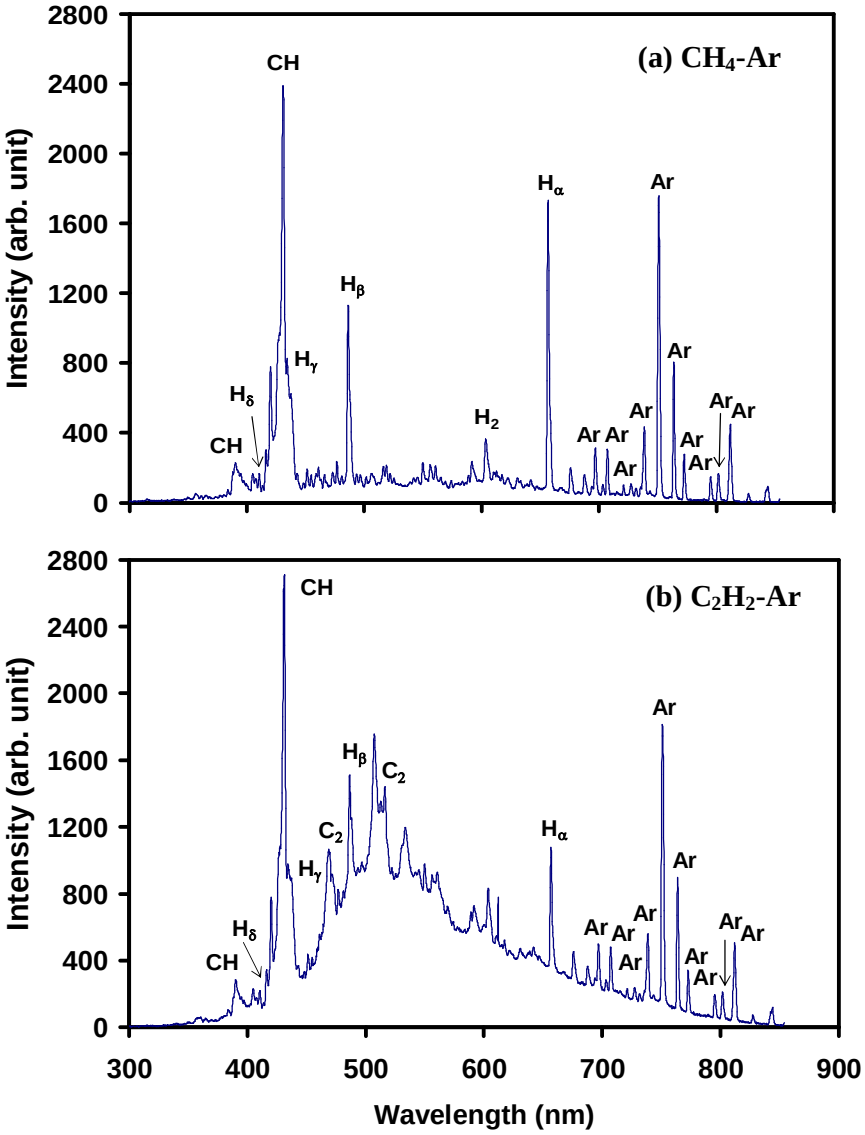

Fig. 2.13 Typical optical emission spectra of CH_4-Ar and C_2H_2-Ar plasmas produced at RF power of 200 W and flow rate of CH_4/C_2H_2 70 sccm and Ar 20 sccm (a) CH_4-Ar and (b) C_2H_2-Ar.

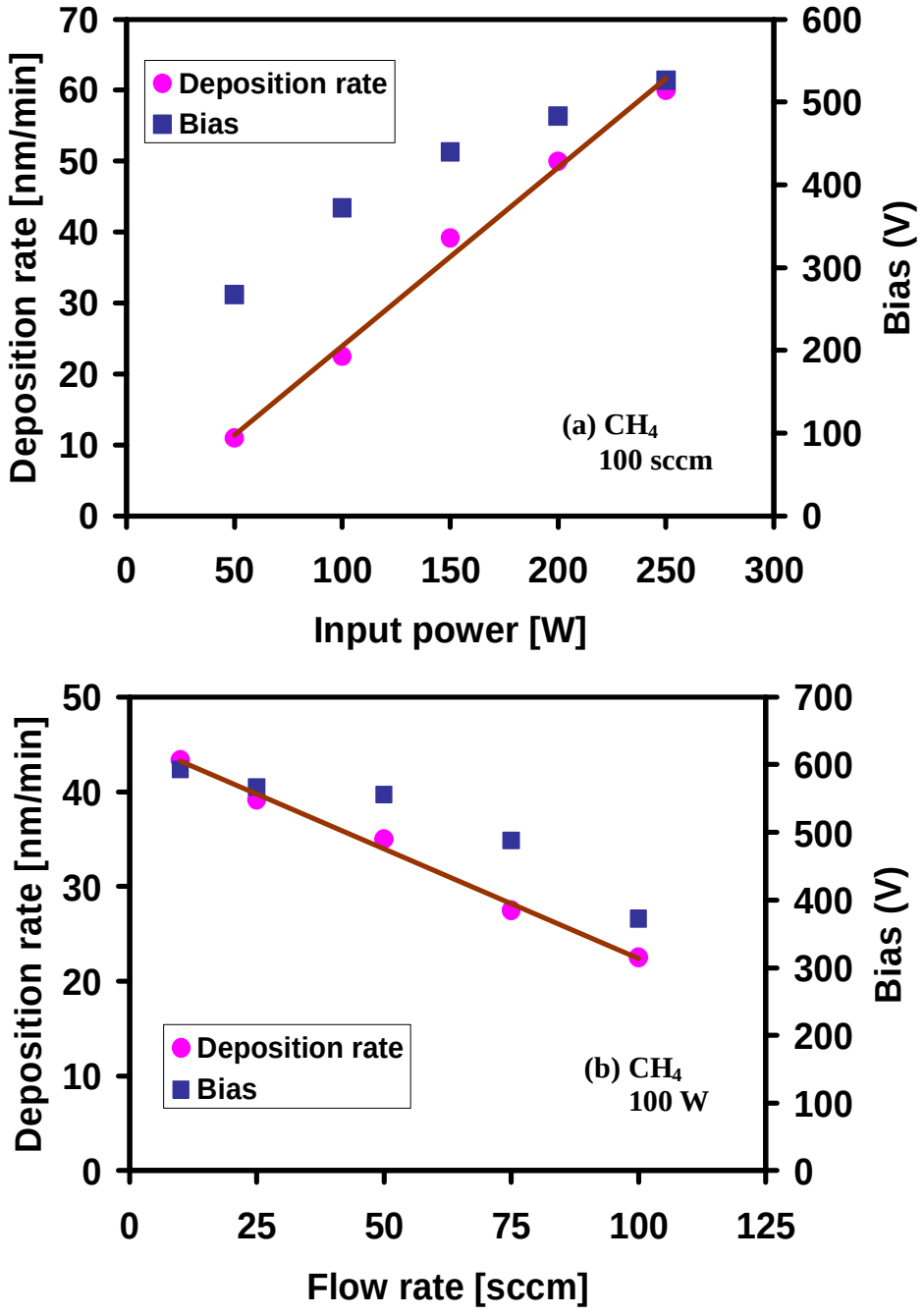

Fig. 2.14 Deposition rate and bias voltage of DLC films as function of RF input power for CH_4 (a) at different RF power and (b) at different flow rate.

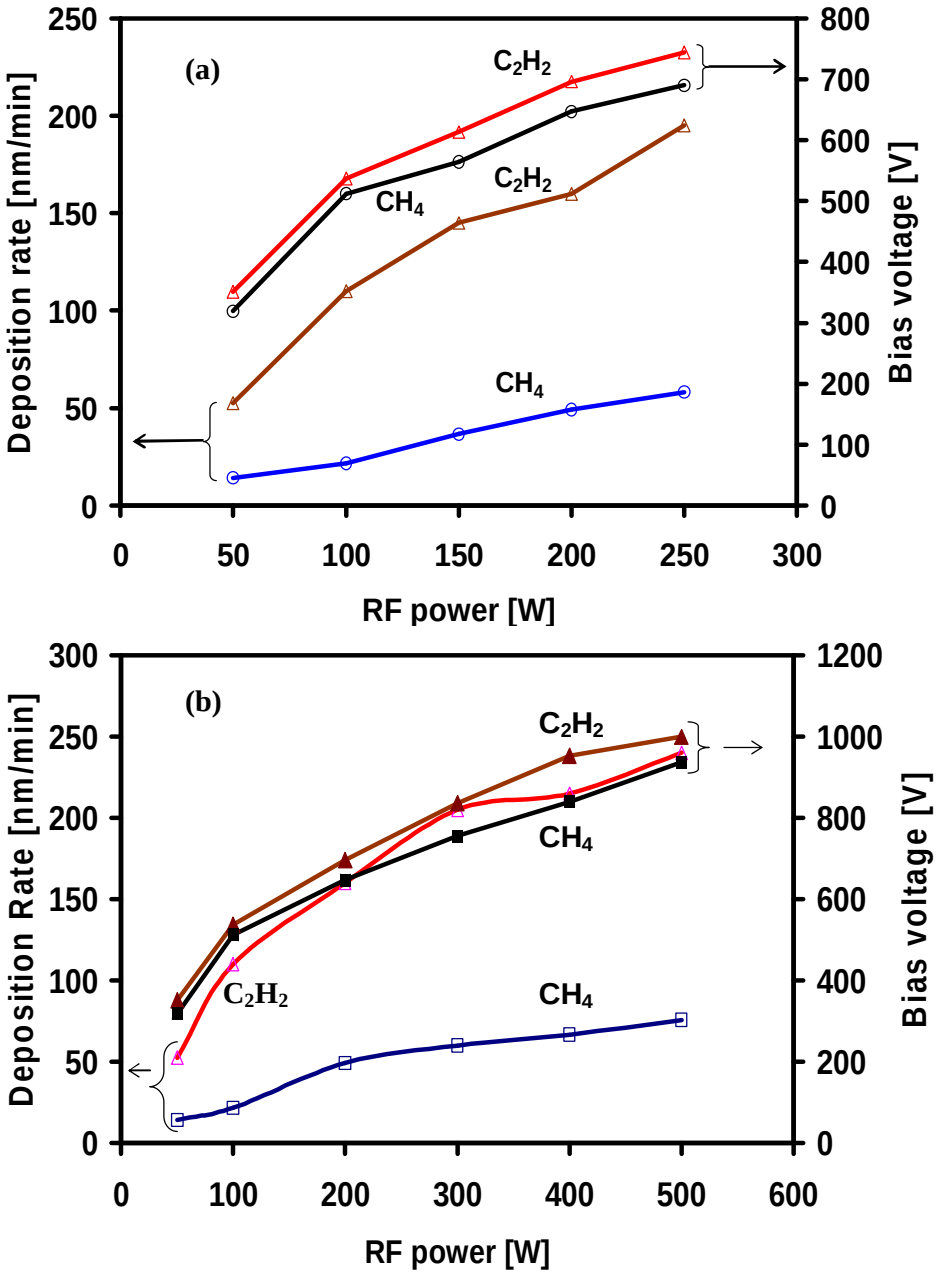

Fig. 2.15 Deposition rate and bias voltage of DLC films as function of RF input power for CH_4 and C_2H_2 and constant flow rate (70 sccm) (a) for RF power 50-250 W and (b) for RF power 50-500 W.

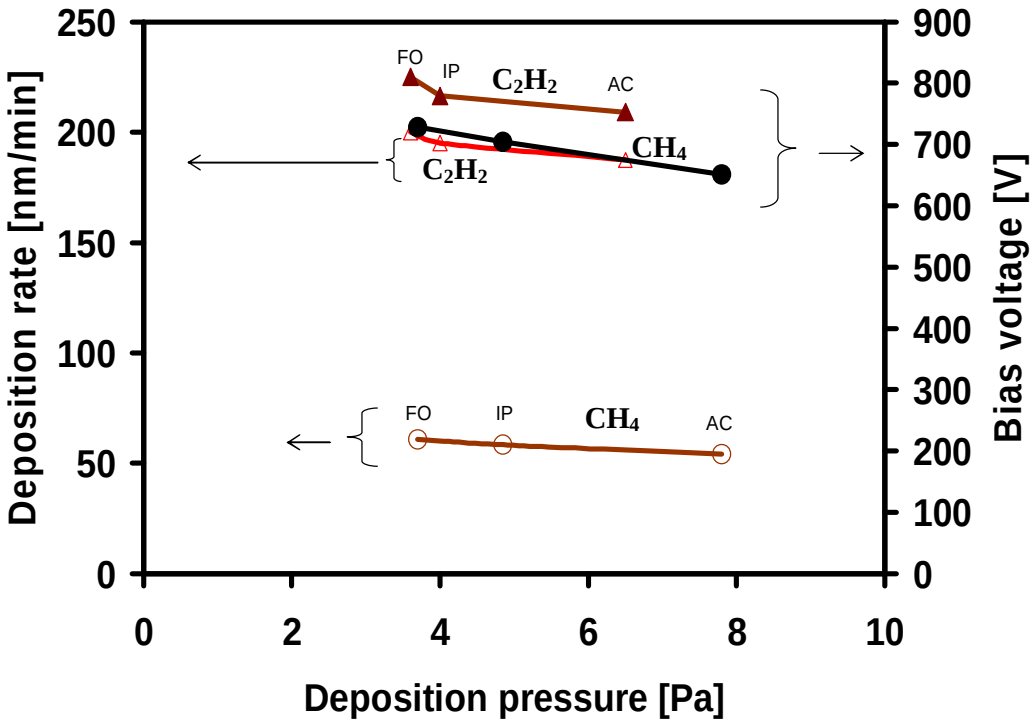

Fig. 2.16 Deposition rate and bias voltage of DLC films as function of deposition pressure for CH_4 and C_2H_2 at 200 W RF power and constant flow rate of (70 sccm).

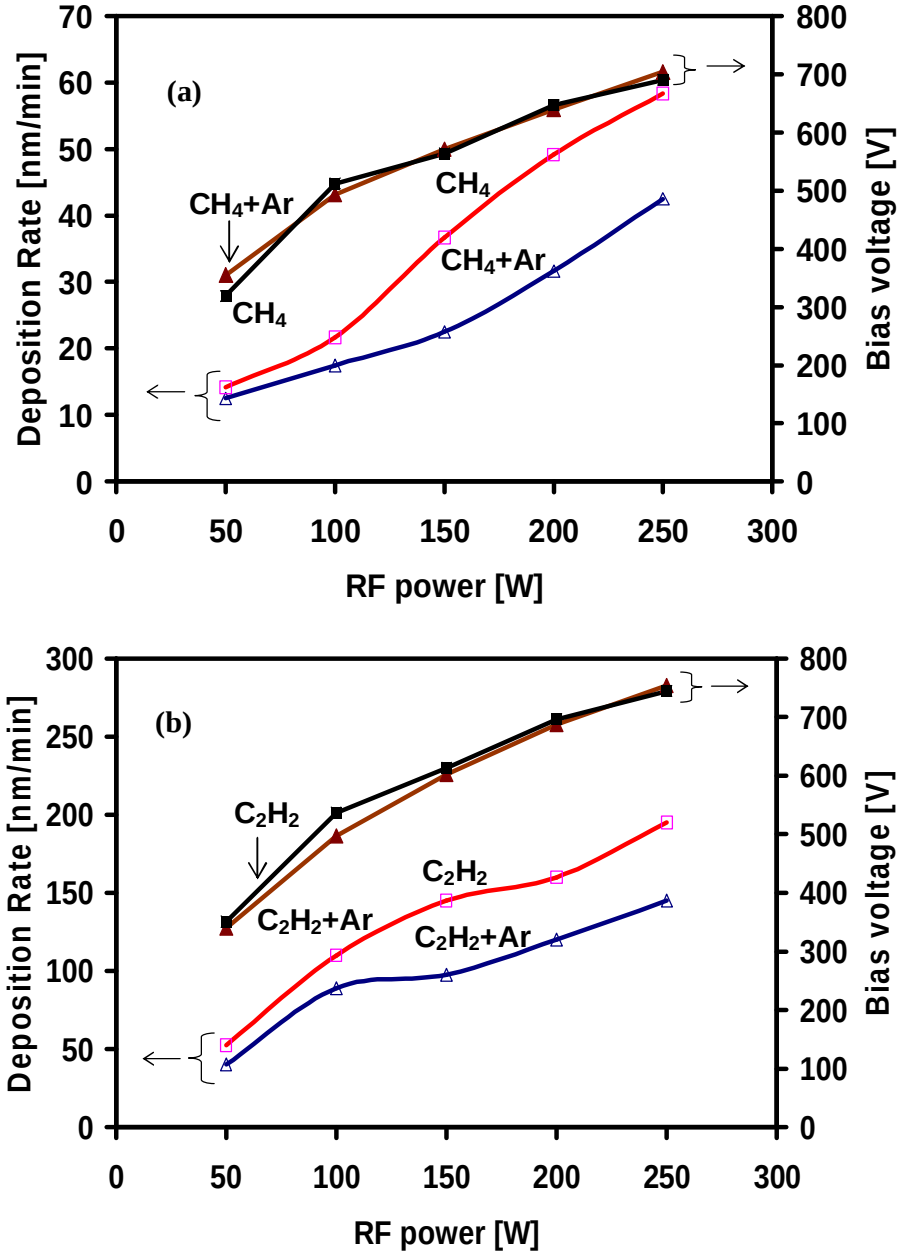

Fig. 2.17 Deposition rate and bias voltage of DLC films as function of RF input power at constant flow rate of CH_4 and C_2H_2 70 sccm and Ar 20 sccm (a) CH_4 and CH_4-Ar and (b) C_2H_2 and C_2H_2-Ar.

References

[1] S. Aisenberg and R. Chabot, J. Appl. Phys., **42** (1971) 2953.

[2] E. G. Spencer, P. H. Schmidt, D. C. Joy and F. J. Sansalone, Appl. Phys. Lett., **29** (1976) 118.

[3] L. Holland, S. M. Ojha, Thin Solid Films, **38** (1976) 17.

[4] A. Anders, S. Anders and I.G. Brown, J. Appl. Phys., **74** (1993) 4239.

[5] D. R. Mckenzie, D. Muller, and B. A. Pailthorpe, Phys. Rev. Lett., **67** (1991) 773.

[6] M. C. Polo, J. L. Andujar, A. Hart, J. Robertson, and W. I. Milne, Diam. Relat. Mater., **9** (2000) 663.

[7] Y. Lifshitz, G. D. Lempert, S. Rotter, I. Avigal, C. Uzansaguy and R. Kalish, Diam. Relat. Mater., **2** (1993) 285.

[8] H. Hofsass, H. Binder, T. Klumpp, E. Recknagel, Diam. Relat. Mater., **3** (1994) 137.

[9] J. Robertson, Diam. Relat. Mater., **12** (2003) 79.

[10] R. J. Narayan, Diam. Relat. Mater., **14** (2005) 1319.

[11] S. R. P. Silva, Properties of Amorphous Carbon (INSPEC, London, 2003) Emis Data Reviews Series No. **29**, Chap. 9, p. 283.

[12] A. Grill and V. Patel, Diam. Relat. Mater., **4** (1994) 62.

[13] V. Anita, T. Butuda, T. Maeda, K. Takizawa, N. Saito and O. Takai: Diam. Relat. Mater., **13** (2004) 1993.

[14] S. Paul and F. J. Clough, Diam. Relat. Mater., **7** (1998) 1734.

[15] M. Zhang, Y. Xia, L. Wang and W. Zhang, Diam. Relat. Mater., **12** (2003) 1544.

[16] M. K. Hassan, B. K. Pramanik and A. Hatta, New Diam. Front. Car. Technol. **16** (2006) 211.

[17] M. K. Hassan, B. K. Pramanik and A. Hatta, Japn. J. Appl. Phys., **45** (2006) 8398.

[18] B. K. Kim and T. A. Grotjohn, Diam. Relat. Mater., **9** (2000) 37.

[19] T. Schwarz-Selinger, A. von Keudell and W. Jacob, J. Appl. Phys., **86** (1999) 3988.

[20] S. F. Yoon, A. Rusli, J. Ahn, Q. Zhang, Y. S. Wu and H. Yang, Diam. Relat. Mater., **7** (1998) 1213.

[21] M. Zarrabian, N. Fourches-Coulon, G. Turban, M. Lancin and C. Marhic., Diam.

Relat. Mater., **6** (1997) 542.

[22] A. Zeinert, B. Racine, K. Zellama, M. Zarrabian, G. Turban and A. Sadki, Diam. Relat. Mater., **7**(1998) 486.

[23] D. Tither, W. Ahmed and E. Ahmed, J. Mater. Sci., **32** (1997) 1931.

[24] A. E.-Raid and F. D. Barlow III, Thin Film Technology Handbook, McGraw--Hill, IEPS, International Society for Hybrid, USA, 1998, Chap.1, p. 2.

[25] J. J. Pouch and S. A. Alterovitz, Properties and Characterization of Amorphous Carbon Films, Material Science Forum Vols. **52** & **53**, Trans Tech Publications, Aedermannsdorf, 1990, p. 42.

[26] S. R. P. Silva, Properties of Amorphous Carbon (INSPEC, London, 2003) Emis Data Reviews Series No. **29**, Chap. 9, p. 282.

[27] A. Bubenzer, B. Dischler, G. Brandt and P. Koidl, J. Appl. Phys., **54** (1983) 4590.

[28] C. B-Hansen, M. D. Bentzon and J. B. Hansen, Diam. Relat. Mater., **3** (1994) 564.

[29] V. Barbarosa, F. Galluzzi, G. Grillo, S. Mercuri and R. Tomaciello, Diam. Relat. Mater., **1**(1992) 328.

[30] G. Cicala, P. Bruno and A. M. Losacco, Diam. Relat. Mater., **13** (2004) 1361.

[31] J. C. Cubertafon, M. Chenevier, A. Campargue, G. Verven and T. Priem, Diam. Relat. Mater., **4** (1995) 350.

[32] Y. Liao, C. H. Li, Z. Y. Ye, C. Chang, G. Z. Wang and R. C. Fang, Diam. Relat. Mater., **9** (2000) 1716.

[33] J. G. Gottling and W. S. Nicol, J. Opt. Soc. Am, **56** (1966) 1227.

[34] E. T. K. Chow, J. Vac. Sci. Technol., **2** (1965) 203

[35] M. Ohring, The Materials Science of Thin Films, Academic Press, U.S.A 1992, p. 261.

[36] J. J. Pouch and S. A. Alterovitz, Properties and Characterization of Amorphous Carbon Films, Material Science Forum Vols. **52** & **53**, Trans Tech Publications, Aedermannsdorf, 1990, p. 177.

[37] A. Bubenzer, B. Dischler, G. Brandt, B. Koidl, J. Appl. Phys., **54** (1983) 459.

[38] C. B. Zarowin, J. Vac. Sci. Technol., **A2** (1984) 1537.

[39] M. A. Liberman and A. J. Lichtenberg, Principles of Plasma Discharges and

Materials Processing, Wiley Interscience, U.S.A., 1994, p. 11.

[40 J. J. Pouch and S. A. Alterovitz, Properties and Characterization of Amorphous Carbon Films, Material Science Forum Vols. **52** & **53**, Trans Tech Publications, Aedermannsdorf, 1990, p. 49.

[41] G. Cicala, P. Bruno and A. M. Losacco, Diam. Relat. Mater., **13** (2004) 1364.

[42] V. Barbarossa, F. Galluzzi, G. Grillo, S. Mercuri and R. Tomaciello, Diam. Relat. Mater., **1** (1992) 329.

[43] Y. Liao, C. H. Li, Z. Y. Ye, C. Chang, G. Z. Wang and R. C. Fang., Diam. Relat. Mater., **9** (2000) 1719.

3.1 Introduction

Electrical properties of thin films are very important from the theoretical and applicative point of view. It is necessary to understand the electrical properties of the material in the form of thin film to fabricate electronic devices. I-V measurement systems determine the electrical output performance of devices. The current voltage characteristics are essential in order to ascertain the dominant conduction mechanism that is taking place in these films [1]. C-V measurements are used to measure the surface states [2], defect densities by measuring the junction capacitance [3]. For insulating films current flows through the film thickness, electrodes are situated on opposite film surfaces [4]. Small evaporated or sputtered circular electrodes frequently serve as a set of equivalent contacts; the substrate usually serves the other contact.

In these studies bulk electrical transport of diamond like carbon thin films deposited by RF-PECVD under different experimental conditions using Au/DLC/n-SI/Au, metal-insulator-semiconductor structure (MIS) were investigated. The as deposited DLC films behave as a semi-insulating material. Au contacts of 2 mm dia. was thermally evaporated on the top sides of the wafer by placing shadow mask to form the metal-DLC insulator-Si MIS structure on n-type Si (100) of low resistivity for electrical characterization of diamond like carbon films. The bottom of the MIS structure was coated with Au by quick coater machine for ohmic contact. I-V and C-V-F measurements were performed on the DLC MIS structure in air at room temperature. The I-V measurements were conducted using a conventional DC power source and a set of digital multimeters. The C-V-F measurements were taken in parallel circuit mode with frequencies ranging from 100 Hz to 200 KHz. The current-voltage (I-V) characteristics were also measured in ambient air in the temperature range of 296-358 K to investigate the temperature dependency. For all the measurements, the Au ohmic contact to the n-type Si was grounded and the top metal (Au) were swept from positive (forward) bias voltage to negative (reverse) bias voltage.

The electrical resistivity is the basic property of materials from the point of view of their electronic application. The diamond like carbon films are generally characterized

by high electrical resistivity ranging from10^7 ohm-cm to 10^{16} ohm-cm depending on the deposition condition and the precursor gases. Extensive studies relating to the electrical conductivities have been carried out during the last two decades [5-8]. If the electrical properties such as intrinsic high resistivity, wide band gap and thermal properties of true diamond materials can be tailored by DLC, then there will be many advantages to using DLC in device applications. This combination of high thermal conductivity and high electrical resistivity makes DLC attractive as a dielectric layer for high temperature device. An example of use of ion beam deposition of DLC in electronic device applications, thin film silicon field effect transistor (FET) with insulating DLC were fabricated [9]. The electrical resistivity of insulating DLC can be reduced by doping with various elements. Mayerson and Smith reported the resistivity of the DLC films deposited by PECVD can be reduced by five orders of magnitude, to 10^7 ohm-cm by doping with phosphine or diborane [10]. Nitrogen incorporation in DLC also reduces the electrical resistivity of the films [11, 12]. The electrical resistivity of the DLC films depends on the other deposition conditions. In particular, the resistivity depends on the RF power, substrate temperature, bias voltage, RF method and precursor gases. More recently the room temperature electrical resistivity can be reduced several orders of magnitude by the incorporation of metal in the DLC films and the conduction behavior ranges from that of semiconductor to metal like depending on the metal content [13, 14].

The origin of properties is believed to lie with in the fully constrained, hydrogen terminated sp^2-sp^3 carbon network which exists within these materials [15]. The observed properties of DLC are related to the hydrogen content of the sample concerned [16].

In general the presence of hydrogen in the gas phase promotes the formation and stabilization sp^3C structures [17]; sp^3 rich hydrogenated carbon films have higher electrical resistivities and higher breakdown voltage [18].

The values of electrical resistivities of DLC films have generally measured at low electric fields and only in few papers dependent on the resistivity on the electric field have been given. Vogel et al. compared the electrical conductivity of DLC films deposited using different methods at electric fields of 10^2-10^6 V/cm and found that the

electrical conductivities of the films displayed ohmic behavior over the entire range of the electric field [19].

3.2 Factors Influencing the Electrical Properties

The following factors influence the films electrical properties [20];

I. Size effect - which covers surface scattering and quantum mechanical tunneling of charge carriers.

II. Method of film preparation - The electrical properties of the metal or insulating films depends on the method of deposition and the deposition parameter. Depending on the deposition conditions employed, structural and electronic defect concentrations, dislocation densities, porosity content, density, chemical composition and stoichiometry, electron trap densities, contact ctc., result with electrical property implication [20].

III. Electrode effect - The electrodes used for measuring electrical properties also influences the film electrical properties. In case of insulating films electrodes are required to deposit that contact their surface. The electrical properties of structure containing insulator (I) or oxide (O) films between metals (MIM), semiconductors (SOS), and mixed electrodes (MIS, MOS) strongly depends on the specific electrode materials used.

IV. Degree of film continuity - Conduction mechanisms in discontinuous, island structure films differ from those in continuous structure films.

V. Existence of high electric field conduction phenomena- Small voltage applied across very small dimension produces high field effects in films.

VI. High chemical reactivity - Corrosion, absorption of water vapor, atmospheric oxidation, and sulfidation and low-temperature solid-state reaction changes in electrical properties.

3.3 Fabrication of Gold Contacts

Top and Bottom gold contacts were fabricated using evaporation and sputtering process, respectively, two of the most important method of physical vapor deposition (PVD) to fabricate the metal-insulator-semiconductor structure (MIS).

3.3.1 Fabrication of the Top Gold Contact

To form the metal/insulator/semiconductor (MIS) structures, circular gold contacts were evaporated onto the surface of the DLC films through a shadow mask in a vacuum evaporator. The vacuum evaporator system used in the experiment was JEOL, JEE-4X (JEOL TECHNICS CO.). The schematic of the vacuum evaporation system is shown in Fig. 3.1. Before making the gold contact, the bel-jar and the chamber was cleaned with ethanol several times then the DLC samples were placed at the centre so that the samples remains under the shutter of the evaporator. Then the suitable metal mask consisting of 2 mm dia holes are placed on the samples. A small piece gold wire approximately 5 mm length and 1.5 mm dia is placed in the W basket, acting as a source material. The evaporation condition for deposition for the top gold contacts is shown in Table 3.1. After fabricating the top gold contacts onto the DLC films by the vacuum evaporator Au/DLC/n-Si structures are formed as shown in Fig. 3.2.

3.3.2 Fabrication of the Bottom Gold Contact

After the formation of the DLC MIS structures, the bottom ohmic contacts were prepared on the back of the n-type silicon by sputtering. The DC sputtering deposition system which was used in the experiment was SANYU-DENSHI, SC 701 HMC, Quick Coater. The schematic of the device with magnet target is shown in Fig. 3.3.

Before deposition, the back of the n-type S is covered with Al foil mask consisting of 15 x 15 mm hole and placed on the sample stage of sputtering system. The sputtering parameter with magnet target holder in this is shown in Table 3.2. The sputtering system consists of a vacuum chamber, which after evacuated, is re-filled with a low-pressure argon gas. A high voltage ionizes the gas, and creates glow discharge near the cathode, consists of an Au target which to deposited. Almost all of

the potential of the high-voltage supply appears across the cathode dark space. The glow discharge consists of argon ions and electrons which have been stripped off them. The electric field accelerates the argon atoms which strike into the Au target. There is an exchange of momentum, and an Au atom is liberated from the target, condenses on to the substrate and forms a Au film.

The Au-DLC-Si-Au structure formed after top Au electrode by vacuum evaporator and bottom Au contact by sputtering device respectively is shown in Fig. 3.4.

3.4 I-V characteristics and Electrical Resistivities

3.4.1 Experimental Circuit Diagram for I-V Measurements

The electrical measurements of the Au-DLC-Si-Au structure were carried in air at room temperature. The current-voltage (I-V), measurements were carried out using a regulated power supply connected in series with the device under investigation and a standard resistor of 1 M-ohm. The circuit diagram for the I-V measurements is shown in Fig. 3.5. The current through the device was calculated by accurately monitoring the potential drop across the standard resistor, while the voltage across the device was obtained as a difference between the supply voltage and the drop across the standard resistor. The data was taken at 1 sec interval using a couple of digital multimeters with storing the data in PC through "PC link system" of SANWA. As can be seen from the figure that, if V_1 is the supply voltage and V_2 is the voltage drop across the resistor, then the voltage drop across the DLC film is given by $V=V_1-V_2$ and the current flow through the circuit is given by $I=V_2/R$. Thus a set of I-V data were collected for plotting the I-V characteristics.

To investigate the variation of electric conductivity with temperature, I-V measurements were performed on few DLC MIS structure which was placed on a heating stage in the temperature range 296-358 K. The I-V data was taken in each run when the stable temperature was achieved.

3.4.2 Current-Voltage (I-V) Characteristics of the DLC Films

From the I-V data, many sets of I-V characteristics of the Au-DLC-Si-Au structure were plotted with different deposition condition and precursors used.

First the I-V characteristics of two sets of DLC films deposited from CH_4 to optimize the deposition condition were plotted. In the first set, the RF power was varied from 50-250 W keeping the flow rate constant at 100 sccm as shown in Fig. 3.6. In case of second set, the flow rate was varied from 10-100 sccm keeping the RF power constant at 100 W as shown in Fig. 3.7.

Secondly, we compared two sets of I-V characteristics for films deposited from CH_4 and C_2H_2 by varying the RF power. First, the RF power was varied from 50 to 250 W, and the flow rate of CH_4 or C_2H_2 was maintained constant at 70 sccm as shown in Fig. 3.8 (a) and (b). In case of the other set, the RF power was varied from 50 to 500 W, and the flow rate of CH_4 or C_2H_2 was maintained constant at 70 sccm as illustrated in Fig.3.9 (a) and (b).

Thirdly, the I-V characteristics of two sets of DLC samples deposited from CH_4 and C_2H_2 by varying pressure were plotted as shown in Fig. 3.10 (a) and (b). In both cases the RF power was 250 W and the flow rate was 70 sccm.

Fig. 11 (a) and (b) shows the I-V characteristics of the of the DLC films from CH_4-Ar and from C_2H_2-Ar mixtures at different RF powers.

The current-voltage (I-V) characteristics over the temperature range of 296-358 K of different DLC samples are plotted as shown in Fig. 3.12 (a) to (d).

3.4.3 Effect of Metal Contact on the I-V Characteristics

The top Au an Al contacts were fabricated on some DLC samples by the vacuum evaporator using the same conditions. Then the I-V measurements of these samples were carried out as before to ascertain the dominant conduction mechanism as shown in Fig. 3.13. This figure shows the I-V characteristics for five a-C:H MIS samples with Au and Al top electrodes. The current was found to vary symmetrically for positive and negative applied voltages, for Au or Al upper contacts. It was expected with the change of electrode from Au to Al, the I-V characteristics should not change. In case of C_2H_2 sample at 100 W RF power, the I-V curve shows no change, i. e.

independent of contact. Little change in current with a change of electrode from Au to Al is observed in case of other four samples deposited from CH_4 and C_2H_2.

3.4.4 Evaluation of Electrical Resistivities of DLC Films

This study, presents and compares the electrical resistivities of diamond-like hydrogenated amorphous carbon (a-C:H) films deposited from CH_4, C_2H_2, CH_4-Ar and C_2H_2-Ar as a function of the electric field strength prepared under a variety of conditions. Electrical resistivities obtained from the current density, voltage and the film thickness plotted against the applied electric field (ratio of the voltage to the film thickness) are shown in Figs. 3.14 to 3.19. Fig. 3.14 (a) and (b) show the variation in electrical resistivity of DLC with applied electric field in log-log plot for CH_4 at various RF powers and at various flow rates respectively. Fig. 3.15 and 3.16 shows the comparison of the electrical resistivities deposited from CH_4 and C_2H_2 at various RF powers. In case of Fig. 3.15, the RF power is varied from 50 to 250 W, while in case of Fig. 3.16, the RF power was varied from 50 to 500 W, keeping the flow constant at 70 sccm in both cases. Variation in electrical resistivity of DLC films at different deposition pressures is shown in Fig. 3.17. Fig. 3.18 investigates and compares the electrical resistivities between the pure CH_4 and CH_4-Ar discharge. Fig. 3.19 investigates and compares the electrical resistivities between the pure C_2H_2 and C_2H_2-Ar discharge. The electrical resistivities of few samples from CH_4 and C_2H_2 at various temperatures ranging from 296-358 K are shown in Fig. 3.20.

3.5 C-V-F Measurements

3.5.1 Experimental Circuit Diagram for C-V-F Measurements

The C-V-F measurements were carried out by a ZM2355 LCR meter. The connection of the test piece is shown in Fig. 3.21. The LCR meter was connected to a four-terminal pair measurement technique, which gives most high precision in measurements. The current supplied from the H CUR terminal flow through the test piece and reaches the L CUR terminal, and thus the current value is measured. The voltage across the H POT and L POT terminal is measured as the voltage applied to

the test piece. With the four terminal pair measurement technique, the measurement current that has followed from H CUR to L CUR through the core conductor of the current cable returns to the signal source, H CUR via the same cable. The test piece and the voltage and current terminals are connected separately with each independent cable with a shielded box as shown in Fig. 3.21 [21].

3.5.2 C-V-F Measurements of the DLC Films

C-V measurements of metal-insulator-semiconductor (MIS) structures are the popular diagnostic tools for material and process characterization. As the charge density in the depletion is not constant but increases towards the junction interface, so the capacitance techniques, which are routinely used to characterize the crystalline semiconductors, can not be directly applied to amorphous semiconductor [22]. Special care was taken to ensure that frequency and temperature provide a full response in capacitance measurement. In this study C-V-F (capacitance-voltage-frequency) measurements were carried out for characterization of Au/DLC/n-Si/Au MIS structure. Capacitance measurements were performed in air using ZM2355 multi-frequency LCR meter and a shielded box for four terminal connections at room temperature. Two sets of DLC samples were taken into consideration for the C-F and C-V measurements. In one set the RF was varied from 50 to 200 W, keeping the flow rate of CH_4 constant at 100 sccm, while in the other set, the flow rate of CH_4 was varied from 10 to 100 sccm keeping the RF power constant at 100 W as shown in the C-F plots in Fig. 3.22 (a) and (b) respectively.

The C-V characteristics on similar sets of DLC samples are shown in Fig. 3.23 (a) and (b) respectively.

3.6. Results and Discussions

These I-V characteristics for all the DLC samples show a symmetrical behavior irrespective of the polarity of the applied voltages. It is also observed that these I-V characteristics are nonlinear for both the current directions. During the measurement it was found that the I-V characteristics were reproducible when the electrode contact point was changed.

From Fig. 3.6, it can be seen that the I-V characteristics of the films grown from 100 to 250 W do not show large variation in current with RF power. But the 50 W samples show highest current. In Fig. 3.7, I-V characteristics of the DLC films grown from 10 to 75 sccm do not show large variation in current with one another. But the sample grown at100 sccm shows large variation of current with respect to other samples.

Fig. 3.8 (a) and (b) shows a comparison of the I-V characteristics of the samples grown from CH_4 and C_2H_2 at different RF powers ranging from 50 to 250 W. The I-V curves obtained from CH_4 do not show large variations in current with RF power. On the other hand, the I-V curves obtained from C_2H_2 show large variations in current with RF power.

Fig. 3.9 (a) and (b) shows a comparison of the I-V characteristics of the samples grown from CH_4 and C_2H_2 at different RF powers ranging from 50 to 500 W. The I-V curves obtained from CH_4 do not show a strong variation of current with RF power. On the other hand I-V curves obtained from C_2H_2 show large variations of current with RF power.

In the case of CH_4, because of the increase in conductivity, the current was almost same when the film thickness increased with RF power. In the case of C_2H_2, the conductivity increased markedly with increasing RF power resulting in an increase in current even though the film thickness increased.

Fig. 3.10 (a) and (b) shows a comparison of the I-V characteristics of the samples grown from CH_4 and C_2H_2 at different deposition pressures. The I-V curves obtained from CH_4 do not show a strong variation of current with pressure. On the other hand I-V curves obtained from C_2H_2 at higher pressure show large variations of current compared to the films deposited at lower pressures.

Fig. 3.11 (a) and (b) shows a comparison of the I-V characteristics of the samples grown from CH_4-Ar and C_2H_2-Ar mixture at different RF powers ranging from 50 to 250 W. Fig. 3.11 (a) shows that I-V curves obtained from CH_4-Ar at 50 and 100 W show very small variation of current with each other. In the same manner, 150, 200 and 250 W samples show very small variation of current with each other. But 50 and 100 W show large variations of current compared to 150, 200 and 250 W samples. In the case of CH_4-Ar, the conductivity decreased markedly in case of high RF powers

(150, 200 and 250 W) with respect to low RF power (50 and 100 W) resulting in a decrease in current even though the film thickness increased with RF powers. As can be seen from Fig. 3.11 (b) that C_2H_2-Ar at 150, 200 and 250 W samples show larger variation of current with each other than the 50 and 100 W samples do. In the case of C_2H_2, the current following increases markedly with increasing RF power even though the film thickness increased.

I-V measurements of the DLC MIS structure at different temperatures ranging from 296-358 K are shown in Figs. 3.12 (a) to (d). These figures show that the forward and reverse current increased with increasing temperature. The temperature dependence of I-V characteristics indicates lower electrical conductivity at room temperature.

It is observed that the I-V curves exhibit a highly non-linear feature. The non-linearity of the I-V characteristics indicates that the prevalent conduction mechanism is non-ohmic in nature. It was observed that the I-V characteristics were reproducible when the counter electrode was biased with either polarity. The current-voltage characteristics of the structures are symmetric with respect of the applied voltages. This indicates that the Si-DLC interface at the bottom and the top Au electrodes were identical in nature. I-V characteristics also indicate lower electrical conductivity of the DLC films.

As can be seen from Fig. 3.13, little change in current with a change of electrode from Au to Al is observed in case of four samples deposited from CH_4 and C_2H_2. All these samples show the same trend. These samples suffer slightly decrease in current in case of Al contacts. The possible reason may be due to the fact that Al is easily oxidize when comes in contact with the O_2 of the air. Let us consider the reaction of aluminum metal to form alumina (Al_2O_3). The balanced reaction is as follows:

$$4Al_{(s)} + 3O_2\left(_g\right) \rightarrow 2Al_2O_3(s) \qquad (3.1)$$

In case of 50, 200 and 400 W samples possibly due to the above redox (oxidation-reduction) reaction the decrease in current observed with the change of electrode from Au to Al. In case of 100 W film from C_2H_2 shows the same current for both contacts. This may be possibly due to no formation of oxide in this sample with this deposition condition.

In Figs. 3.14 to 3.19 it is observed that the resistivities of the DLC films deposited from CH_4, C_2H_2, CH_4-Ar and C_2H_2-Ar strongly depend on electric field strength. This means DLC films do not show ohmic behavior. The plot also shows that the resistivities of the films decrease with an increase in RF power and increase with the increase of flow rate and pressure. At electric fields below the order of 10^5 V/cm, electrical resistivities are almost similar, but at electric fields above this value, the resistivities decrease gradually. The Figs. also show that the resistivities are dependent on the deposition parameter. Comparison of the curves deposited from CH_4, C_2H_2 as shown in Figs. 3.15 and 3.16 also show that the resistivities of the DLC films deposited under similar conditions are strongly dependent on the used precursors. Figs. 3.18 and 3.19 show that Ar addition effects the resistivities of DLC films.

As can be seen from Fig. 3.14 (a), the resistivities of the films grown using CH_4 at RF powers of 150, 200 and 250 W do not show strong variations from one another. In the case of 50 and 100W samples, a large variation in resistivity is observed among films. The largest resistivity is obtained in the films deposited at a RF power of 50 W. In the case of Fig. 3.14 (b), the films grown at 75, 50, 25 and 10 sccm do not show large variation of resistivity from one another. The largest resistivity is obtained in the film deposited at flow rate of 100 sccm.

From Fig. 3.15, it is observed that the resistivities of the films grown using CH_4 at RF powers of 150, 200 and 250 W do not show strong variations from one another. In the case of C_2H_2, a large variation in resistivity is observed among films grown at different RF powers. The largest resistivity is obtained in the films deposited at a RF power of 50 W in both cases.

Fig. 3.16 shows that, the resistivities of the films grown from CH_4 using RF powers of 300, 400 and 500 W do not show strong variations from each other. In the case of C_2H_2, a large variation of resistivity is observed among films grown using RF powers of 50, 100, 200 and 300 W but a similar resistivity is observed for 400 and 500 W samples. The largest resistivities are obtained for the films deposited at 50 W RF power in both cases.

Fig. 3.17 shows that, the resistivities of the films grown from CH_4 using different pressures do not show strong variations from each other. In the case of C_2H_2, large

variation of resistivity is observed among films grown using different deposition pressures. Films deposited at higher pressures showed higher resistivities in both cases.

Fig. 3.18 shows that the resistivities of the films deposited from CH_4 decrease with an increase in RF power. At electric fields below the order of 10^5 V/cm, electrical resistivities are almost constant, but at electric fields above this value, the resistivities decrease gradually. The resistivities of the films grown from CH_4 using RF powers of 150, 200 and 250 W do not show strong variations from each other. In the case of CH_4-Ar, a variation of resistivity is observed among films grown using different RF powers. The largest resistivities are obtained for the films deposited at 50 W RF power in both cases. Fig. 3.18 also shows the variation of resistivities with CH_4-Ar. The resistivities of the films grown from CH_4-Ar mixture using RF power of 50 W and 100 W decreases than that of pure CH_4 based films. On the other hand, DLC films grown from CH_4-Ar using RF powers of 150, 200 and 250 W show higher resistivities than that of pure CH_4-based films for the same value of RF power. But the CH_4-Ar sample grown at 250 W behaves differently at low electric field.

Fig. 3.19 (a) and (b) shows the electrical resistivities of the pure C_2H_2 and C_2H_2-Ar discharge plotted against the applied electric field. In this figure it is observed that the resistivities of the films deposited from C_2H_2 and C_2H_2-Ar strongly depend on electric field strength. The plot also shows that the resistivities of the films decrease with an increase in RF power. In both case of C_2H_2 and C_2H_2-Ar, a large variation of resistivity is observed among films grown using RF powers of 50 to 250 W. The largest resistivities are obtained for the films deposited at 50 W RF power in both cases.

Fig. 3.19 also shows the variation of resistivities with Ar gas dilution in the C_2H_2. The resistivities of the films grown from C_2H_2-Ar mixture using RF power of 50 W to 250 W, increases than that of pure C_2H_2-based films.

Fig. 3.20 show that the electrical resistivities decreases with the increase of temperature. At room temperature the density of free charge carriers is extremely low which prevents electrical conduction. As the temperature increases the density of charge carriers also increases and hence the resistivity decreases.

The resistivity of a-C:H films mainly depends on hydrogen content and the percentages of sp^3 and sp^2 bonds [23]. Such resistivity increases if hydrogen content or the percentage of sp^3 bonds increases [24]. Hydrogen plays an important role in the formation and stabilization of C=C bond from sp^2 to sp^3, in missing π-bonding electrons being available for the electrical conductivity. At a high power, i.e., by increasing self-bias voltage, the sp^3 fraction and hydrogen content decrease owing to ion bombardment and the resistivity of the films decreases. On the other hand, at a high flow rate and high deposition pressure, i.e. by decreasing the self-bias voltage, the sp^3 fraction and hydrogen content decrease is not significant owing to the less ion bombardment and the resistivity of the films increases.

In case of CH_4, owing to the sufficient fraction of hydrogen in the source gas, a small variation in resistivity was observed even when RF power was increased. On the other hand, in case of using C_2H_2, the fraction of hydrogen was insufficient to terminate sp^2 bonds in rapidly growing films at high RF powers.

In case of CH_4, the dominant gas species flowing out of the chamber during the discharge is molecular hydrogen. When Ar is added in chamber, the dominant gas species are molecular hydrogen and Ar. In CH_4-Ar case, the dominant ionic species bombarding the surface include both Ar and hydrogen. At low RF powers 50 and 100 W due to addition of Ar the molecular H_2 emission in CH_4-Ar plasma is much more predominant than the pure CH_4 plasma. This causes much hydrogen molecules flowing out of the chamber. Due to the combined effect of Ar ion bombardment and hydrogen evolution, the hydrogen content decreases and hence the resistivity of the films at 50 and 100 W decreases with Ar dilution.

In literature, Ar percentage results in more sp^3 carbon bonds [25, 26]. This may be due to the destruction of the weak graphitic sp^2 bonds as a result of high Ar ion bombardment [25, 26]. In case of higher power 150, 200 and 250 W from CH_4-Ar, owing to the high Ar ion bombardment, the resistivity of the films increases due to the breaking of the sp^2 bonds, results in increasing sp^3 fraction in the films with Ar addition. In case of C_2H_2-Ar, owing to the high Ar ion bombardment, the resistivity of the films increases due to the breaking of the sp^2 bonds, results in increasing sp^3 fraction in the films with Ar addition.

The films grown at low RF powers were actually highly resistive. It is feared that the hydrogen termination of sp^2 will result in polymer-like films. However, for the improvement in semi-conducting properties, it seems necessary to increase the resistivity of the DLC films by decreasing the sp^2 fraction without hydrogen incorporation.

Fig. 3.22 (a) and (b) shows the C vs. F plot for the DLC samples at various RF power from 50-200 W keeping the flow rate constant at 100 sccm and at different flow rates from 10-100 sccm keeping RF power constant at 100 W, respectively. The figures represent the dependency of capacitance C on frequency f. The capacitance decreases with the increase of frequency, and is particularly frequency dependent at lower frequencies. A wide dispersion in the capacitance value is observed at lower frequencies. At higher frequencies the curves tends to approach a common capacitance value. The observed variation in capacitance could be due to the high resistivity of the layer/or the well-known dispersion effect which occurs when a deep level is unable to follow the high frequency voltage modulation and contribute the net space charge in the depletion region [27]. In DLC, the high resistivity can also contribute to the decrease in capacitance at higher frequency. A decrease in capacitance with increasing frequency has been reported by many researchers in several other thin film materials [28-29]. The frequency dispersion in the depletion region is due to the response of interface traps to the applied frequency. The frequency dependence to the interface traps which when filled gives rise to dissipation and the capacitance changes. These phenomena can be explained by the model proposed by Goswami and Goswami [30]. According to the model, C', the depletion capacitance, which is voltage dependent but frequency and temperature independent, with a discrete temperature-dependent resistive element R due to the DLC films in parallel with C', both elements in series with a constant low value resistance r due to lead length, etc. According to this model the measured series capacitance is given by

$$C = C' + \left(\frac{1}{\omega^2 R^2 C'} \right). \tag{3.2}$$

From the above equation (3.2), it can be clearly explained that the measured capacitance should decrease with increasing frequency, and at very high frequencies

reaching a constant value of capacitance C'. In addition, the difference in the frequency dependence of capacitance between different samples may be due to the difference in the sample resistivity.

Fig. 3.23 represents a typical set of C-V curves at room temperature. The total measured capacitance is the series sum of the insulator capacitance and the semiconductor depletion layer capacitance per unit area. With a positive gate bias, an n-type semiconductor is in accumulation and the capacitance measured is simply due to the parallel plate capacitor with the a-C:H as the dielectric. At sufficiently negative bias voltage, all the curves show the voltage independent minimum value (Cm) which is a series combination of the insulator capacitance (C_I) and the semiconductor capacitance (Cs). At sufficiently negative voltage, curves show the voltage independent maximum value which is approximately equal to the insulator capacitance. The turn on condition of the capacitance response of the in depletion regime is satisfied. Then the C-V curves show an abrupt change from strong depletion capacitance into the accumulation capacitance. The C-V curves of 200 W and 250 W shows almost same capacitance with the voltage. The other curves exhibit several interesting features in depletion regime of bias voltage. In the deep depletion, the curves show a bias independent flat level (Cm) which is a series combination of DLC capacitance (C_I) and the semiconductor geometric capacitance (C_S). Then the capacitance starts to increase with bias voltage at constant slope. The constant slopes of C-V curves are related to the uniform defect density of DLC bulk region. Then in case of 50 W, 75 sccm and 50 sccm, curves show a decreased slope, indicating the increased number of defects states involved in the measurements. In the accumulation region the curves exhibit almost the same changes according to the bias voltage. The curves finally start to saturate to their maximum level C_I and further increase in bias voltage causes the capacitance to decrease. The constant slopes of C-V curves in are related to the uniform defect density of a-C:H bulk region [31, 32].

The capacitance of the 200 and 250 W samples with applied bias indicating a poor depletion region formation at the top and bottom metal/a-C:H interfaces.

3.7 Summary

I-V, C-V and C-F measurements were carried out to investigate the electrical properties of the DLC films deposited by RF-PECVD.

The I-V characteristics for all the samples display non-ohmic behavior. These I-V characteristics for all the DLC samples show a symmetrical behavior irrespective of the polarity of the applied voltages. The I-V curves obtained from CH_4 do not show a strong variation of current with RF power and deposition pressure. On the other hand, I-V curves obtained from C_2H_2 show large variations of current with RF power and deposition pressure. The temperature dependence of I-V characteristics indicates lower electrical conductivity at room temperature and variable activation energy at high temperature.

The electrical resistivities of the DLC films were found to dependent on the substrate bias and the precursors. With an increase in RF power, resistivity decreased whereas the resistivity increased with an increase of flow rate and deposition pressure. The CH_4-based films were more insulating than C_2H_2-based films at high RF powers. Highest resistivity of the films was obtained for both the CH_4 and C_2H_2 at low RF power.

In the case of higher power, the sp^3 fraction and hydrogen content will decrease due to ion bombardment and the resistivity of the films will decrease. At higher flow rate or deposition pressure, the sp^3 fraction and hydrogen content increase owing to the less ion bombardment and the resistivity of the films increases.

In case of CH_4, owing to the sufficient fraction of hydrogen in the source gas, a small variation in resistivity was observed even when RF power was increased. In case of C_2H_2, the fraction of hydrogen was insufficient to terminate sp^2 bonds in rapidly growing films at high RF powers.

Ar dilution with CH_4 and C_2H_2 affect the resistivity of the DLC films. Addition of Ar with CH_4 decreased the resistivity of the DLC films at low RF powers whereas the resistivity increased at high RF powers. The resistivity of the C_2H_2-Ar-prepared films was found to increase.

The resistivity increase was possibly due to the transformation of carbon bonds from sp^2 to sp^3 with hydrogenation.

C-V-F measurement confirmed that the measured capacitance varies with the applied bias and frequency. The frequency dependence of capacitance was attributed to the series resistance effect of the material. At high frequencies device with high series resistance has declining capacitance and reaching an almost constant value. The C-V characteristics of the DLC MIS structure were explained in terms of standard depletion approximation.

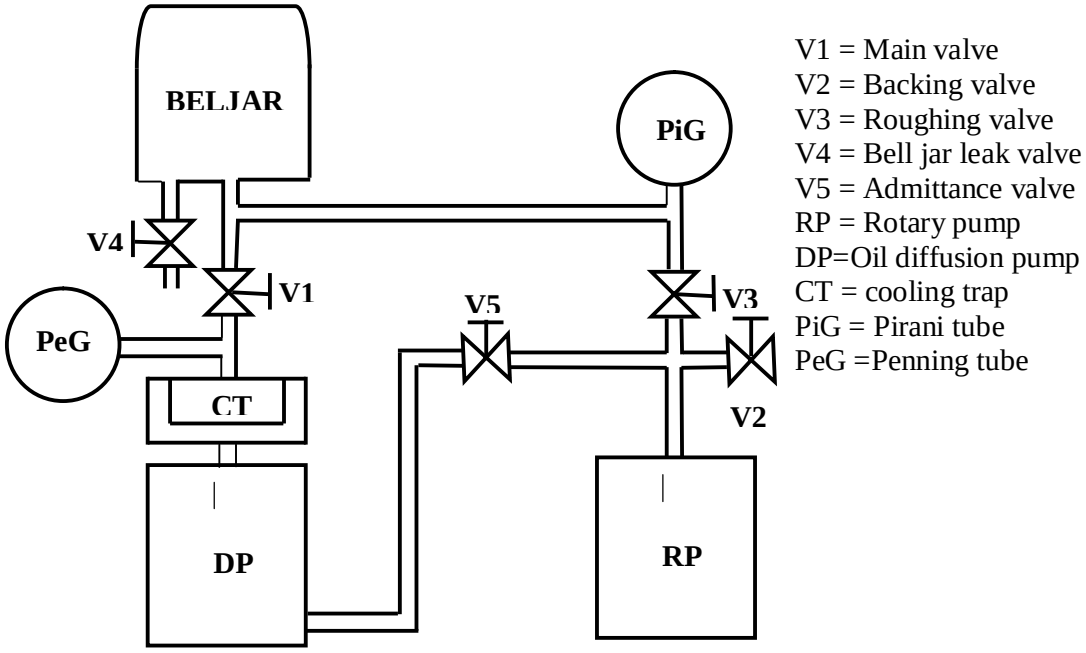

Fig 3.1 The schematic of the JEOL, JEE-4X vacuum evaporation systems.

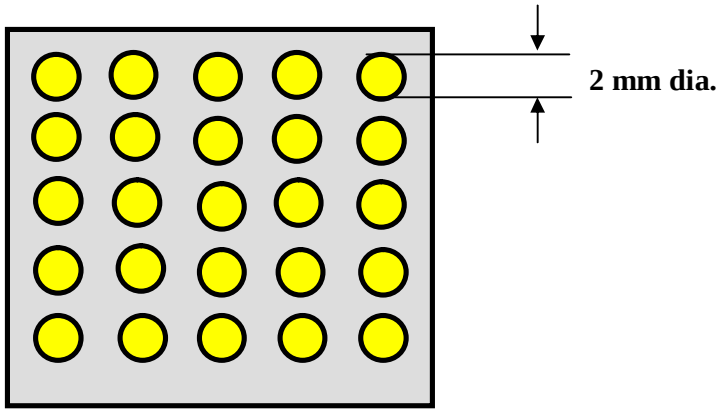

Fig. 3.2 Plane view of the DLC with top Au electrode pattern fabricated by vacuum evaporator.

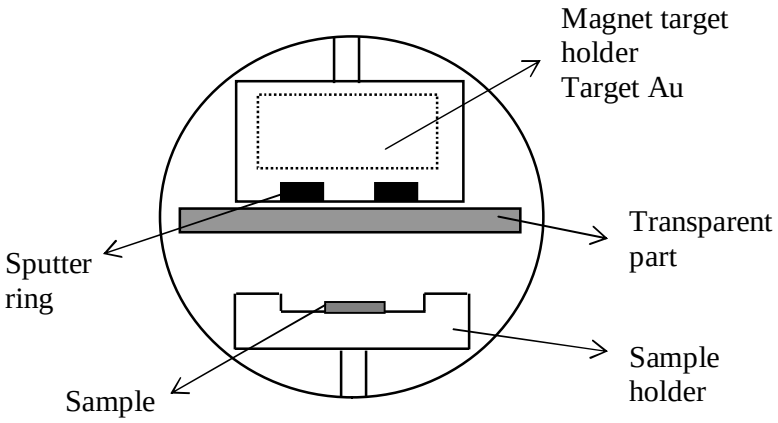

Fig. 3.3 A schematic of the quick coater (SANYU-DENSHI, SC-701 HMC) sputtering device with magnet target.

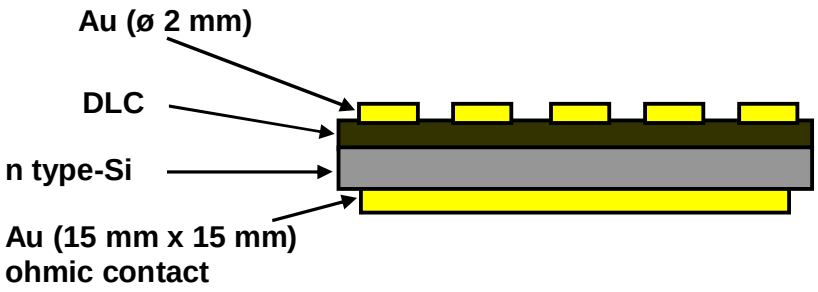

Fig. 3.4 Schematic diagram of the Au-DLC-Si-Au structure after fabricating top and bottom gold contact.

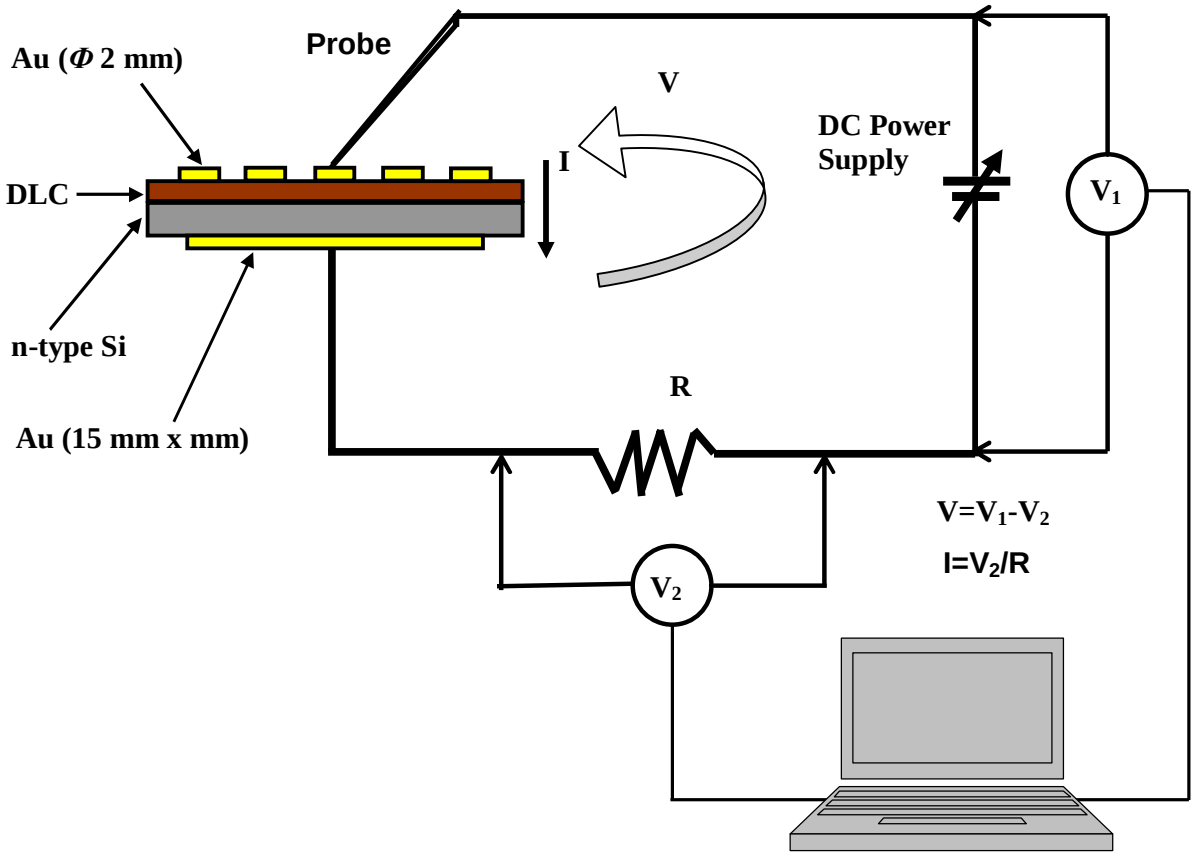

Fig. 3.5 Experimental circuit diagram for the current-voltage (I-V) measurement.

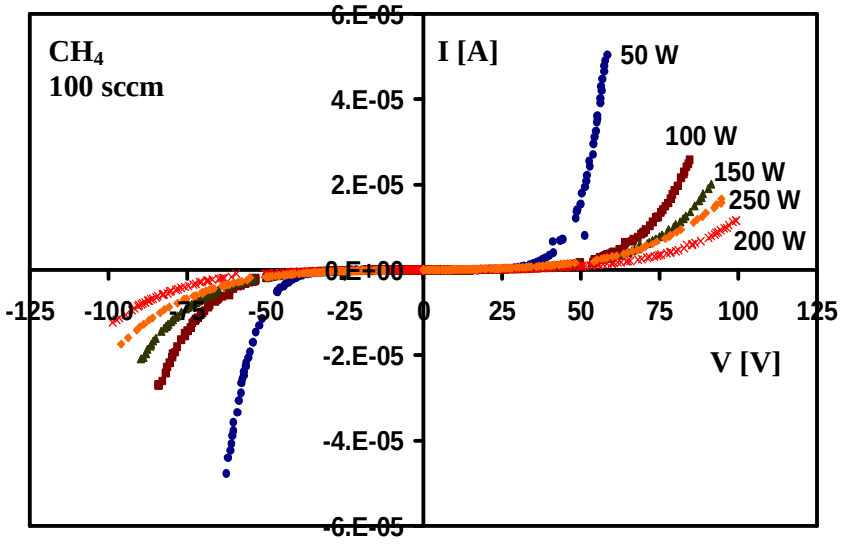

Fig.3.6 I-V characteristics of Au/DLC/n-Si/Au structure of CH_4 for various RF power and flow rate of 100 sccm.

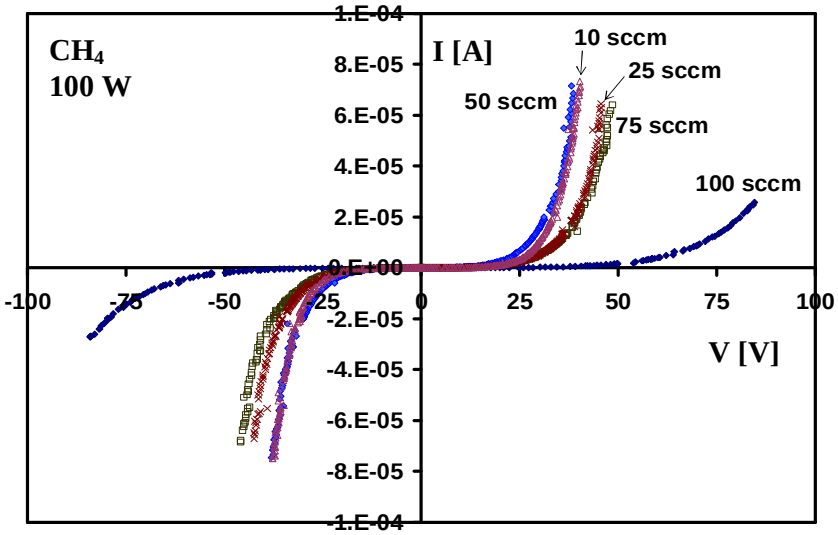

Fig.3.7 I-V characteristics of Au/DLC/n-Si/Au structure of CH_4 films for various flow rate and RF power of 100 W.

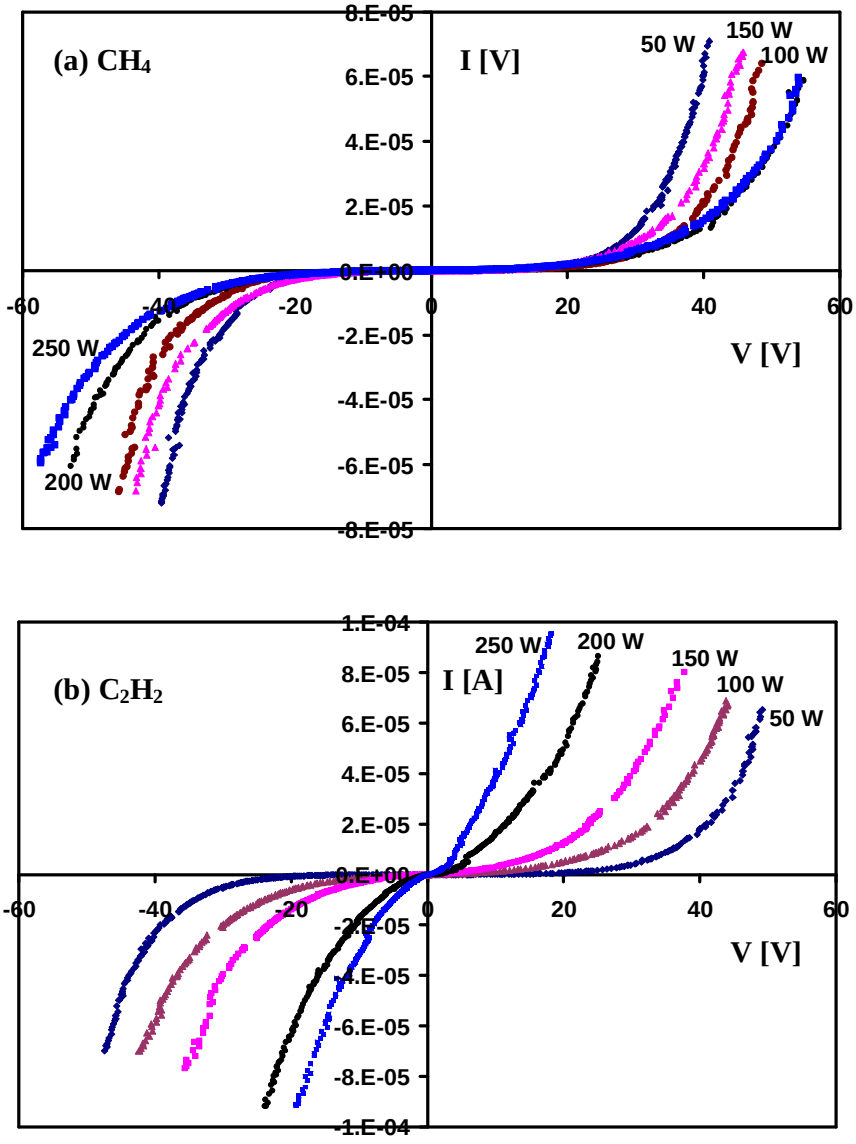

Fig. 3.8 I-V characteristics of Au/DLC/n-Si/Au structure of CH_4 and C_2H_2 films for various RF powers ranging from 50-250 W and flow rate of 70 sccm (a) CH_4 and (b) C_2H_2.

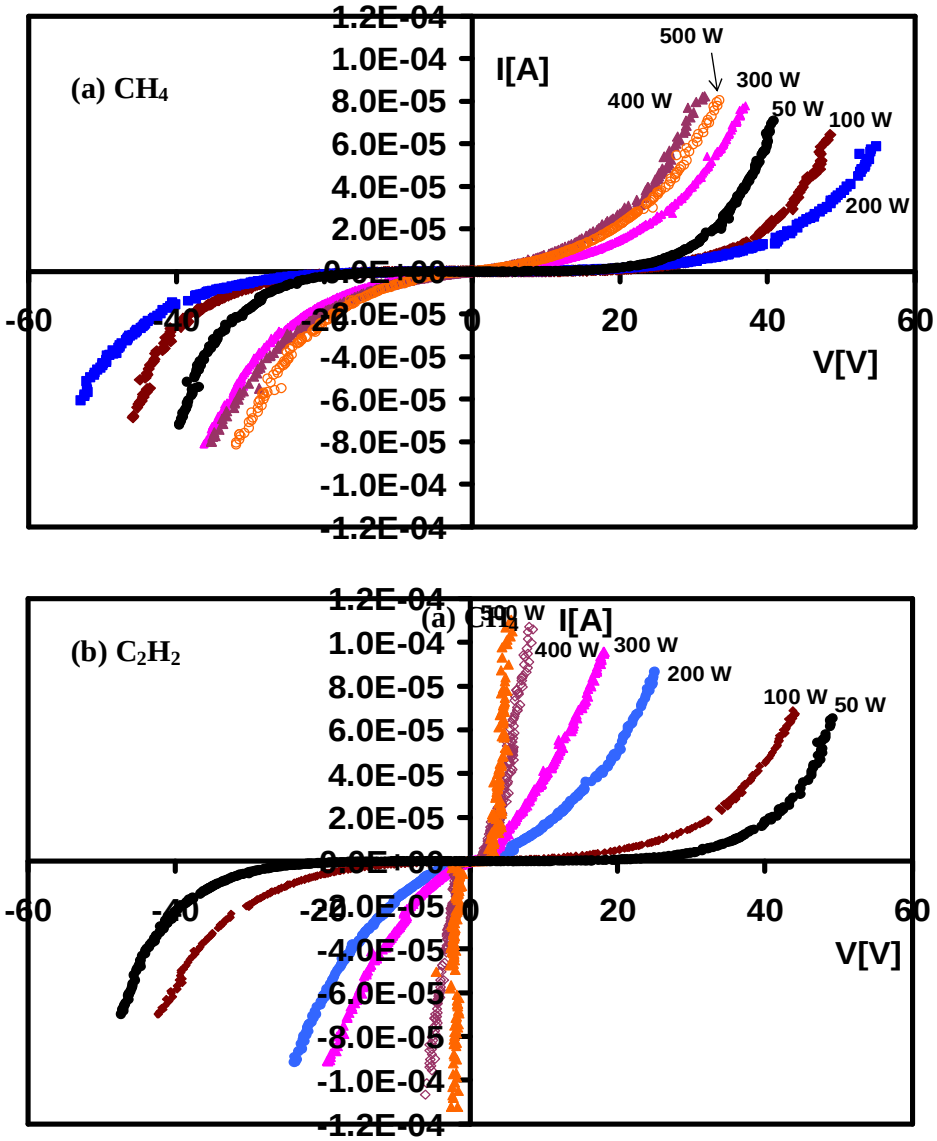

Fig. 3.9 I-V characteristics of Au/DLC/n-Si/Au structure of CH_4 and C_2H_2 films for various powers RF ranging from 50-500 W and flow rate of 70 sccm (a) CH_4 and (b) C_2H_2.

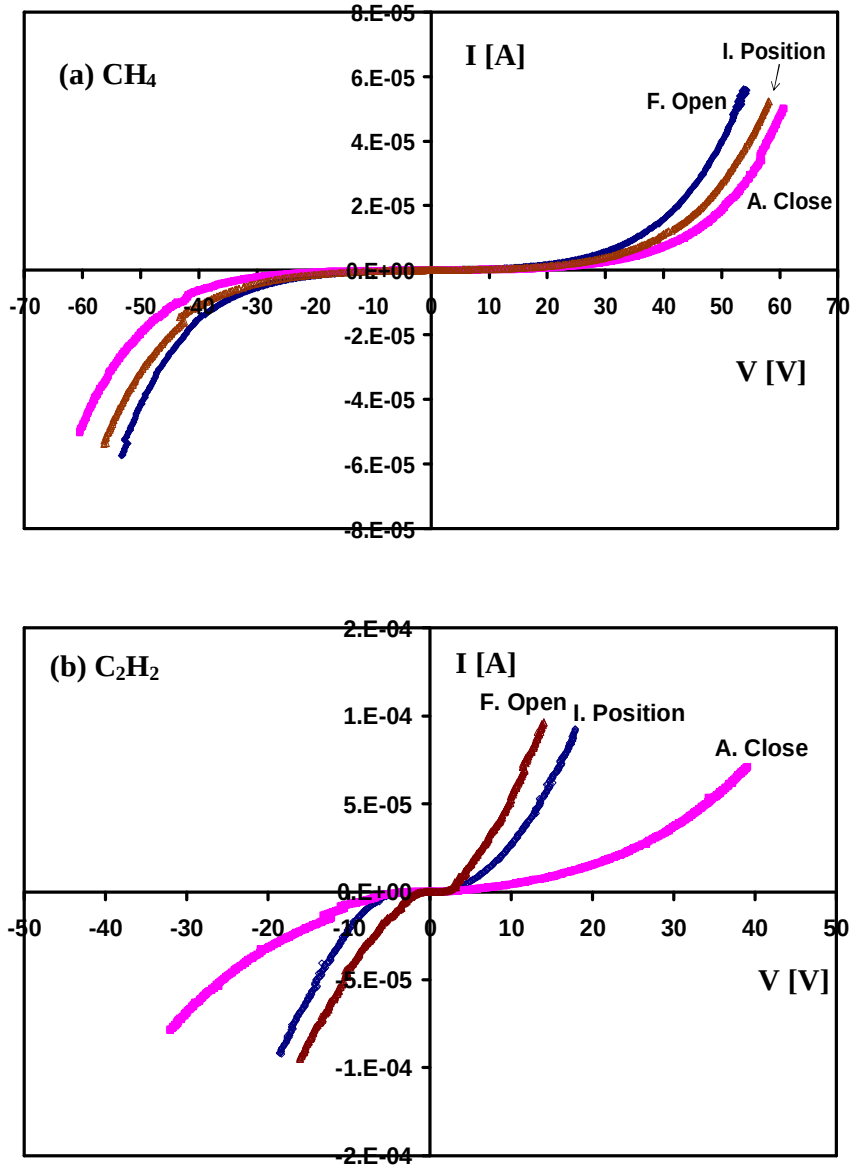

Fig. 3.10 I-V characteristics of Au/DLC/n-Si/Au structure of CH_4 and C_2H_2 films for various deposition pressures (a) CH_4 and (b) C_2H_2.

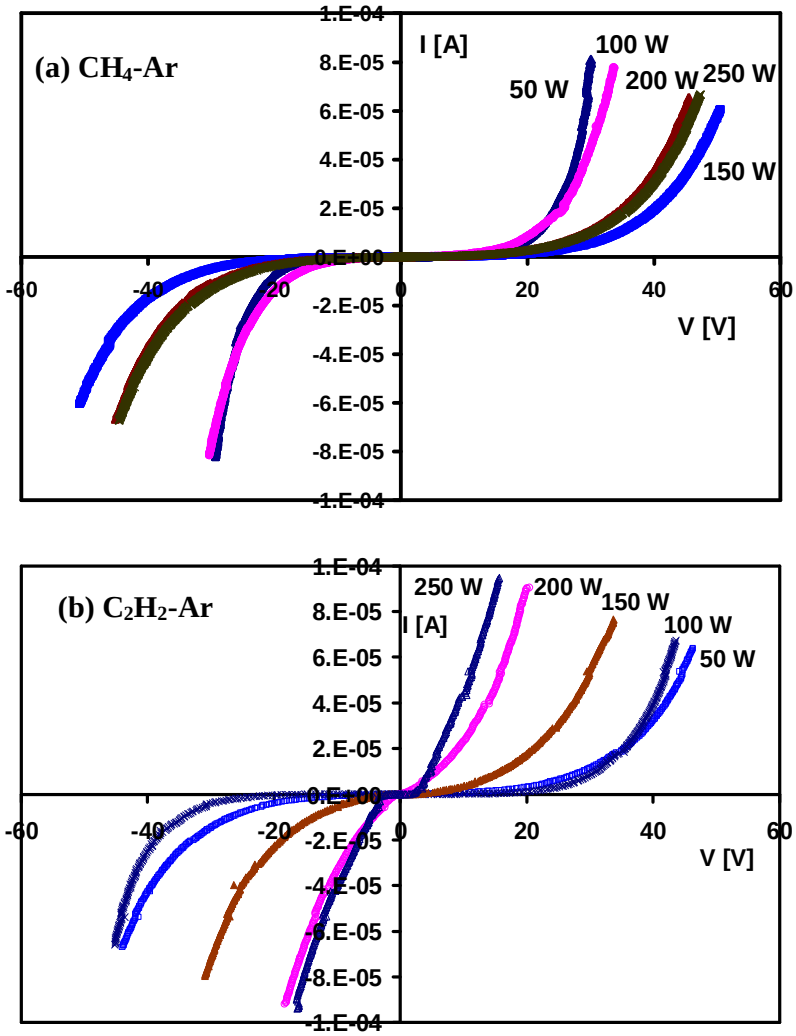

Fig. 3.11 I-V characteristics of Au/DLC/n-Si/Au structure of CH_4-Ar and C_2H_2-Ar mixtures films for various RF powers and flow rate of CH_4/ C_2H_2 70 sccm and Ar 20 sccm (a) CH_4-Ar and (b) C_2H_2-Ar.

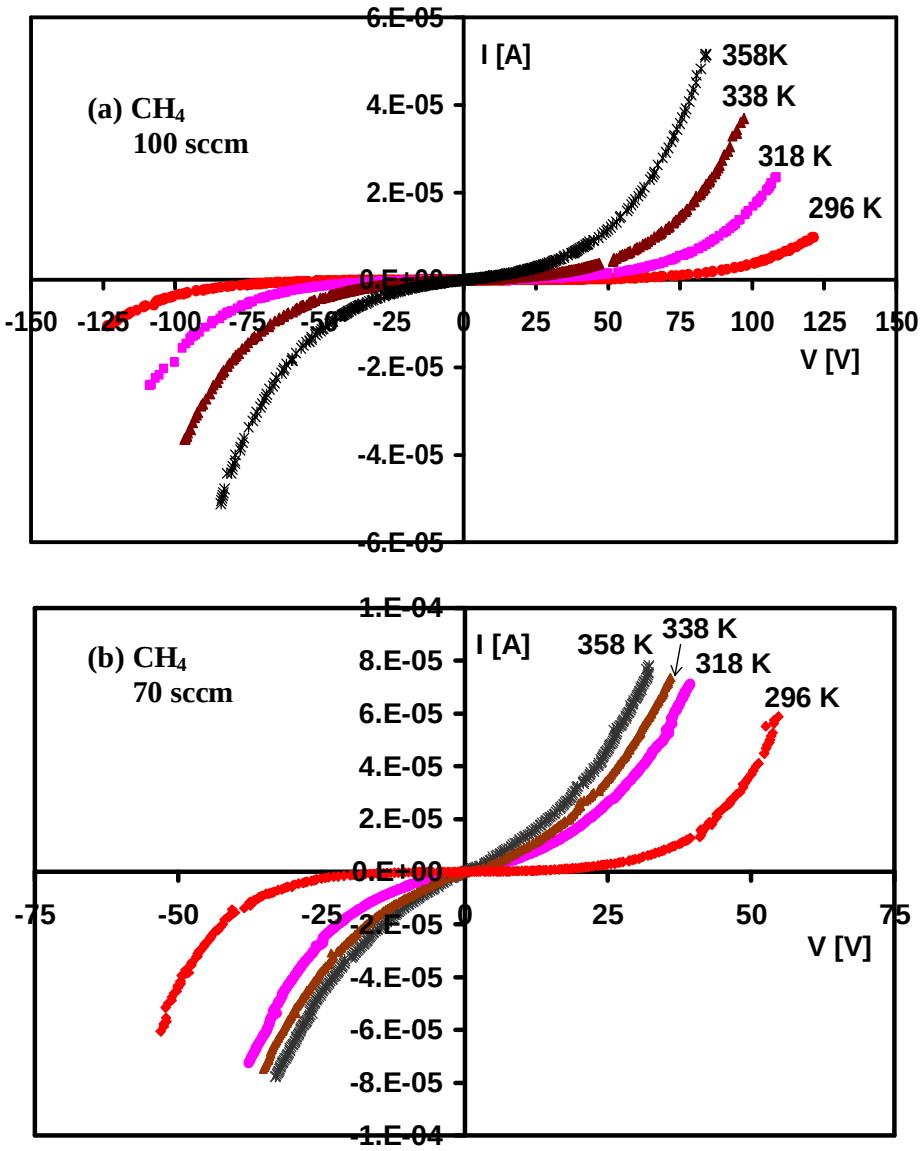

Fig. 3.12 I-V characteristics of Au/DLC/n-Si/Au structure of CH_4 at 200 W films at various temperatures (a) CH_4 (100 sccm) and (b) CH_4 (70 sccm).

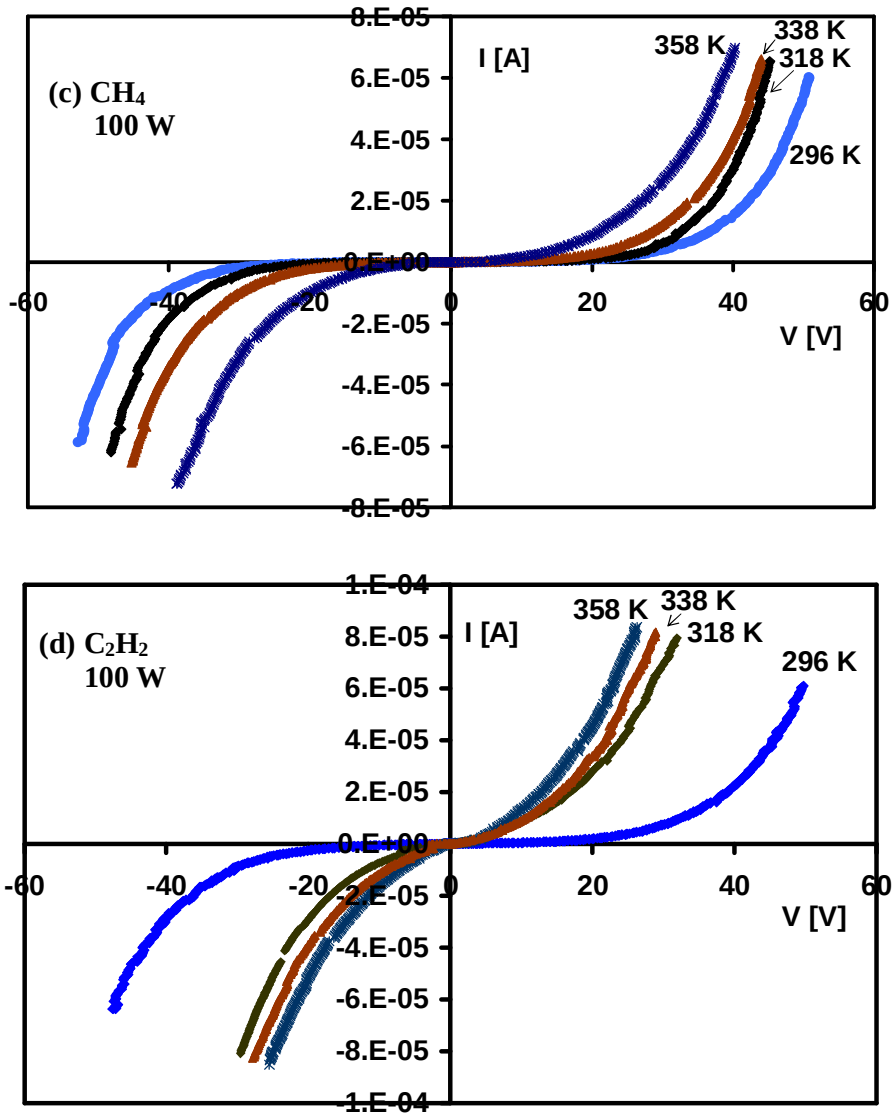

Fig. 3.12 I-V characteristics of Au/DLC/n-Si/Au structure at various temperatures and flow rate of 70 sccm (c) CH_4 (100 W) and (d) C_2H_2 (100 W).

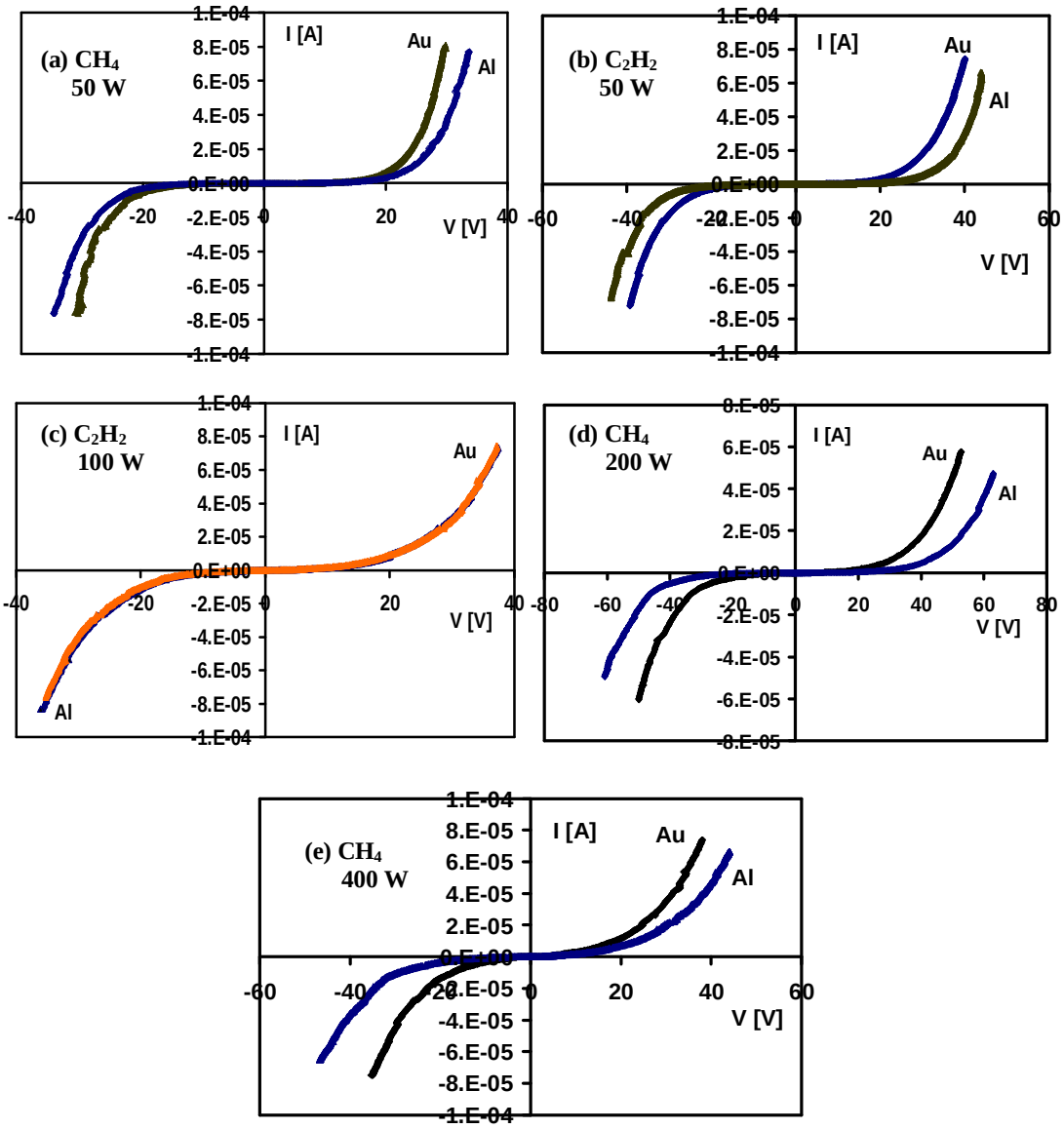

Fig. 3.13 I-V characteristics of Au/DLC/n-Si/Au structure of CH_4 and C_2H_2 films for various RF powers using Au and Al contact to the same sample (a) CH_4, 50 W (b) C_2H_2, 50 W (c) C_2H_2, 100 W (d) CH_4, 200 W (e) CH_4, 400 W.

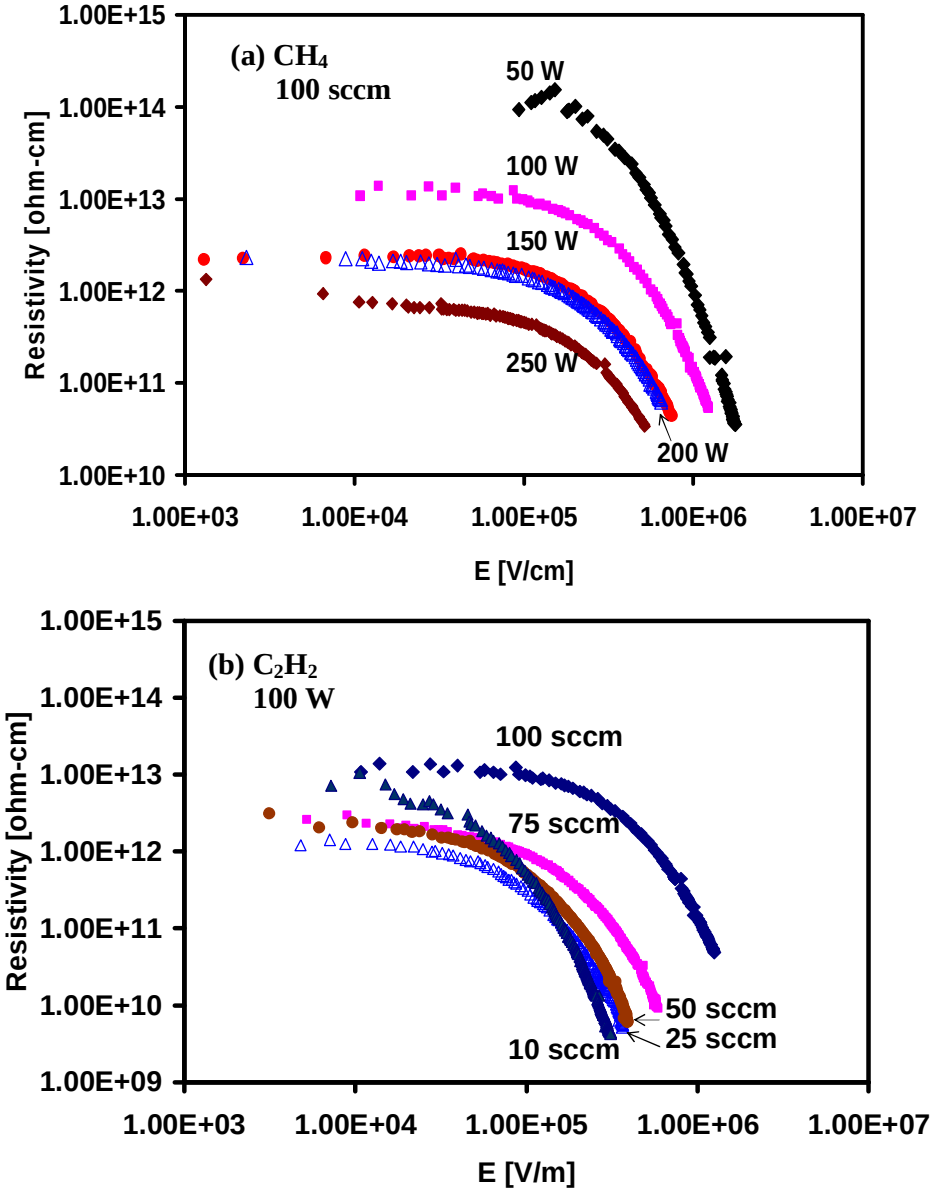

Fig. 3.14 Variation in electrical resistivity of DLC from CH_4 with applied electric field in log-log plot (a) for different RF powers and (b) for different flow rates.

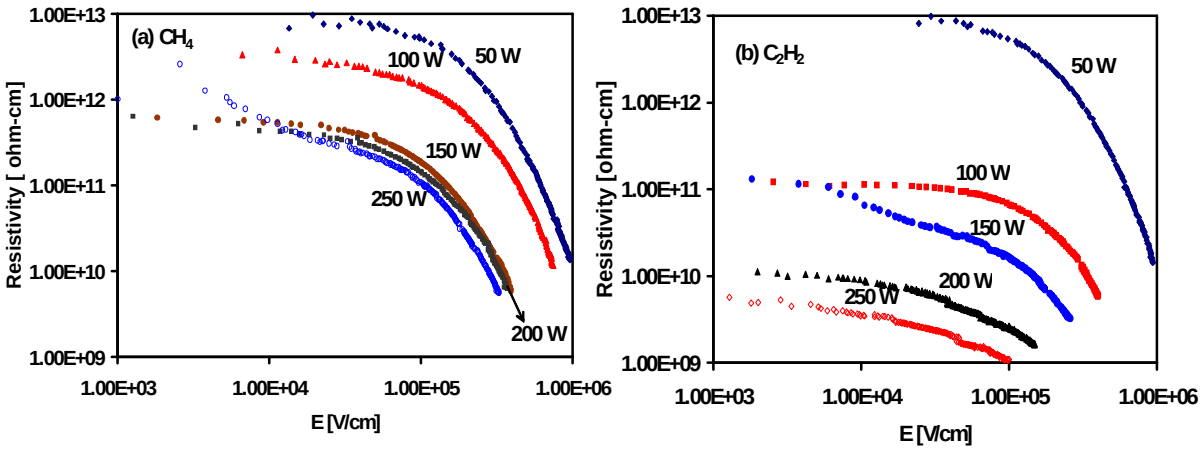

Fig. 3.15 Variation in electrical resistivity of DLC with applied electric field in log-log plot for various powers RF ranging from 50-250 W and flow rate of 70 sccm (a) CH_4 and (b) C_2H_2.

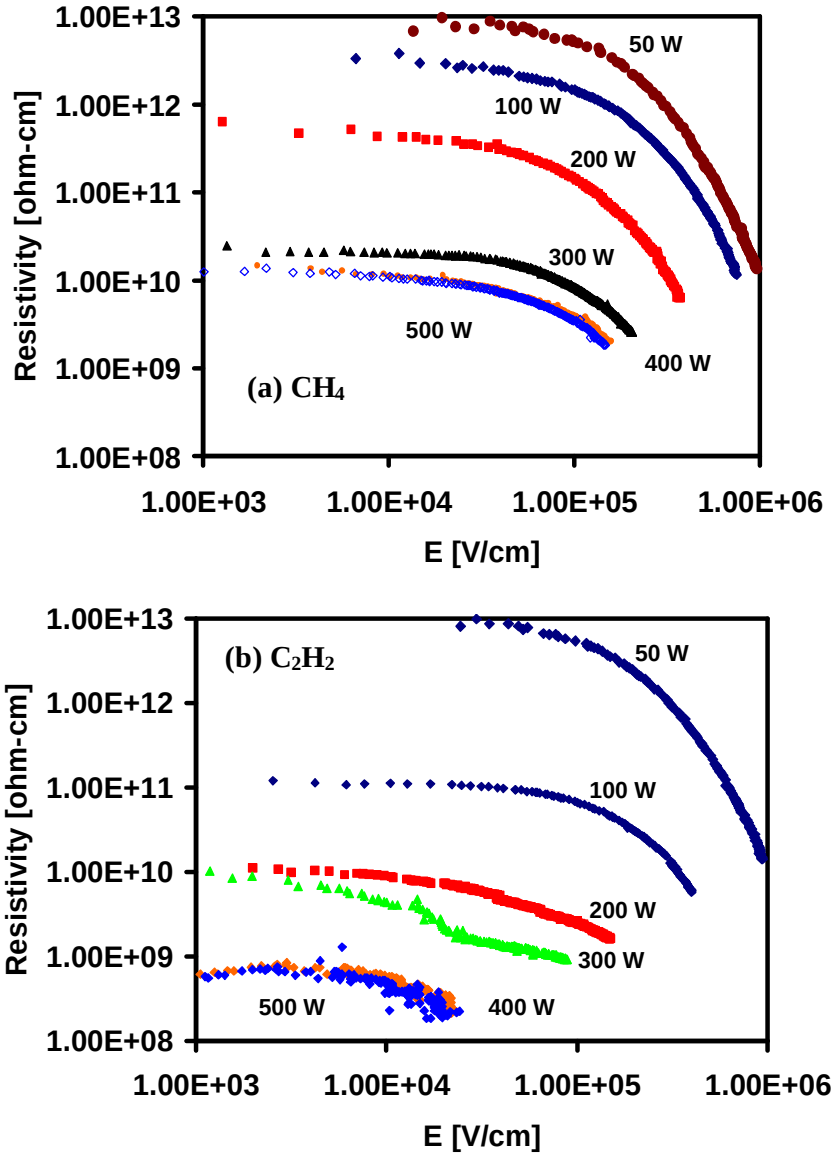

Fig. 3.16 Variation in electrical resistivity of DLC with applied electric field in log-log plot for various powers RF ranging from 50-500 W and flow rate of 70 sccm (a) CH_4 and (b) C_2H_2.

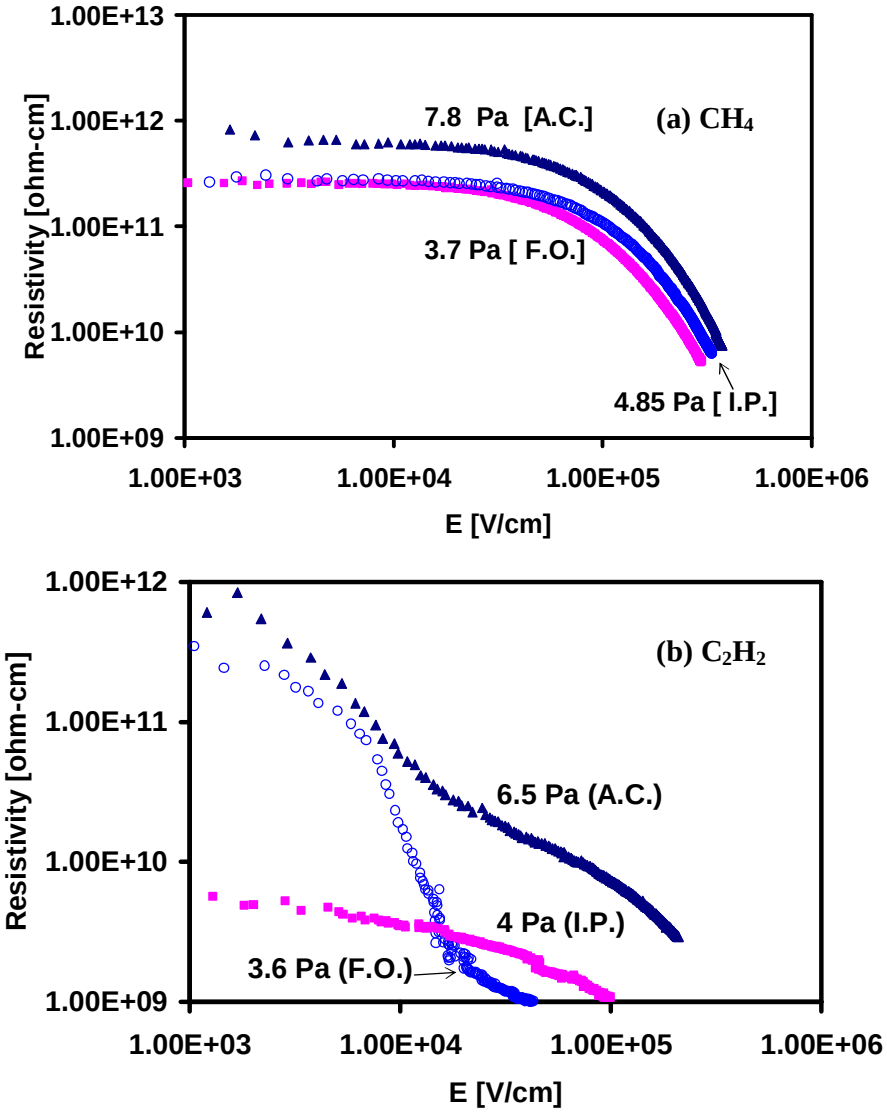

Fig. 3.17 Variation in electrical resistivity of DLC at different deposition pressures with applied electric field in log-log plot for RF power of 250 W and 70 sccm flow rate (a) CH_4 and (b) C_2H_2.

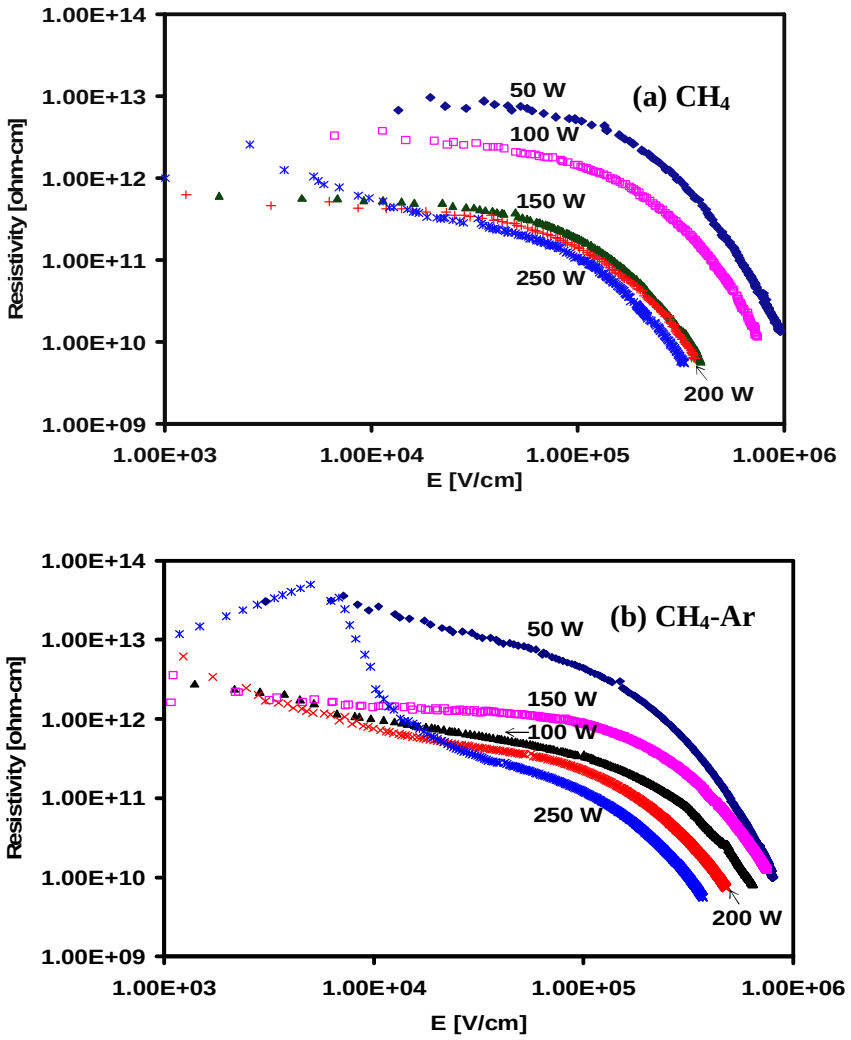

Fig. 3.18 Variation in electrical resistivity of DLC with applied electric field in log-log plot for various RF powers and flow rate of CH_4 70 sccm and Ar 20 sccm (a) CH_4 and (b) CH_4-Ar.

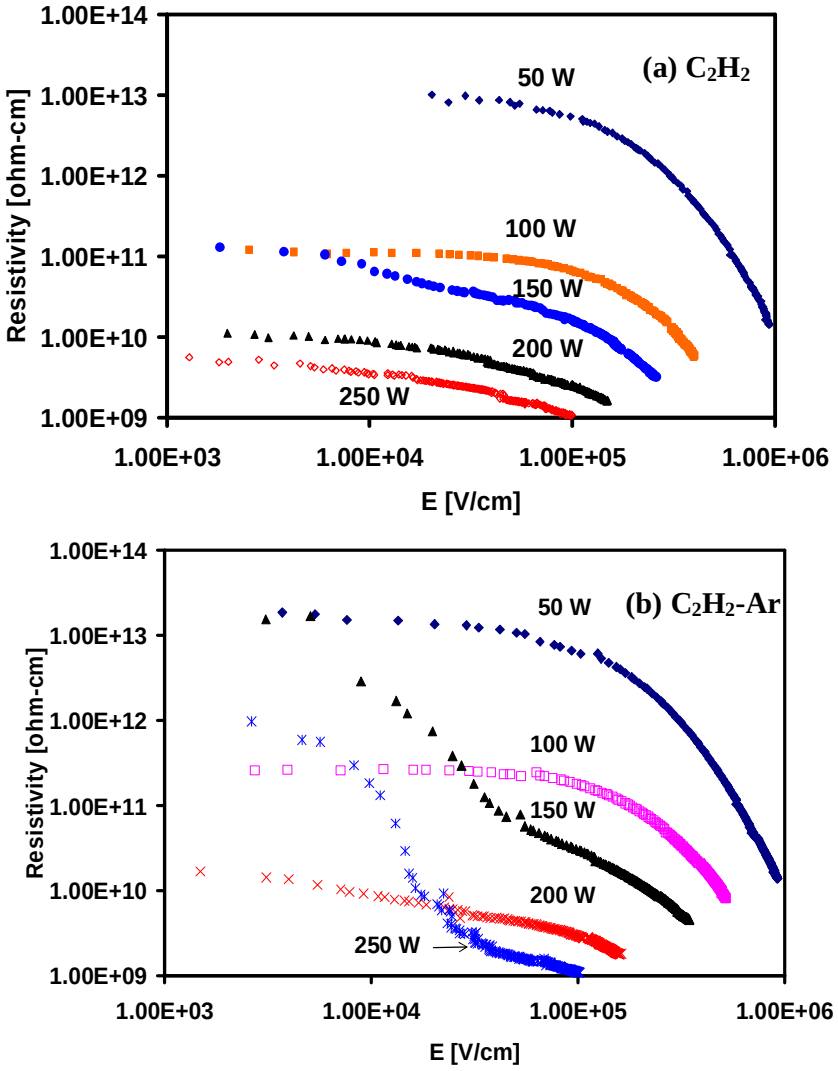

Fig. 3.19 Variation in electrical resistivity of DLC with applied electric field in log-log plot for various RF powers and flow rate of C_2H_2 70 sccm and Ar 20 sccm (a) C_2H_2 and (b) C_2H_2-Ar.

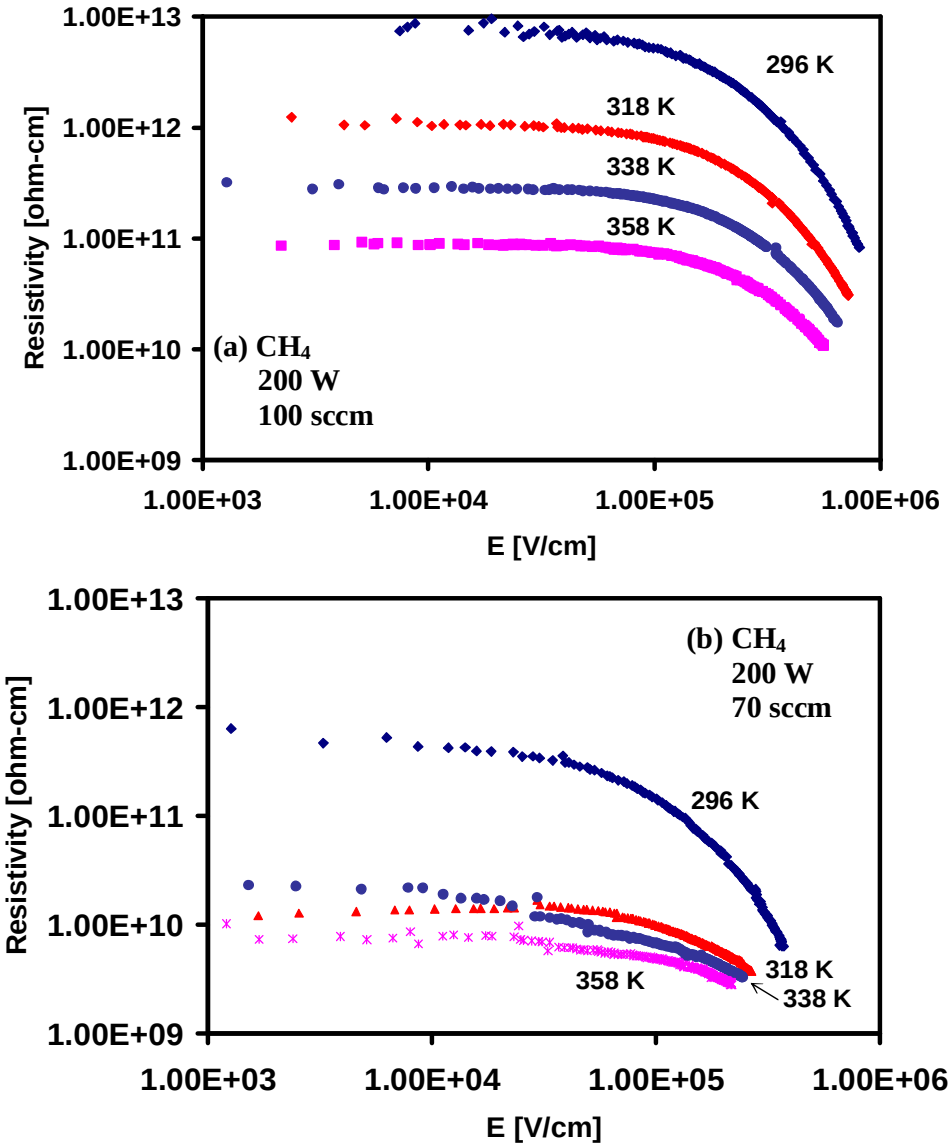

Fig. 3.20 Variation in electrical resistivity of DLC with applied electric field in log-log plot at various temperature (a) CH_4 (100 sccm, 200 W) and (b) CH_4 (70 sccm, 200 W).

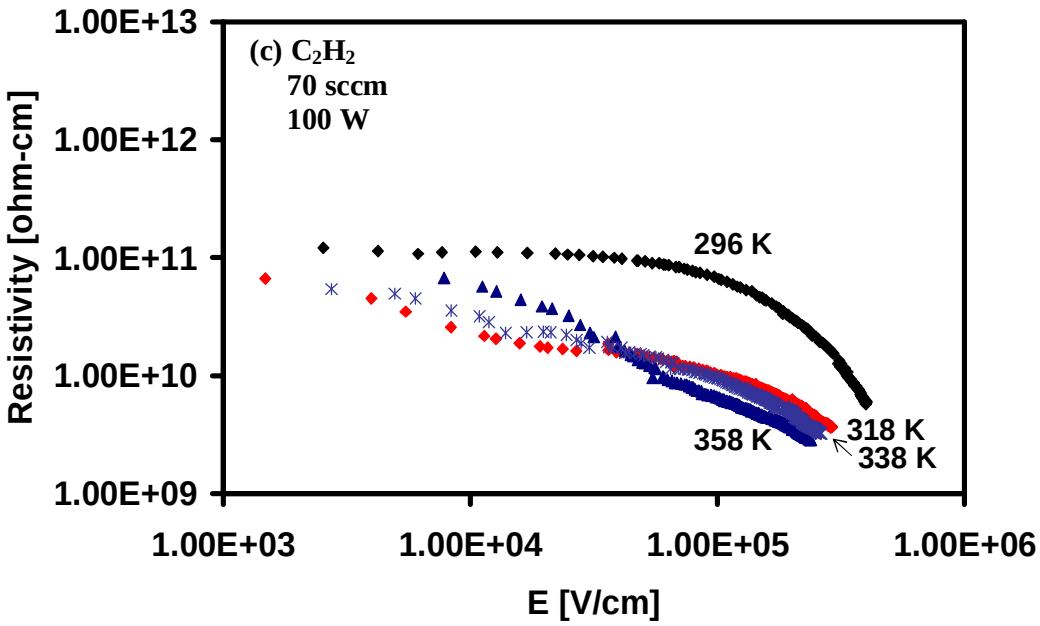

Fig. 3.20 Variation in electrical resistivity of DLC with applied electric field in log-log plot at various temperature (c) C_2H_2 (70 sccm, 100 W)

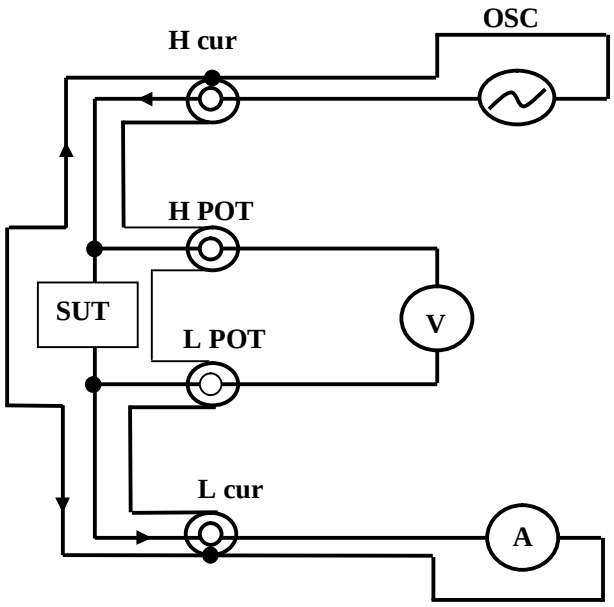

Fig. 3.21 Experimental arrangement of four terminal pair connection for measuring C-V-F curves.

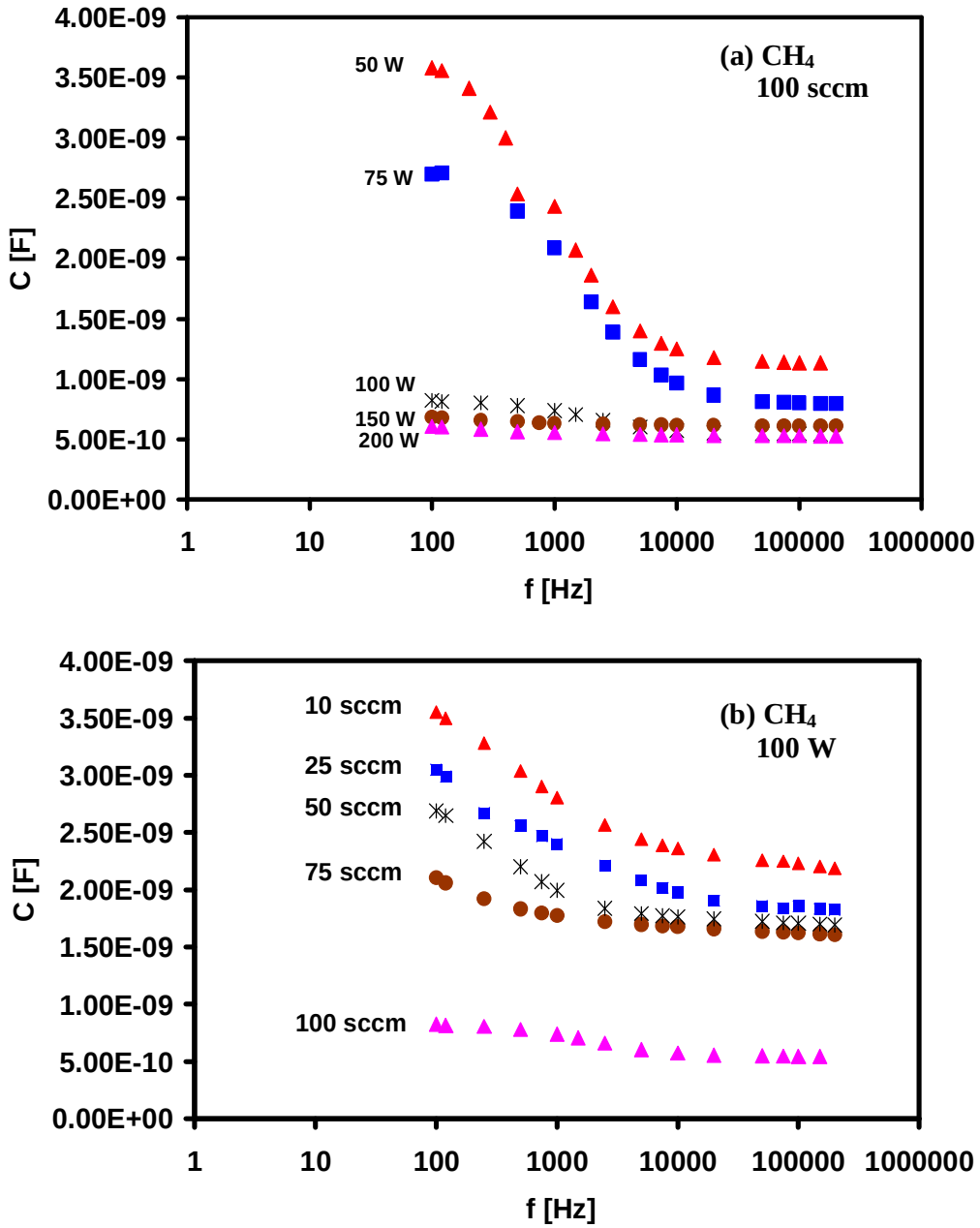

Fig. 3.22 Dependence of capacitance on frequency for Au/DLC/n-Si/Au MIS structure at room temperature from methane (a) at various RF powers and (b) at various flow rates.

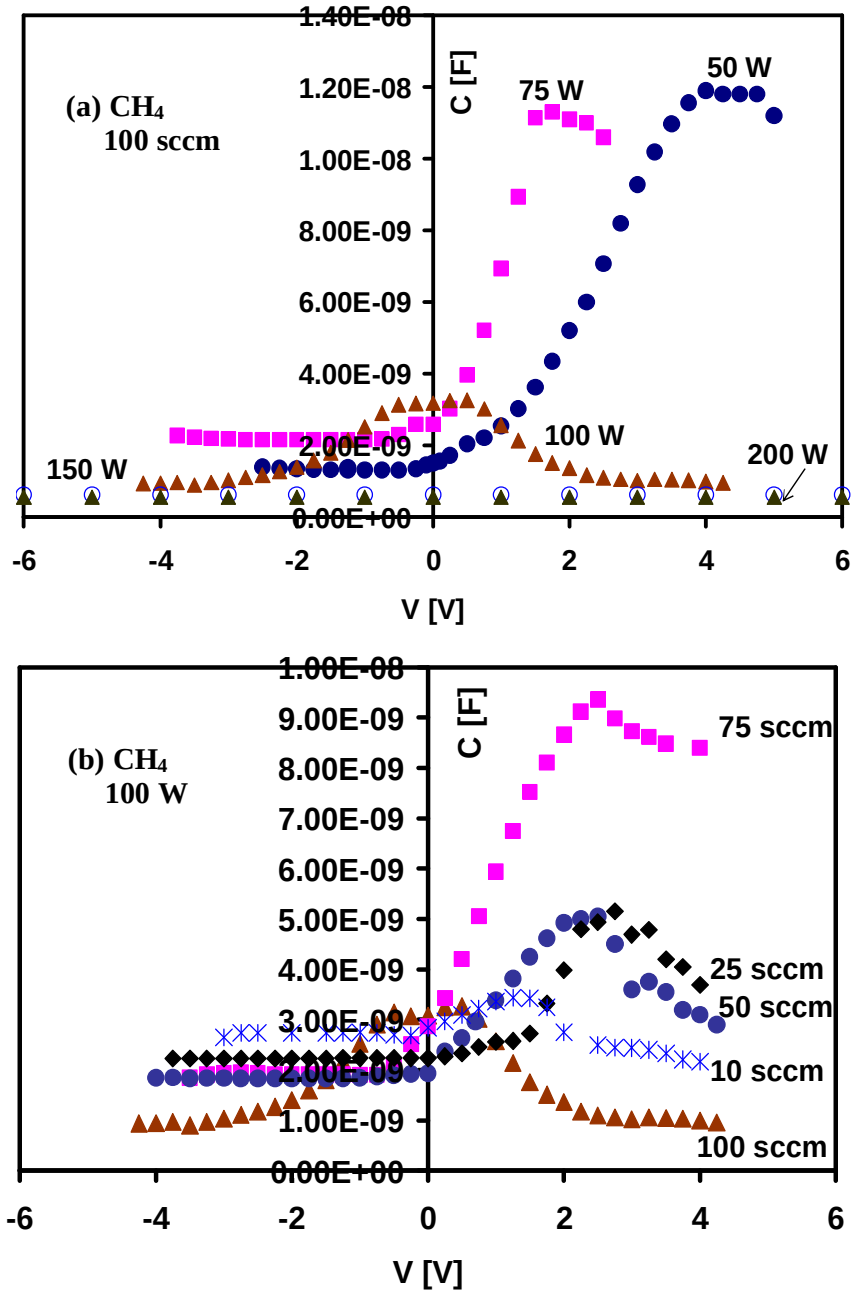

Fig. 3.23 Capacitance vs. bias voltage for Au/DLC/n-Si/Au MIS structure at room temperature (a) at various RF powers and (b) at various flow rates.

Table 3.1 Evaporation parameters for the fabrication top Au electrode.

Source material	Basic vacuum pressure (Pa)	Evaporation pressure (Pa)	Heater current (A)	Evaporation Time (min)
Au	$2x10^{-4}$	$5x10^{-4}$	30	3 min

Table 3.2 Sputtering parameters for the fabrication bottom Au contact.

Target	Voltage KV	Holder	Current (mA)	Chamber pressure(Pa)	Sputtering time (min)
Au	0.4	Magnet	10	2.5 ~ 2	3.5

References

[1] S. R. P. Silva, Properties of Amorphous Carbon (INSPEC, London, 2003) Emis Data Reviews Series No. 29, Chap. 6, p. 214.

[2] J. J. Pouch and S. A. Alterovitz: Properties and Characterization of Amorphous Carbon Films, Material Science Forum Vols. **52** & **53**, Trans Tech Publications, Aedermannsdorf, 1990, p. 20.

[3] H.-R. Park and S.-H. Lee, J. Korean Phys. Soc., **39** (2001) 141.

[4] M. Ohring, The Material Science of Thin Film, Academic Press, U.S.A. 1992, Chap. 10, p. 453.

[5] S. R. P. Silva and J. D. Carey, Diam. Relat. Mater., **12** (2003) 151.

[6] C. Godet, Diamond Relat. Mater, **12** (2003) 159.

[7] G. Lagar, M. Clin, S. Charvet, M. Therasse, C. Godet and K. Zellama, Diam. Relat. Mater., **12** (2003) 201.

[8] M. K. Hassan, B. K. Paraminik and A. Hatta, New Diam. and Front. Carbon Technol., **16** (2006) 211.

[9] J. J. Pouch and S. A. Alterovitz: Properties and Characterization of Amorphous Carbon Films, Material Science Forum Vols. **52** & **53**, Trans Tech Publications, Aedermannsdorf, 1990, p. 26.

[10] B. Meyerson and F. Smith, Solid State Commun., **34** (1980) 531.

[11] O. Amir and R. Kalish, J. Appl. Phys., **70** (1991) 4958.

[12] V. Anita, T. Butuda, T. Maeda, K. Takizawa, N. Saito and O. Takai, Diam. Relat. Mater., **13** (2004) 1993.

[13] C. P. Klages and R. Memming, Mater. Sci. Forum, **52-53** (1989) 609.

[14] H. Dimigen, H. Hubsch and R. Memming, Appl. Phys. Lett., **50** (1987) 1056.

[15] J.C. Angus and F. Jansen, J. Vac. Sci. Technol., **6** (1998)1778.

[16] R. B. Jackman and L. H. Chua, Diam. Relat. Mater., **01** (1992) 895.

[17] J. Robertson, Amorphous Carbon Adv. Phys., **35** (1986) 317.

[18] A. P. Mousinho, R. D. Mansano, P. Verdonck, Diam. Relat. Mater., **13** (2004) 315.

[19] M. Vogel, O. Stenzel, W. Gruenewald and A. Barna, Thin Solid Films, **209** (1992) 195.

[20] M. Ohring, The Material Science of Thin Film, Academic Press, USA, 1992, Chap. 10, p. 452.

[21] Instruction manual, LCR Meter, ZM2355, Chap. 8, p. 1.

[22] H.-R. Park and S.-H. Lee, J. Korean Phys. Soc., **39** (2001**)** 141.

[23] S. R. P. Silva, Properties of Amorphous Carbon (INSPEC, London, 2003) Emis Data Reviews Series No. **29**, Chap. 1, p. 16.

[24] B. K. Kim and T. A. Grotjohn, Diam. Relat. Mater., **9** (2000) 42.

[25] K. Chakrabarti, J. B. Kim, J. I. B. Wilson and C. Lee, Phys. Stat. Sol., **194** (2002) 116.

[26] J. Kim and C. Lee, J. of the Korean Phys. Soc., **42** (2003) S958.

[27] G. H. Glover, Solid-State electron, **16** (1973) 973.

[28] B. B. Ismail and R. D. Gould, Proc. SPIE, **2780** (1996) 46.

[29] K. T. McCarthy, S. B. Arnason, and A. F. Hebard, Appl. Phys. Lett., **74** (1999) 302.

[30] A. Goswami and A. P. Goswami, Thin Solid Films, **16** (1973) 175.

[31] P. Viktorovitch, J. Appl. Phys**., 52** (1981)1392.

[32] J. P. Kleider and D. Mencaraglia, J. Appl. Phys., **78** (1995) 3857.

4.1 Introduction

The various types of conduction mechanism in insulating film have been extensively studied [1-9]. In general an insulator possesses very few free charge carriers at normal temperatures. It has large energy band gap. In most cases, insulating films are amorphous in nature and the usual model of sharply defined energy bands can not be readily applied, but fuzzy tails arise both at the top of the valence band and the bottom of the conduction band [10]. A relatively high density of charge carriers may be present due to structural imperfection. They tend to be localized or trapped at these centers which cause the insulating property having very low mobilities.

In general, amorphous carbon has very complicated conduction mechanism, in which electrons, holes and ions influence on the current transport. Different electrical phenomena may arise by insulating films when sandwiched between combinations of metal and semiconductor electrodes. The various conduction processes may take place in case of wide gap semiconductor and insulators, depending on the trap density, the depth of the trap energy levels below the conduction band and the size of the Schottky barrier at the contacts. Under the influence of an applied electric field, electrons, holes and ions may migrate giving rise to the conduction current. Two main categories of carrier transport mechanism are summarized bellow:

1. Charge carrier injection through potential barriers from contacts (Barrier-Limited):

The potential barrier at the interface between the metal electrode and the insulator (or a semiconductor) prevents the easy injection of electron from the metal into the insulator [11]. When a depletion layer is formed on the insulator side near the interface, the conduction becomes electrode limited because the free carrier concentration in this case is higher in the bulk than what the contact can provide. This means the current-voltage characteristics are controlled by the charge carrier injection from the injecting contacts. Charge carriers injection from an electrode to an insulator/semiconductor may happen either by Schottky emission or quantum-mechanical tunneling.

2. Bulk-Limited:

In this case the electrical contact must be ohmic. For electrical conduction involving mainly one type of charge carriers, say electron, the cathode region can be considered a carrier reservoir that supplies charge carriers to the anode region by the applied voltage. Examples include space charge-limited, intrinsic and Poole-Frenkel conduction mechanism.

The main features of current transport in insulating films are current-voltage or field characteristics are nonohmic, and, with the exception of tunneling, the conduction mechanism is thermally activated.

4.2 Mechanisms Affecting the Current Transport

The different mechanism affecting the current transport through a thin MIS structure is illustrated schematically in the energy band diagram as shown in Figs. 4.1 and 4.2 in the presence of applied electric field [10]. From the diagram, the different electrical transport mechanisms that observed are summarized below:

Mechanism 1 (Schottky Emission): From the diagram it is observed that electron can be injected into the conduction band of the insulator by means of thermal activation over the potential barrier at the metal-insulator interface, this process is referred to as Schottky emission. Schottky emission is considered as electrode limited conduction mechanism [11].

Mechanism 2 (Tunneling): Electrons may also tunnel directly into the conduction band of the insulator from either the cathode. If an insulating film is extremely thin or contains a large number of imperfections, or both, electrons can tunnel directly between the metal electrodes and produces a current without the movement of carriers in the conduction band or in the valence band.

Mechanism 3 (Space-charge-limited (SCL) conduction): This bulk-limited mechanism occurs because the rate of carrier injection from the contacts exceeds the rate at which charge can be transported through the film. If the cathode emits more electrons per second than the space can accept, the remainder will form a negative space charge, which creates a field to reduce the rate of electron emission from the

cathode. Hence the current is controlled not by the electron injecting electrode but by the bulk of the insulator i.e. by the carrier mobility in the space inside the material.

Mechanism 4 (Ionic conduction): High temperature conduction in thick film and bulk insulators frequently occurs by ionic rather than electronic motions. Ionic conduction occurs if the actual impurities or defects in the film migrate. The most distinguishing feature of ionic conduction is the extremely low mobility of the carriers and high activation energy. There will also be mass transport through the film to an electrode.

Mechanism 5 (Intrinsic Conduction): This mechanism involves direct electronic excitation from the valence to the conduction band. Eg is large in insulator, intrinsic conduction is negligible.

Mechanism 6 (Poole-Frenkel emission): Electrons may also be thermally excited into the conduction band of the insulator from trapping levels in its forbidden bands. The mechanism of this effect is associated with field enhanced thermal excitation (or detrapping) of trapped electrons or holes, which is very similar to the Schottky effect in the thermionic emission.

Furthermore, the transport mechanism through the insulator may occur through the presence of impurities, for example foreign atoms or defects, such as Schottky defects or Frenkel defects, causing either impurity or ionic conduction.

A number of above mechanism may operate simultaneously at a particular applied potential difference across the device, but generally one mechanism will dominate the observed current. Some of the above mentioned conduction process will now be considered in greater details.

4.2.1 Schottky Emission

The Schottky effect is the emission of electrons into the conduction band of an insulator from the metal contact electrode (or semiconductor) by thermal activation over the field lowered metal insulator interfacial barrier. The phenomena, that the lowering of the potential barrier height by the interaction of the applied electric field and the image force is called Schottky effect. The emission mechanism is shown in Fig. 4.3 [12]. This figure shows that the potential barrier height is ϕ_m - χ provided the

image force is ignored and no applied electric field. Considering the applied and the image force, the total lowering of the potential barrier height

$$\Delta\phi_B = (\phi_m - \chi) - \phi_B$$

$$= \left(\frac{q^3 F}{4\pi\varepsilon}\right)^{1/2} = \beta_{sc} F^{1/2}, \tag{4.1}$$

where $\beta_{SC} = \left(\frac{q^3}{4\pi\varepsilon}\right)^{1/2}$ is called the Schottky constant.

So the effective potential barrier height can be written as

$$\phi_B = (\phi_m - \chi) - \left(\frac{q^3}{4\pi\varepsilon}\right)^{1/2} = \phi_B - \Delta\phi_B, \tag{4.2}$$

this is field dependent.

This type of electron emission from the electrode at a negative potential is analogous to thermionic emission except that the applied electric field lowers the barrier height ϕ_B is given by Richardson equation

$$J = A^* T^2 \exp\left[-(\phi_B - \Delta\phi_B)/kT\right] \times \left[\exp(qV/kT) - 1\right]$$

$$= J_0\left[\exp(qV/kT - 1)\right]. \tag{4.3}$$

where J_0 is the saturation current density, which may be written in the form

$$J_O = A^* T^2 \exp\left[-(-\phi_B - \Delta\phi_B)/kT\right]$$

where T is the absolute temperature of the emitter and A is the Richardson constant which is given by

$$A^* = A = \frac{4\pi mqk^2}{h^3}. \tag{4.4}$$

For most metals, A is about 60-120 $Acm^{-2}k^{-2}$. In expression, k is the Boltzmann constant, h is Plank's constant, and m is the electronic mass.

Because of the image-force lowering of the potential barrier, the electrode limited current does not saturate according to the Richardson equation, but, rather, obeys the Richardson-Schottky law. If we let the current density under this condition be identified by J then

$$J = J_O \exp\left(\frac{\beta_S E^{1/2}}{KT}\right). \tag{4.5}$$

In deriving the equation (4.4), Schottky neglected the electron-electron interaction term in calculating the carrier density using the Fermi-Dirac statistics. This assumption is practically not true because the emission current has a significant magnitude and hence there is always the possibility of electron-electron interaction. He also assumes a constant value of work function. In practice, however, the work function will increase if an electronic space charge exists in the vicinity of the contact. It also decreases with increasing field strength. In addition, the emitting area is much less than the actual surface area because of filamentary injection [13-14]. The value of the dielectric constant ε is less than the DC or static value of ε in the vicinity of the contact [15-16]. The presence of this discrepancy suggests that a rigorous fit of theoretical and experimental results can not be expected.

Crowell (17) has shown that the effect of an electron having differing masses in the metal and insulator implies that an effective mass m* must be used in the constant A. The actual shape of the potential barriers deviates from the ideal one because of imperfections such as surface states.

Dalapati *et al*. observed Schottky emission electrical conduction in ultra thin ZrO_2 films deposited on $Si_{0-y}C_y$ heterolayers [1]. Huang *et al*. has reported the Schottky emission conduction of multiwalled carbon nanotube [2]. Silva *et al*. reported the Schottky barrier-lowering conduction mechanism in amorphous carbon film [3].

4.2.2 Poole-Frenkel (PF) Emission and Its Modification

The original theory of the Poole-Frenkel effect was put forward by Frenkel [18]. The Poole-Frenkel effect is sometimes called the internal Schottky effect, since the mechanism of this effect is associated with the field enhanced thermal excitation (detrapping) of trapped electrons or holes, which is very similar to the Schottky effect in the thermionic emission. It is a bulk-limited conduction process. In this process emission of electrons occurs from trapping centers in semiconductors and insulators by the joint effect of temperature and electric field. It is also called the field-assisted thermal ionization. Fig 4.4 depicts the Poole-Frenkel emission mechanism. In this diagram, the solid lines represent the normal potential energy of the electron as a

function of distance x from the positive ion. The potential energy ϕ_{PF} of the electron at a distance x_0 is given by

$$\phi_{PF} = -\frac{q^2}{4\pi\varepsilon x_0} \tag{4.6}$$

where ε is the dielectric constant for low or high frequencies depending on whether or not the medium surrounding the donor can polarize within the emission time.

In the presence of an external field E, the Coulomb potential is reduced by a factor $-qEx_0$. The resultant potential barrier for thermal excitation of a trapped electron into the conduction band is shown by the dashed curve in Fig. 4.4. The resultant potential at a distance x_0 is given by

$$\Delta\phi = -\frac{q^2}{4\pi\varepsilon x_0} - qEx_0 . \tag{4.7}$$

If x_0 is defined as the distance from the ion at which the potential energy has its maximum value, then

$$\frac{d}{dx_0}\left(\frac{-q^2}{4\pi\varepsilon x_0} - qEx_0\right) = 0 ,$$

this gives

$$x_0 = \left(\frac{q}{4\pi\varepsilon E}\right)^{1/2} . \tag{4.8}$$

Using (4.8) in (4.7) we have,

$$\Delta\phi_{PF} = -2\left(\frac{q^3 E}{4\pi\varepsilon}\right)^{1/2} . \tag{4.9}$$

Equation (4.9) gives the reduction of the Poole-Frenkel barrier. The resultant barrier is now $(\phi_{PF} - \Delta\phi_{PF})$. Thus the emission current density J_{PF} in the presence of field is given by

$$\begin{aligned} J_{PF} &= q\mu n_C E \exp\left[-(\phi_{PF} - \Delta\phi_{PF})/2kT\right] \\ &= J_0 \exp(\Delta\phi_{PF}/2kT) \end{aligned}$$

$$J_{PF} = J_0 \exp\left(\frac{\beta_{PF} E^{1/2}}{2KT}\right) \tag{4.10}$$

where

$$J_0 = q\mu n_C E \exp\left(-\frac{\phi_{PF}}{2kT}\right).$$

In equation (4.10), μ is the electronic mobility and n_C is the effective density of states in the conduction band of the insulator. The Poole-Frenkel field lowering co-efficient β_{PF} in relation to equation (4.9) is given by

$$\beta_{PF} = \left(\frac{q^3}{\pi\varepsilon}\right)^{1/2}. \qquad (4.11)$$

Equation (4.10) is called the normal Poole-Frenkel equation.

A. A. Dakhel observed the Poole-Frenkel electrical conduction in Eu_2O_3 (europium oxide) films deposited on Si (100) at high electric field [4]. J. P. Chang has reported the Schottky emission at low electric field and Poole-Frenkel emission type conduction mechanism at high electric field [5]. S. Egret *et el.* reported that the dominant transport mechanism in M/a-C:H/M structures with a symmetrical I-V characteristics is Poole-Frenkel conduction [6].

The current-voltage measurements [19] on thin insulating films of SiO, Al_2O_3 and Ta_2O_5 are in qualitative agreement with the electric field and temperature dependencies predicted by equation (4.10). However the resulting constant β was somewhat smaller than β_{PF} equation (4.11) and in some cases in near aggrement with Schottky β. To explain the anomaly there are many other modification of the original Poole-Frenkel model based on various assumptions depends on: (a) the presence of discrete trapping levels; and (b) the mobile donor concept.

The first explanation regarding the value of β was put forward by Simmons [19]. He proposed a model based on the neutral trapping centers and field-assisted thermionic emission from the donor centers. His model is shown in Fig. 4.5. He firstly determined the position of the Fermi level by equating the number of electrons missing from the donor centers to the number of occupied traps, assuming the number of electrons in the conduction band to be negligibly small. He then estimated the current density which is given by:

$$J_{(PF)_{AN}} = J_0 \exp\left(\frac{\beta_{PF} E^{1/2}}{2kT}\right) \tag{4.12}$$

where

$$J_0 = q\mu n_c E\left(\frac{n_d}{n_t}\right)\exp\left(\frac{-(Ed + Et)}{2kT}\right).$$

In this expression n_d, E_d and n_t, E_t are the concentration and energy level, respectively, of donor and trapping centers. From the equation, it is seen that the field lowering co-efficient is now $\beta_{PF}/2(\equiv \beta_S)$, although the conductivity is not electrode-limited.

The explanation of the anomalous value of β is due to Hill [20] who made a detailed analysis of electrical conduction in amorphous solids. The basis of this analysis is the ionization of local defects by an applied field. He derived an expression of the generalized current J of the form

$$J \propto \alpha^2 Sinh\alpha \tag{4.13}$$

or

$$J \propto \alpha^{-1}(\alpha Cosh\alpha - Sinh\alpha), \tag{4.14}$$

where J is given by

$$J = IT^{-n}\exp\left(\frac{E_i}{kT}\right), \tag{4.15}$$

E_i is the ionization energy of the centre and α is $\frac{\beta E^{1/2}}{kT}$.

Equation (4.13) corresponds to emission from the donor centre occurring along the electric field direction with n equal to 4 in equation (4.15), whereas equation (4.14) corresponds to spherically uniform emission from the centers in which case n is equal to 3 in equation (4.15).

To explain the anomalous value of β, Hill assumed that donors and traps co-exist. He also assumed that the density of ionized donors is a small fraction of the total density of the ionizable donors. If this is the case then ionization of a donor by Poole-Frenkel emission can stimulate further ionization of other processes (other than Poole-Frenkel emission). The initial ionized donor can act as a capture centre for the electron released from the second donor, giving rise to an effective mobile donor and

an anomalous value of β. Hill has expressed β_{AN} (called the anomalous β) in terms of normal β_{PF} by the relation

$$\beta_{AN} = \beta_{PF}(2\nu_e - \nu_h)/2\nu_e \tag{4.16}$$

where ν_e and ν_h are the velocities, respectively, of the free carriers and mobile donors. As the ionization of the second donor must always be dependent on the availability of the first donor it is unlikely that $\nu_h > \nu_e$ so the range of the anomalous Poole-Frenkel constant is from β_{PF} to $1/2\beta_{PF} (\equiv \beta_S)$.

There are many other modifications of the original Poole-Frenkel model based on various assumptions.

4.2.3 Space-Charge-Limited (S.C.L.) Flow

If the cathode supplies large number of free carriers in the dielectric or the semiconductor near the injecting electrode, a space-charge will build up within the insulator or semiconductor. A field will be created to reduce the rate of electron from the cathode. Current flows through the insulator will then saturate. For low values of potential difference, if the injected carrier density is lower than the thermally generated free carrier density $n_{0,}$ Ohm's law will be obeyed, and the current density J_{SC} is given by

$$J_{SC} = qn_O \mu V / d \tag{4.17}$$

where V is the applied DC potential difference across the device and d the insulator thickness. When the injected carrier density is greater than the free carrier density the current becomes space-charge-limited.

Two requirements need to be fulfilled in order to observe SCL current flow of significant magnitude. These are: (i) at least one of the two electrodes must make an ohmic contact with the insulator, and (ii) the insulator must be relatively free from trapping defects.

The mechanism of SCLC in solids was first proposed by Mott and Gurney [21]. They obtained the current density J_{SC} for the simple case of single carrier trap-free SCLC in an insulator as

$$J_{SC} = \frac{9}{8}\varepsilon\mu\frac{V^2}{d_3} \tag{4.18}$$

where the symbols have their usual meanings.

This is the well known Mott-Gurney equation and is sometimes referred to as the square law for trap-free SCL currents. The interesting features of relation are that it predicts that J_{SC} is directly proportional to V^2 and inversely proportional to d^3. However, equation (4.18) predicts much higher current than are observed in practice, and also that SCLC is temperature insensitive.

The deviations from the trap free theory are readily observed in case of more realistic insulators, which contains trap.

The theory of SCLC in defect insulators was put forward by Rose [22]. In the presence of traps, a large fraction of the injected space charge will condense therein, which means that the free-carrier density will be much lower than in a perfect insulator. Since the occupancy of traps is a function of temperature, the SCL current will be temperature-dependent.

If the insulator contains n_t shallow traps, all assumed to be at the same energy level E_t below the bottom of the conduction band, the ratio θ of the free charge to the total carriers (free and trapped) charge is given by

$$\theta = \left(\frac{n_c}{n_t}\right)\exp\left(\frac{-E_t}{kT}\right). \tag{4.19}$$

The current density, including the effect of shallow traps is given by J

$$J_{(SC)_T} = \frac{9}{8}\varepsilon\mu\theta\frac{V^2}{d^3}. \tag{4.20}$$

Since θ is independent of *V*, $J_{(SC)T}$ is directly proportional to V^2, as in the trap free case. As θ is very small temperature-dependent quantity, the inclusion of shallow traps in the insulator satisfies the theory with the experimental observation.

Lampert [23] has modified the equation (4.20) by replacing *d* with d_{eff}, which can be considered as effective thickness. The difference between d_{eff} and *d* can be attributed to the inhomogeneous spatial distribution of free and trapped carriers.

Now, if sufficient charge is injected into the dielectric, the traps will become filled and the current density will again be given by the Mott-Gurney equation. The voltage at which this occurs is called the trap-filled-limited (TFL) voltage, and is given by

$$V_{TFL} = qn_t d^2 / 2\varepsilon . \tag{4.21}$$

Fig. 4.6 represents the SCL I-V characteristics for an insulator containing shallow traps. It is evident from this diagram that there are four distinct zones. These are (A) ohmic, (B) governed by a modified Mott and Gurney law, (C) a trap-filled-limit region, and (D) governed by the trap-free Mott and Gurney law.

In general the traps will not be localized to shallow levels as considered above and the form of the space charge law will depend on the particular trap distribution. For a trap density decreases exponentially as the energy from the band edge increases, the current density for the applied potential difference V is given by

$$J_{(SC)_T} = q\mu n_C \left(\frac{\varepsilon}{qn_0 T_X k} \right)^X \left(\frac{V^{X+1}}{d^{2X+1}} \right) \tag{4.22}$$

where x is a parameter which characterizes the particular distribution of traps and T_X is the temperature used to characterize the trap distribution.

Shaila Wagle observed this effect in vacuum deposited $Sb_2Pb_1Se_7$ films [7]. S. Ashok has reported space-charge-limited current in thin-film diamond [8]. P.W. May also reported the SCLC model in CVD as grown and doped diamond [9].

4.2.4 Distinction between Schottky and Poole-Frenkel Emission

Both Poole-Frenkel and Schottky emission $\log I$ vs. $E^{1/2}$ are expected to be linear. The gradient of the linear region may be of the same value. In both cases the current density are exponentially proportional on 1/T. These criteria however, are not sufficient for distinguishing between the two emission processes. The following factors will discriminate the two emission process clearly:

1. Both effects are due to columbic interaction between the escaping electron and a positive charge, but they differ in that the positive charge is fixed for the Poole-Frenkel trapping barrier, while the positive charge is a mobile image charge for the Schottky barrier.

2. The lowering of the barrier due to the Poole-Frenkel effect are twice that due to the Schottky effect. Because the columbic attractive force to the electron is $\frac{q^2}{4\pi\varepsilon(r_{PF})^2}$ for Poole-Frenkel effect and $\frac{q^2}{4\pi\varepsilon(2x_m)^2}$ for Schottky effect.
3. The Poole-Frenkel effect is observed when electric conduction is bulk limited, and the Schottky effect is observed when electric conduction is electrode limited.
4. The current- voltage characteristics of an MIS/MIM device using metals with different work function will be highly asymmetric for Schottky emission and symmetric for Poole-Frenkel emission.
5. The two emission characteristics have different voltages and temperature dependencies. For Schottky emission

   $$J_S \propto T^2 \exp(\beta_S E^{1/2} / kT)$$

   A graph of $\ln J_S / T^2$ vs. $1/T$ may be drawn at a given electric field E and for a given temperature T, a plot of $\ln J_S$ vs. $E^{1/2}$ can also be drawn, and for Poole-Frenkel emission

   $$J_{PF} \propto E \exp(\beta_{PF} E^{1/2} / 2kT).$$

   The corresponding graph is $\ln J_{PF}$ vs. $1/T$ at a given field E, and for a given temperature T, $\ln(J_{PF} / E)$ vs. $E^{1/2}$ may be drawn.
6. The height of the barrier at the contact for a wide band gap insulator is expected to be above 0.8 eV whereas much lower activation energies are indicated with bulk-limited emission.

4.3 Electrical Conduction Mechanism and Schottky Plots of DLC Films

The leakage current conduction mechanism of the DLC films has investigated. To determine the conduction mechanism of the DLC film, a series of log J vs. $E^{1/2}$ curves are plotted the Schottky plots for the DLC MIS structures from the I-V data.

The graphs of log J vs. $E^{1/2}$ are plotted for CH_4 films at different flow rates from 10 to 100 sccm keeping the RF power constant at 100 W is shown in Fig. 4.7. On the other hand Fig. 4.8 shows the log J vs. $E^{1/2}$ curve for CH_4 films at different RF power from 50 to 250 W keeping the flow rate constant at 100 sccm.

Figs. 4.9 and 4.10, show the current density plotted in the logarithm scale along with the square root of the electric field strength at different RF powers for both CH_4 and C_2H_2. In Fig. 4.8 the RF power was varied from 50-250 W while in Fig. 4.9 it was 50-500 W, but the flow rate was 70 sccm in both cases.

Fig. 4.11 shows the log J vs. $E^{1/2}$ curves for both CH_4 and C_2H_2 at different deposition pressures.

Fig. 4.12 shows the plot of log J vs. $E^{1/2}$ for both CH_4-Ar and C_2H_2-Ar mixtures at different RF power ranging from 50-250 W. The flow rate of CH_4 and C_2H_2 was 70 sccm and Ar 20 sccm.

The logarithm of the current density versus square root of field for Au and Al upper contacts is shown in Fig. 4.13.

Fig. 4.14 shows the Schottky plots of few CH_4 and C_2H_2 samples at various temperatures ranging from 296-358 K.

Fig. 4.15 shows the Arrhenius plot of temperature dependent of the current for DLC films for both CH_4 and C_2H_2 samples deposited at RF power of 200 W and 70 sccm flow rate.

4.4 Results and Discussions

Electrical conduction in DLC MIS structure may be controlled by several mechanisms. These are, mainly, Schottky emissions, Poole-Frenkel emission, Foeler-Nordheim tunneling, and space charge limited current.

The graphs of log J vs. $E^{1/2}$ as shown in Figs. 4.7 and 4.8 for CH_4 films vary approximately linearly with the square root of field. In the case of CH_4 shown in Fig. 4.8, all the experimental data with different RF powers show a similar slope. But in Fig 4.7 the experimental data with different RF powers show a different slope.

Figs. 4.9 and 4.10; (a) and (b) and show the current density plotted in a logarithm scale along with the square root of the electric field strength, a Schottky plot. In the

case of CH_4 shown in Fig. 4.9 (a) and 4.10 (a) all the experimental data with different RF powers show a similar slope. It suggests that the electrical conductivity in the DLC films from a CH_4 source gas is well explained by the Poole-Frenkel model.

Both the Schottky and Poole-Frenkel emission stem from lowering a Coulombic potential barrier for free carrier generation out of a defect centre or trap under an applied electric field. It is also considered that the carrier injection from the electrodes through the Schottky potential induced at the interface between the electrode and the dielectric material shows the same trend as the Poole-Frenkel model. From the fact that the experimental data of I-V curves were symmetrical for both the gold contact on the DLC and the n-type Si substrate interface, it was concluded that the conduction mechanism was not due to Schottky injection but due to the internal carrier excitation following the Poole-Frenkel model. This was also confirmed by comparison of the other experimental results of the I-V characteristics using aluminum electrodes instead of gold.

In the low-electric-field region below 10kV/cm, as shown in Fig. 4.9 (a) and 4.10 (a), the current density was smaller than the linear extension of the Poole-Frenkel line. It is assumed in the Poole-Frenkel model that the carrier velocity is saturated at a high electric field. At a low electric field, however, the carrier velocity depends on the electric field strength. By assuming this, at the low electric field, the current depends on the carrier velocity governed by the electric field, whereas at the higher electric field it follows the conventional Poole-Frenkel model as

$$j = j_0\{1-\exp(-\frac{E}{E_0})\}\exp\{\frac{\beta_{PF}\sqrt{E}}{2kT}\} \qquad (4.23)$$

where E_0 is the electric field strength necessary for the saturation of carrier velocity. By fitting eq. (4.23) to the experimental data, the solid lines in Fig. 4.10 (a) and 4.10 (b) were obtained. The experimental results were well explained by this model.

The constant β_{PF} appearing in the Poole-Frenkel model is obtained from the unit charge and the dielectric constant as

$$\beta_{PF} = \sqrt{\frac{e^3}{\pi\varepsilon}}\,. \qquad (4.11)$$

The slope of the Schottky plot is determined only by the dielectric constant. From the experimental results, the dielectric constant for the DLC films deposited from CH_4 was almost 4. The result was a reasonable value as compared with other measurements [24, 25].

In the case of C_2H_2, only lower-powered films at 50, 100 W and 150 W exhibited the same trend as the CH_4 samples. At 200, 250 and 300 W, a similar trend also appeared briefly in the higher-current-density region of nearly $1mA/cm^2$. In the lower-electric-field region, however, the results did not follow eq. (4.23) but the current increased rapidly as the exponent of the square root of the electric field. The slope of the lower-electric-field region was almost 3 times larger than that of the higher-electric-field region, which is in agreement with Poole-Frenkel model. At 400 and 500 W, the current increased rapidly in the low electric field. The poor resistivity of the DLC films from C_2H_2 at higher RF powers originated from the different conduction mechanism as compared with that from CH_4 at higher RF powers. However at 400 and 500 W for low electric field may be hopping conduction appears to be the dominant mechanism.

As can be seen from Fig. 4.11 (a) all the samples with different experimental data at different deposition pressure show the similar slope. The current density varies approximately linearly with the square root of electric field. In case of C_2H_2 film deposited at highest pressure (6.5 Pa) show the same trend as the CH_4 samples deposited at different pressures. But the C_2H_2 films deposited at lower pressures (3.6 and 6.5 Pa), a similar trend also appeared shortly in the higher-current-density region. In the lower-electric-field region, however, the results did not follow eq. (4.23) but the current increased rapidly as the exponent of the square root of the electric field. The slopes of the lower electric field region were larger than the higher-electric field region following the Poole-Frenkel conduction.

In the case of CH_4-Ar as shown in Fig. 4.12 (a) only films at 50 and 200 and 250 W exhibited the same trend as the CH_4 samples as in Fig. 4.9 (a) and 4.10 (a) . At 100 and 150 W the slope is slightly lower than the other cases but they also show straight line in Schottky plot. The experimental data of I-V curves 100 and 150 W CH_4-Ar were also symmetrical for both the gold contact on the DLC and the n-type Si substrate interface, it was concluded that the conduction mechanism was not due to

Schottky injection but due to the internal carrier excitation following the Poole-Frenkel model.

In the case of C_2H_2-Ar, only lower-powered films at 50, 100 and 150 W exhibited the same trend as the samples of 50, 100 and 150 W from pure C_2H_2 as in Fig. 4.9 (b) and 4.10 (b). At 200 and 250 W, a similar trend also appeared briefly in the higher-current-density region of nearly 10mA/cm^2. In the lower-electric-field region, however, the results did not follow eq. (4.23) but the current increased rapidly as the exponent of the square root of the electric field. The slope of the lower-electric-field region was almost 3 times larger than that of the higher-electric-field region, which is in agreement with Poole-Frenkel model.

As can be seen from Fig. 4.13 (a) and (b) all the experimental data from CH_4 and C_2H_2 for Au and Al upper contact at different RF powers show the similar slopes. In case of C_2H_2 100 W sample almost no change of log J vs. $E^{1/2}$ plot is observed. Little change of current density with the field was observed with a change of electrode from Au to Al. But in case Au electrode all the samples showed higher current density than the Al electrodes. Little change of current density with a change of electrode from Au to Al, indicates that the leakage current conduction is primarily governed by bulk-limited conduction [26]. In each case, the logarithm of current density varied approximately linearly with the square root of the voltage, as expected for Poole-Frenkel conduction. The current was also found to vary symmetrically for both positive and negative applied voltages, for Au or Al contacts. This showed that the current is limited by the bulk, not the contacts, which was in agreement to Poole-Frenkel conduction.

The Schottky plot at various temperatures also shows the same trend of the CH_4 samples as shown in Fig. 4.14.

The conduction mechanism was also studied further by finding the temperature dependent of current for samples CH_4 and C_2H_2 for 200 W at constant applied voltages 4.25 V and 2.90 V respectively as shown in Fig. 4.15, the Arrhenius plots. The Arrhenius plots of conductivity shows an approximate linear dependence of ln I against T^{-1}, giving activation energies 0.60 and 0.62 eV respectively. A linear dependence of ln I vs. T^{-1} is expected for Poole-Frenkel emission.

4.5 Summary

This research investigated the electrical transport properties of DLC film deposited from RF-PECVD with the Au/DLC/n-Si/Au structure at room temperature over a wide range of applied electric field of up to 10^6 V/cm. The electrical conductivity of DLC films from CH_4 followed a Poole-Frenkel-type conduction mechanism. This means that conduction occurs due to the thermal excitation of electrons from traps into the conduction band of the insulator (DLC). In the case of C_2H_2, however, films at 50, 100 and 150 W completely followed and films at 200, 250 and 300 W partially followed Poole-Frenkel conduction whereas films at 400 and 500 W had a completely different conduction mechanism from CH_4. In case of C_2H_2, different conduction mechanism at high RF powers was possibly due to the higher sp^2 bonds not terminated by hydrogen due to insufficient hydrogen supply during the film growth.

In case of films from CH_4-Ar also supported the assignment of Poole-Frenkel-type conduction mechanism. In case of C_2H_2-Ar, however the low-powered-films deposited at 50, 100 and 150 W completely followed and the films at 200 and 250 W partially followed Poole-Frenkel conduction.

The Poole-Frenkel type conduction were found to occur for the DLC samples fabricated at different deposition pressure from CH_4 and the C_2H_2 sample deposited at higher pressure of 6.5 Pa. On the other hand, films from C_2H_2 at relatively lower pressure partially followed the Poole-Frenkel conduction model.

The conduction mechanism identified for both the top Au and Al top electrode as Poole-Frenkel emission which suggested that conduction is independent of the electro- negativity of the contact metals.

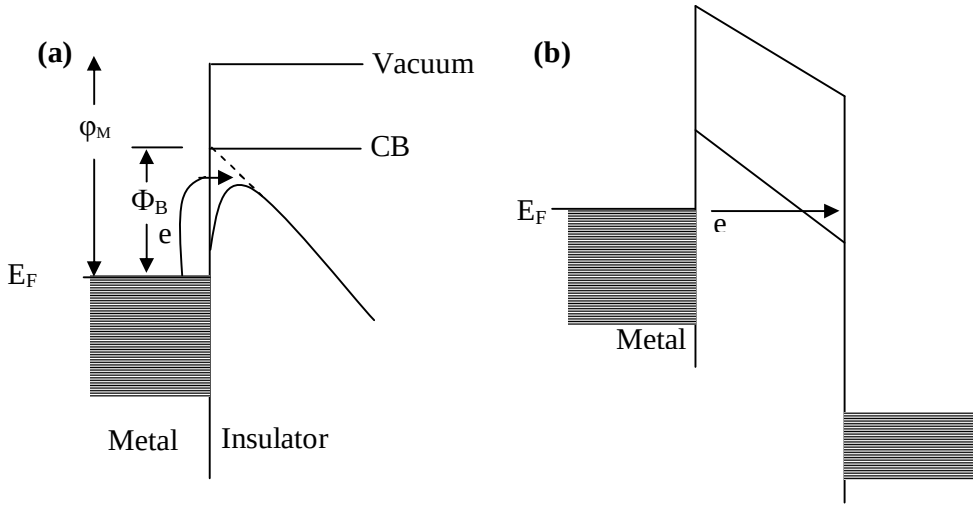

Fig. 4.1 Barrier limited conduction mechanism (a) Schottky emission and (b) Tunneling [10].

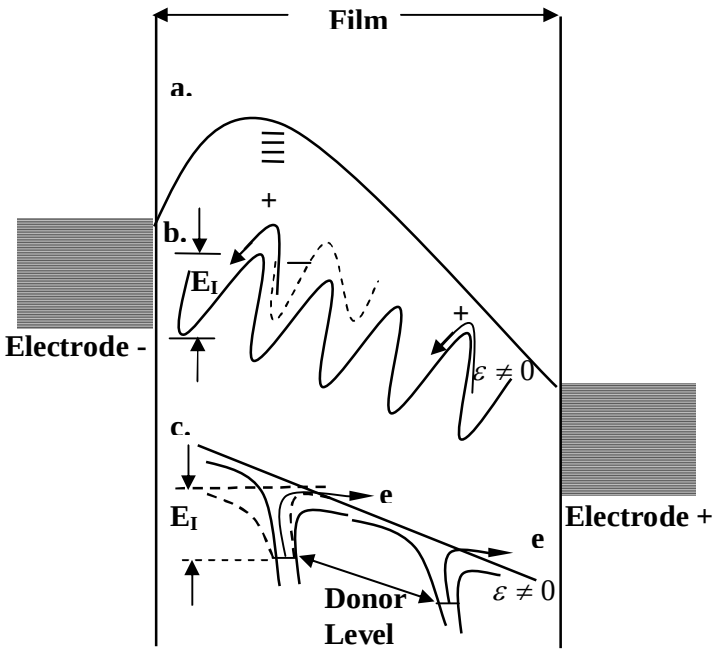

Fig. 4.2 Bulk-limited conduction mechanisms (a) Space-charge-limited (b) Ionic conduction of cations (c) Poole-Frenkel [10]

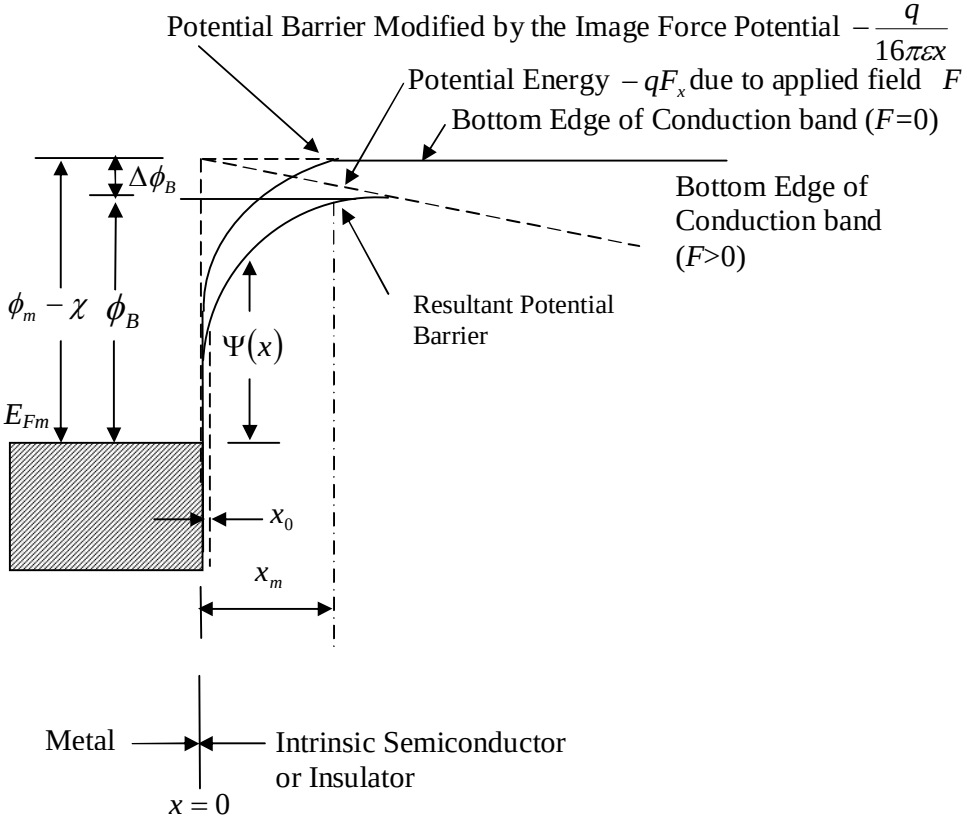

Fig. 4.3 Energy level diagram showing the lowering of the potential barrier due to the combination of image force and the applied uniform field (Schottky effect) [12].

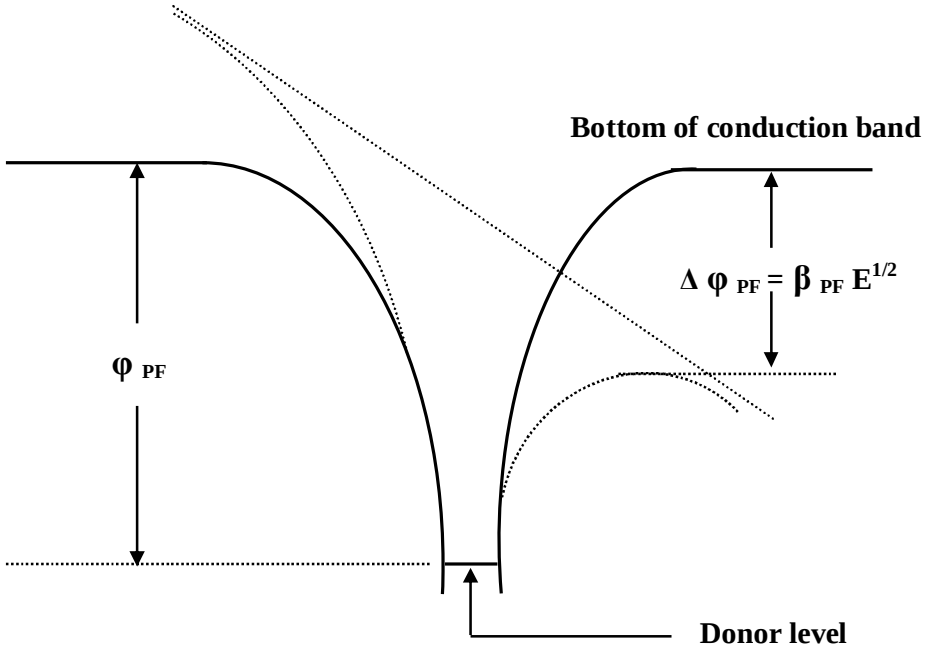

Fig. 4.4 Poole-Frenkel effect at a donor centre

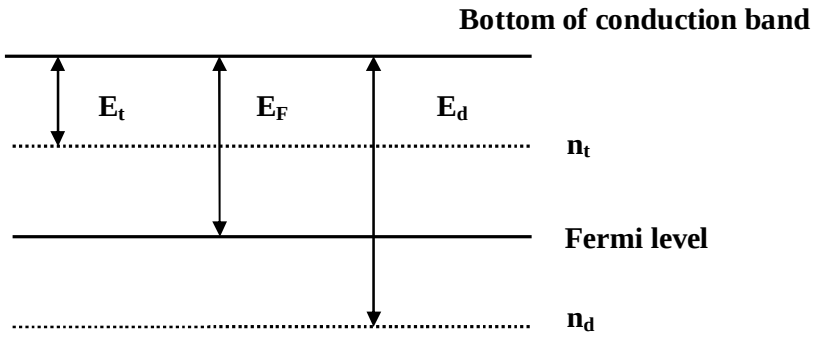

Fig. 4.5 Anomalous Poole-Frenkel effect (Simmons model).

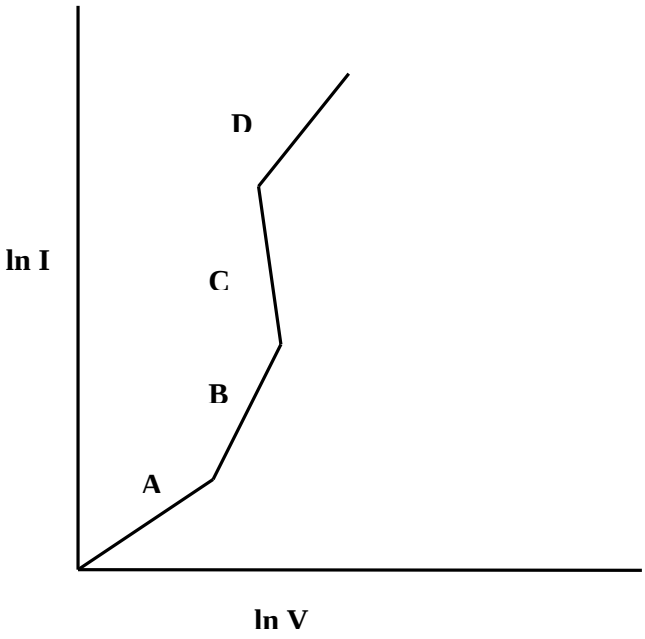

Fig. 4.6 SCLC I-V characteristics for an insulator containing shallow traps.

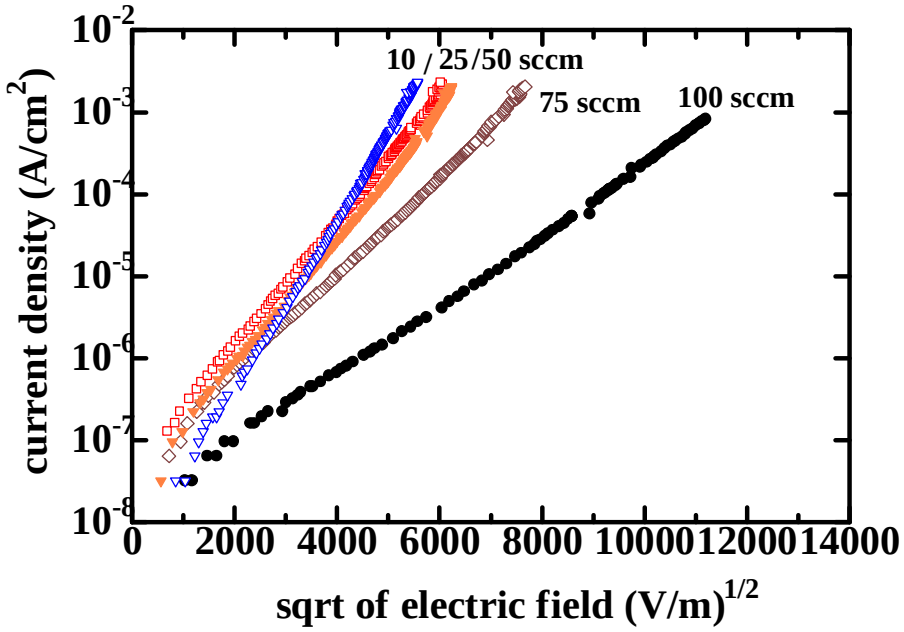

Fig. 4.7 Current density vs. sqrt of electric field of DLC films at various flow rates from CH_4 and RF power of 100 W.

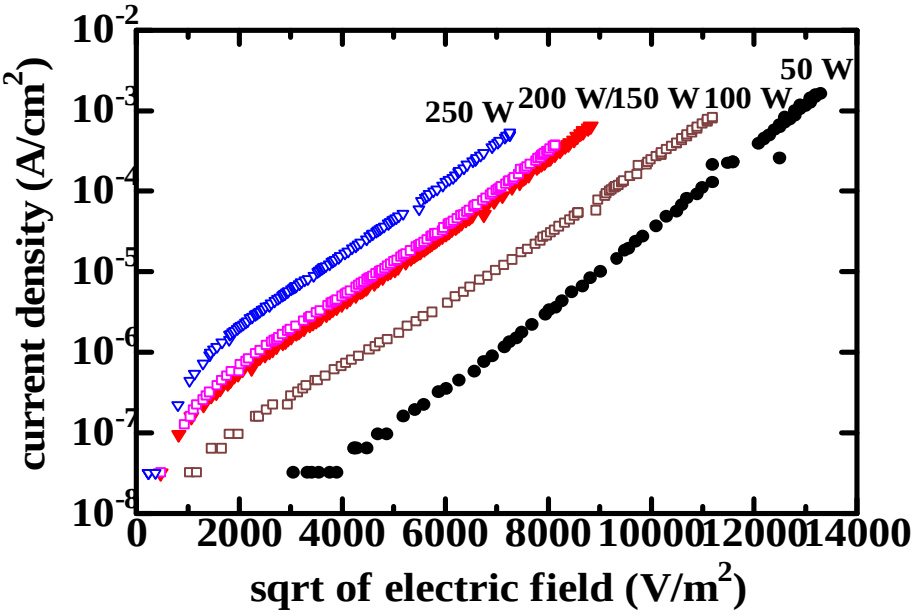

Fig. 4.8 Current density vs. sqrt of electric field of DLC films at various RF powers from CH_4 and flow rate of 100 sccm.

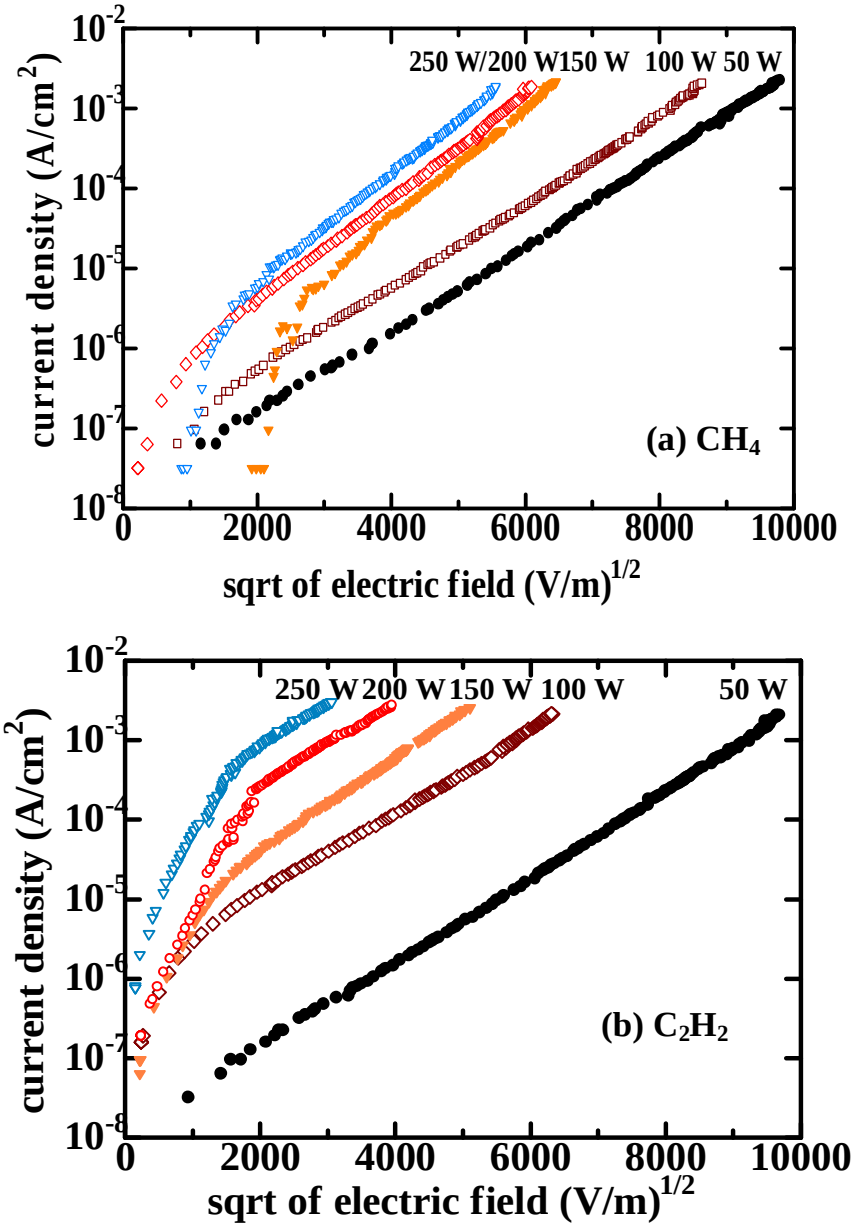

Fig. 4.9 Current density vs. sqrt of electric field of DLC films at various RF powers ranging from 50-250 W and constant flow rate of 70 sccm (a) CH_4 and (b) C_2H_2.

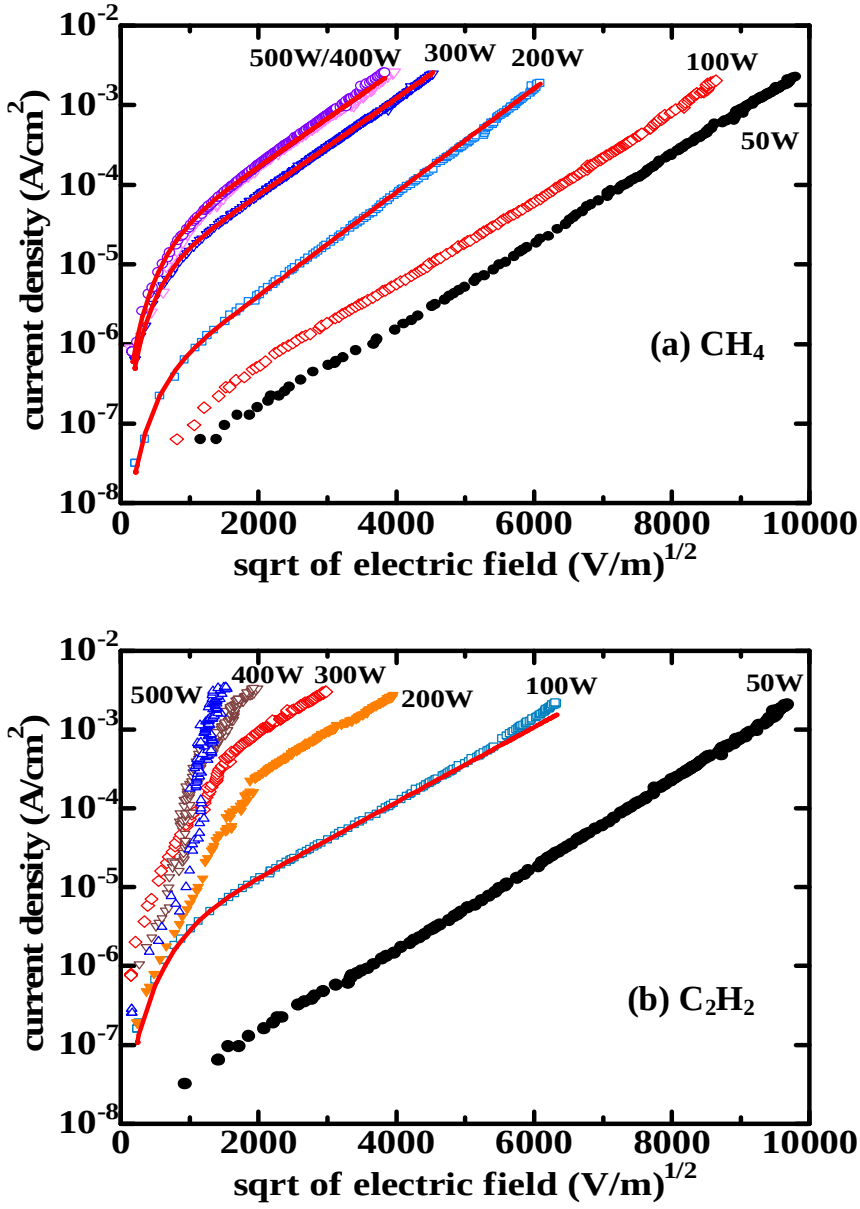

Fig. 4.10 Current density vs. sqrt of electric field of DLC films at various RF powers ranging from 50-500 W and constant flow rate of 70sccm (a) CH_4 and (b) C_2H_2.

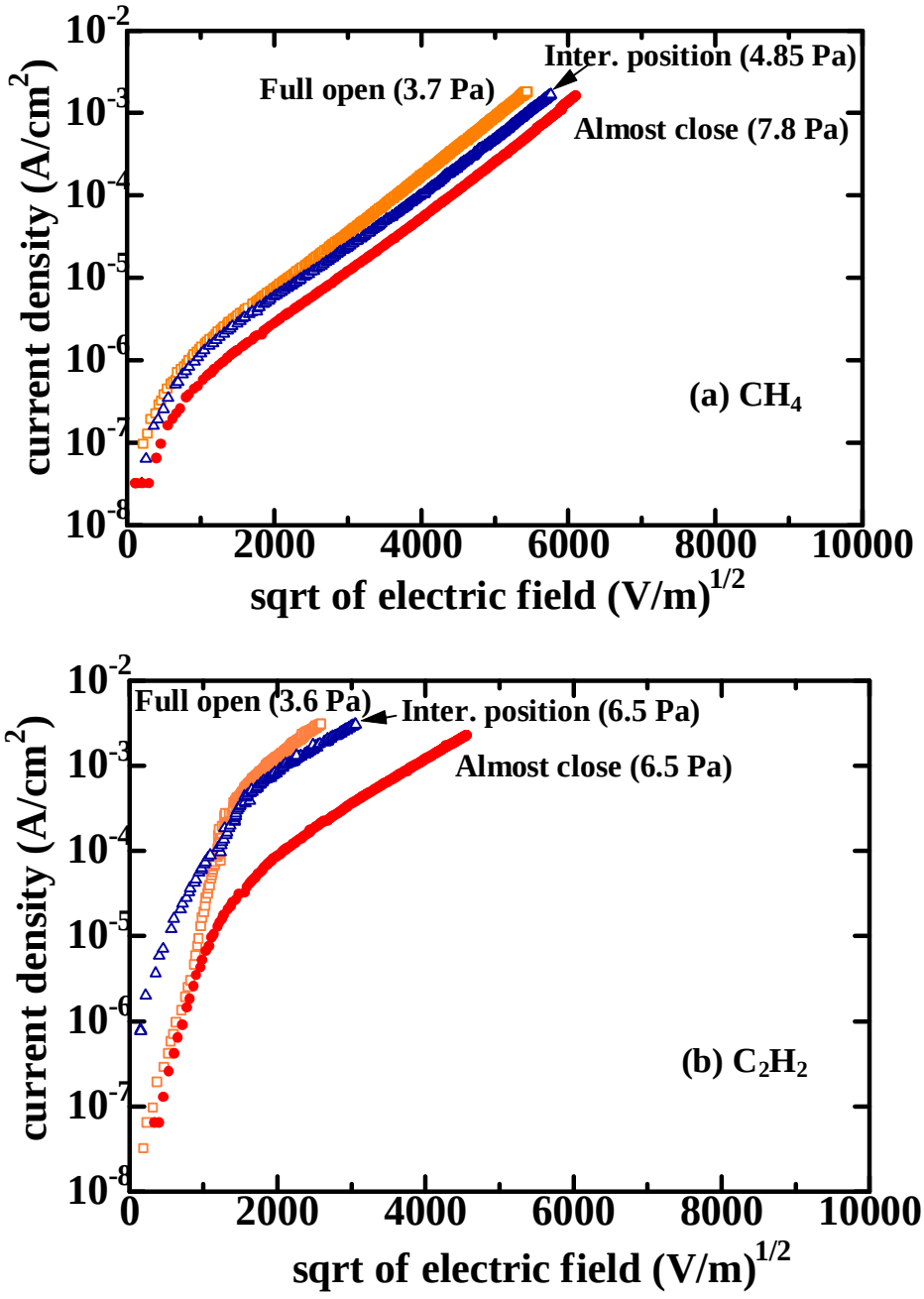

Fig. 4.11 Current density vs. sqrt of electric field of DLC films at various deposition pressure for RF power of 250 W and 70 sccm flow rate (a) CH_4 and (b) C_2H_2.

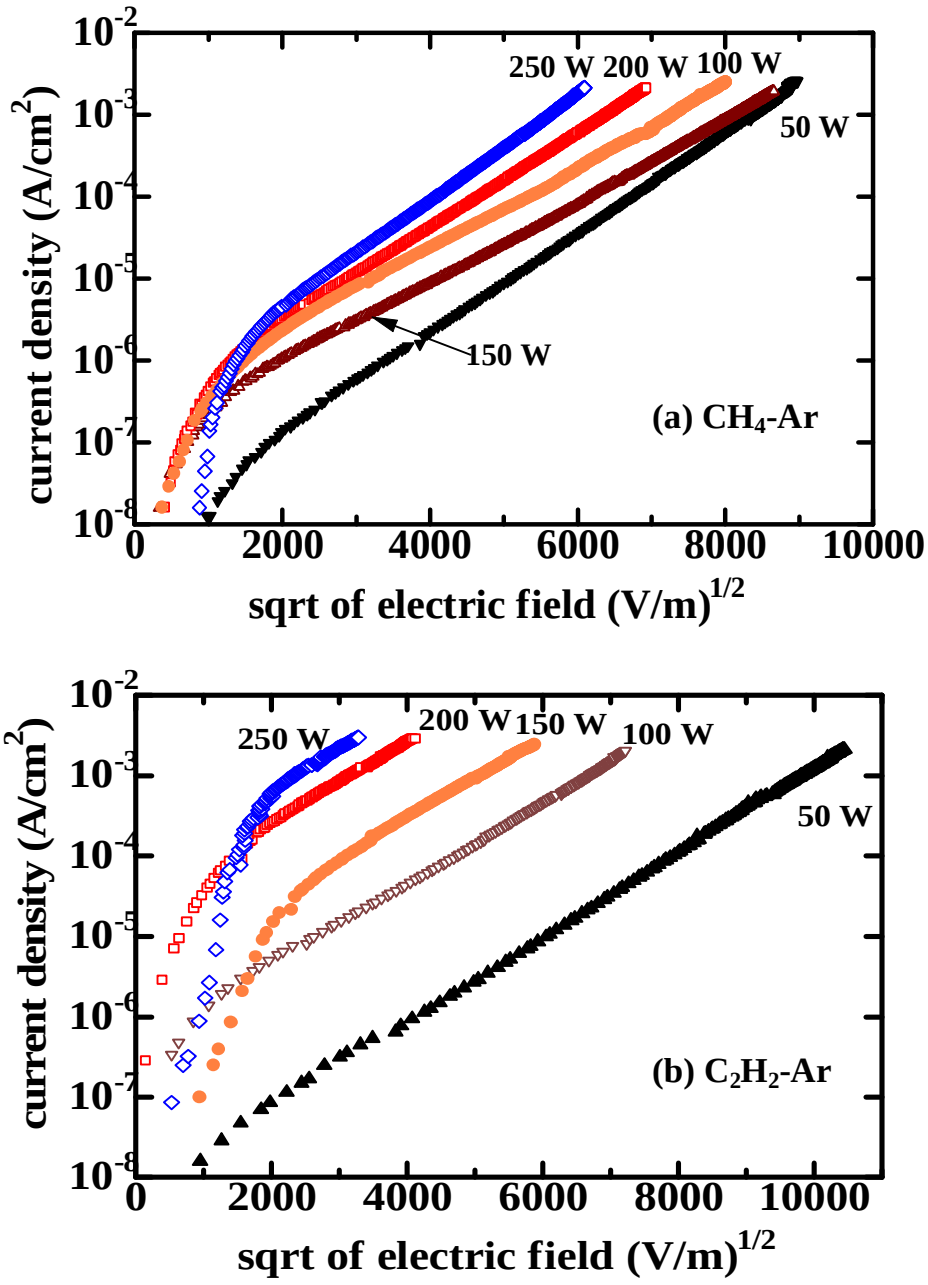

Fig. 4.12 Current density vs. sqrt of electric field of DLC films at various RF power flow rate of CH_4/ C_2H_2 70 sccm and Ar 20 sccm (a) CH_4-Ar and (b) C_2H_2-Ar.

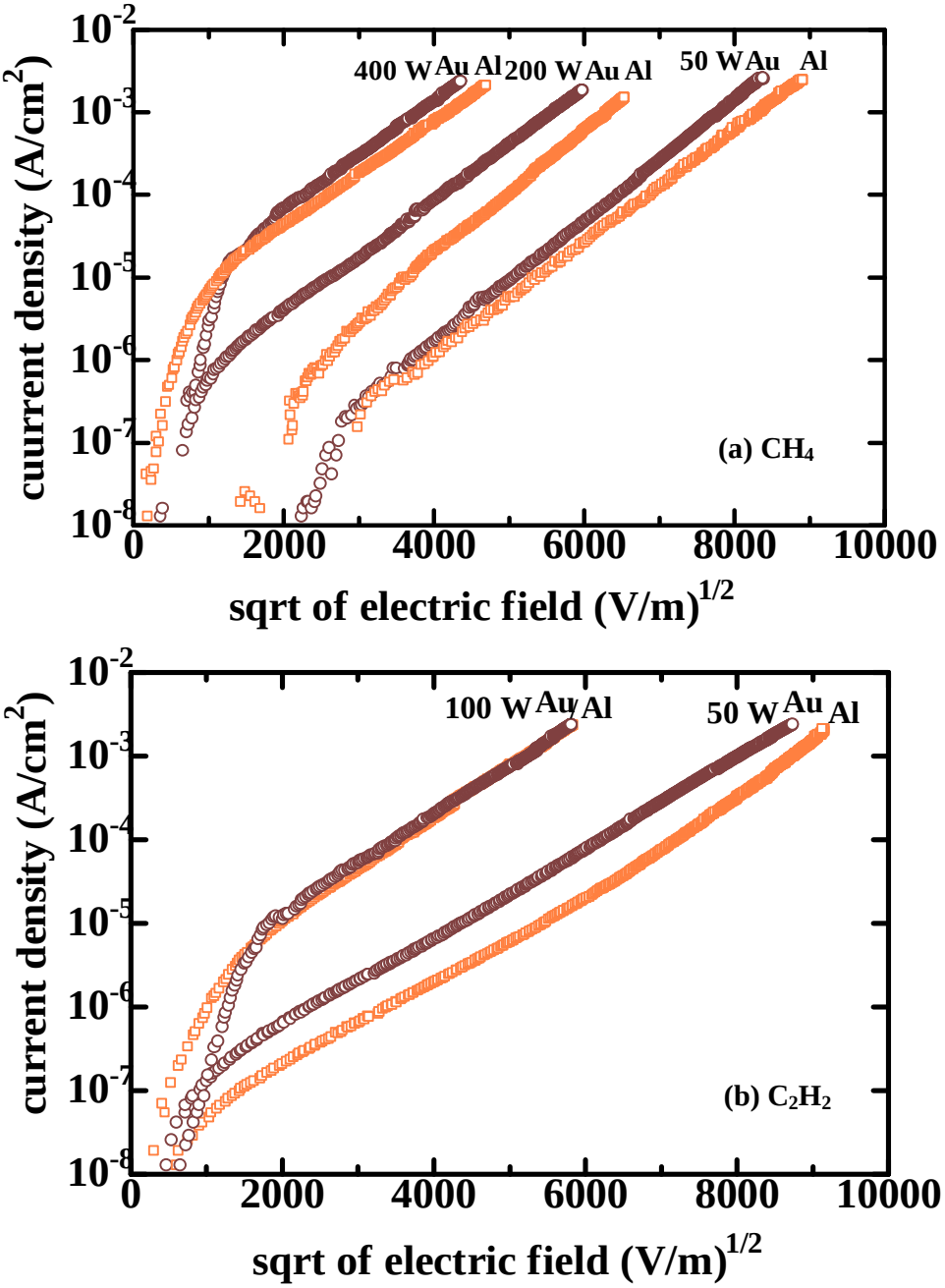

Fig. 4.13 Current density vs. sqrt of electric field of DLC films at various RF powers and flow rate of 70 sccm for both Au and Al top contact (a) CH_4 and (b) C_2H_2.

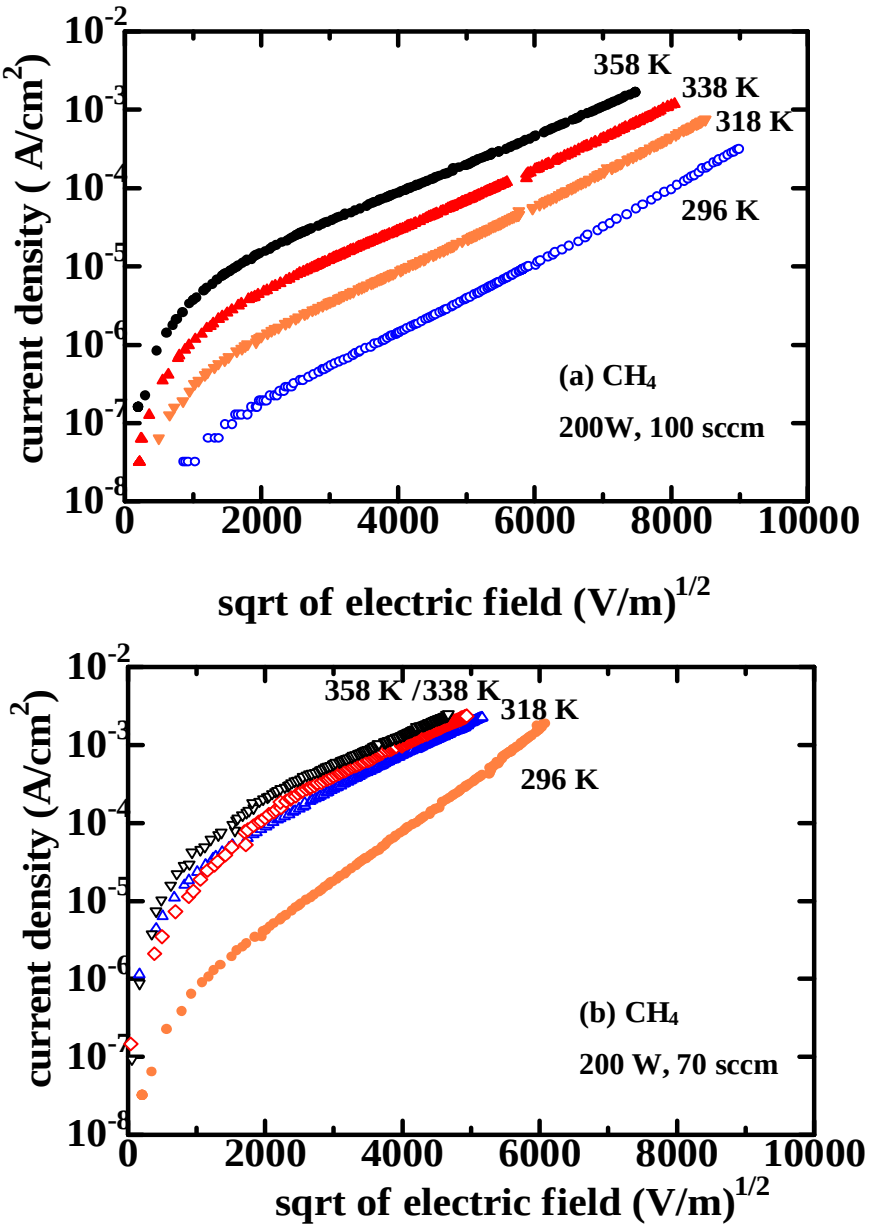

Fig. 4.14 Current density vs. sqrt of electric field of DLC films at various temper--atures (a) CH_4 (100 sccm, 200 W) and (b) CH_4 (70 sccm, 200 W)

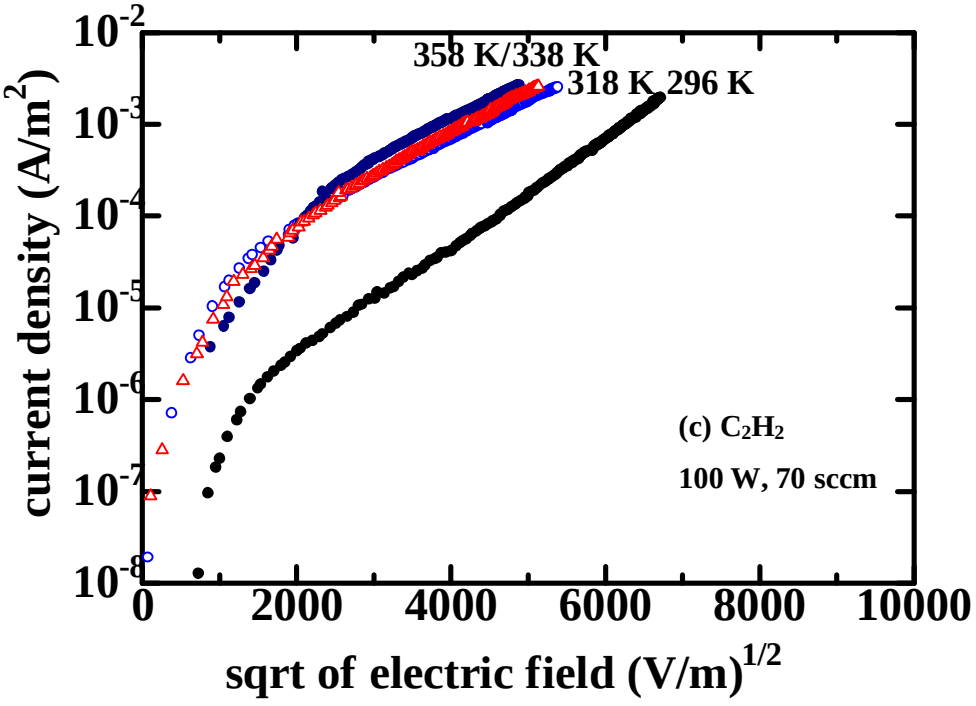

Fig. 4.14 Current density vs. sqrt of electric field of DLC films at various temperatures (c) C_2H_2 (70 sccm, 100 W)

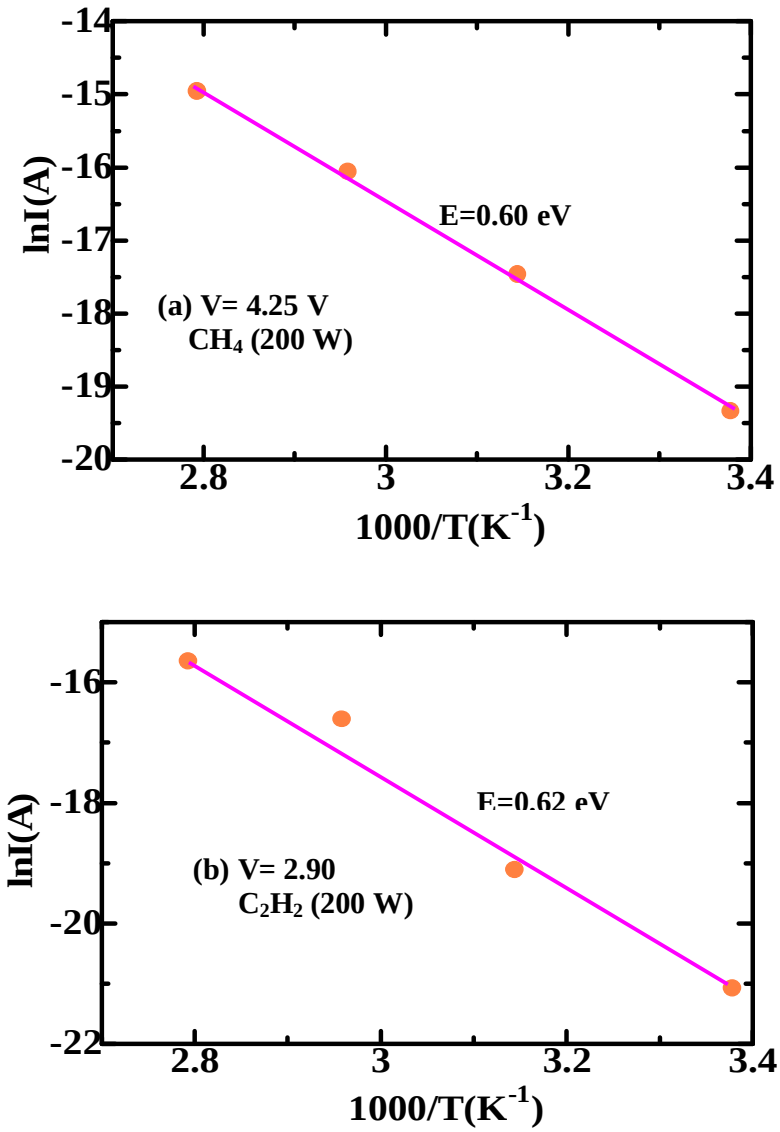

Fig. 4.15 Arrhenius plot of temperature dependent of the current for DLC films (a) CH_4 (200 W, 70 sccm) and (b) C_2H_2 (200 W, 70 sccm)

References

[1] G. K. Dalapati, S. K. Samanta, S. Chatterjee, P. K. Bose, S. Varma, S. Patil and C. K. Maiti, Jpn. J. Appl. Phys., **43** (2004) 3501.

[2] B. R. Huang, C. S. Huang, C. F. Hsieh and Y. F. Liu, Diam. Relat. Mater., **13** (2004) 2133.

[3] S. R. P. Silva and J. D. Carey, Diam. Relat. Mater., **12** (2003) 154.

[4] A. A. Dhakel, Cryst. Res. Technol., **38** (1971) 971.

[5] J. P. Chang and Y.-S. Lin, Appl. Phys. Lett., **79** (2001) 3667**.**

[6] S. Egret, J. Robertson, W.I. Milne and F. J. Clough, Diam. Relat. Mater., **6** (1997) 880**.**

[7] S. Wagle and V. Shirodkar, Brazilian J. Phys., **30** (2000) 382.

[8] S. Ashok, K. Srikanth, A. Badzian, T. Badzian, and R. Messier, Appl. Phys. Lett., **50** (1987) 764.

[9] P. W. May, M.-T. Kuo and M. N. R. Ashfold, Diam. Relat. Mater., **8** (1999) 1493.

[10] M. Ohring, The Material Science of Thin Film, Academic Press, USA, 1992, Chap. 10, p. 465-467.

[11] K.C. Kao, Dielectric Phenomena in Solids, Elsevier Academic Press, USA, 2004, Chap 6, p. 345.

[12] K.C. Kao, Dielectric Phenomena in Solids, Elsevier Academic Press, USA, 2004 Chap 6, p. 346.

[13] K.C. Kao, IEEE Trans. Electr. Insul., **EI-11** (1976) 121.

[14] W. Hwang and K. C. Kao, J. Chem Phys., **60** (1974) 3845.

[15] S. M. Sze, C. R. Crowell and D. Kahng, J. Appl. Phys., **35** (1964) 2534.

[16] K. K. Thornber, T. c. McGill. and C. A. Mead, J. Appl. Phys., **38** (1967) 2384.

[17] C. R. Crowell, Solid State Elect., **8** (1965) 395.

[18] J. Frenkel, Phys. Rev., **54** (1938) 647.

[19] J. G. Simmons, Phys. Rev., **15** (1967) 657.

[20] R. M. Hill, Phil. Mag., **23** (1971) 59-86.

[21] N. F. Mott and R. W. Gurney, Electronic Process in Ionic Crystals (Dover, New York, 1940).

[22] A. Rose, Phys. Rev., **97** (1955) 1538.

[23] M. A. Lampert, Phys. Rev., **103** (1956) 1648.

[24] S. R. P. Silva, Properties of Amorphous Carbon (INSPEC, London, 2003) Emis Data Reviews Series No. 29, Chap. 10, p. 326.

[25] A. Grill, Diam. Relat. Mater., **10** (2001) 234.

[26] M.-H. Jo and H.-H. Park, Appl. Phys. Lett., **71** (1998) 1392.

One of the most popular techniques for the deposition of diamond-like carbon (DLC) films using radio frequency plasma enhanced chemical vapor deposition (RF-PECVD) has been demonstrated in this research work. A systematic investigation of the results concerning the deposition and the electrical characterization of the diamond like carbon films synthesized in different experimental conditions and from two different saturated and unsaturated hydrocarbon source gases to be presented. The control of deposition and the properties of DLC have been studied by changing the deposition condition. The relationship between the process parameters and the film properties were investigated systematically.

It was also shown that the precursor gas substantially influences the film growth rate and electrical properties. Optical emission spectroscopy (OES) was found to be useful tool for the investigation of the glow discharge plasma. The growth kinetics and properties of the film reflected clearly the plasma composition.

In this research, electrical characterization of DLC have been performed using I-V, C-V, C-F and the resistivity measurements of the films are also studied at different deposition conditions. In the light of experimental results and their analysis the main conclusions of this research are summarized as follows:

Chapter 2. Synthesis of DLC films by using RF plasma CVD

DLC thin films were prepared by RF-PECVD using CH_4, C_2H_2 and the admixture of CH_4-Ar and C_2H_2-Ar gases. The self-bias voltage was the critical factors influencing the growth rate and the film properties. The growth rate and the bias voltage increase with the increase of RF power and decrease with flow rate and the deposition pressure. The findings of this work shown that highest deposition rates were obtained for the films deposited at highest RF power, lowest flow rate or lowest deposition pressure.

The small fragments, such as C, C_2 or CH may be regarded as the actual precursors for a-C:H growth. In both cases of CH_4 and C_2H_2, the intensity of CH radicals were similar, but the intensity of H_α in the C_2H_2 plasma was about one-half that in the CH_4 plasma.

The highest deposition rate was obtained with high content of carbon atoms in the molecule as in C_2H_2. The growth rate of DLC films prepared using the C_2H_2 plasma was more than threefold that of the CH_4-plasma-prepared films.

Ar addition to the CH_4 and C_2H_2 plasmas decreases the growth rate due to the sputtering effect of Ar ions.

Chapter 3. Electrical Characterization of the DLC films

I-V and C-V and C-F measurements of the Au-DLC-Si-Au structure were carried out to investigate the electrical properties of the DLC films deposited by RF-PECVD.

The overall features of the I-V characteristics of the DLC films deposited by RF-PECVD were similar. I-V characteristics of the DLC films have shown that the films display non-ohmic behavior irrespective of the polarity of the applied voltage. The I-V curves obtained from CH_4 do not show a strong variation of current with RF power and deposition pressure. On the other hand, I-V curves obtained from C_2H_2 show large variations of current with RF power and deposition pressure.

C-V-F measurement confirmed that the measured capacitance is bias and frequency dependent. The frequency dependence of capacitance was attributed to the series resistance effect of the material. The C-V characteristics of the DLC MIS structure were interpreted on the basis of depletion approximation.

The electrical conductivity of the films increases with increasing measurement temperature because of the semi-conducting behavior.

It is found that the resistivity of the deposited DLC films varied a wide range of the order 10^9 ohm-cm to 10^{14} ohm-cm. The electrical resistivities of the DLC films were found to be dependent on the substrate bias and the precursors. With an increase in RF power, resistivity decreased, whereas with an increase of flow rate and deposition pressure resistivity increased. The CH_4-based films were more insulating than C_2H_2-based films at high RF powers. Highest resistivity of the films was obtained for both the CH_4 and C_2H_2-based films at low RF power, higher flow rate and higher deposition pressure.

Addition of Ar with CH_4 decreased the resistivity of the DLC films at low RF powers whereas the resistivity increased at high RF powers. The resistivity of the C_2H_2-Ar-prepared films was found to increase.

The resistivity increase was possibly due to the transformation of carbon bonds from sp^2 to sp^3 with hydrogenation.

Chapter 4. Conduction Mechanism of DLC films

The electrical conduction properties of the Au-DLC-Si-Au structures were investigated at room temperature over a wide range of electric field up to $6x10^6$ V/m. The dominant conduction mechanism of the DLC films was identified as Poole-Frenkel process. This means that conduction occurs due to the thermal excitation of electrons from traps into the conduction band of the insulator (DLC).

The electrical conductivity of DLC films from CH_4 followed a Poole-Frenkel-type conduction mechanism. In the case of C_2H_2, however, films at 50, 100 W and 150 W completely followed and films at 200, 250 and 300 W partially followed Poole-Frenkel conduction whereas films at 400 and 500 W had a completely different conduction mechanism from CH_4. In case of C_2H_2, different conduction mechanism at high RF powers was possibly due to the higher sp^2 bonds not terminated by hydrogen due to insufficient hydrogen supply during the film growth.

Addition of Ar does not change the conduction mechanism of the DLC films. Change of electrical top contact does not change the conduction process suggesting that conduction is independent of the electro-negativity of the contact metals.

List of Publications

1. Comparative Study on Chemical Vapor Deposition of Diamond-Like Carbon Films from Methane and Acetylene Using RF Plasma
   Md. Kamrul Hasan, Bimal Kumar Pramanik and Akimitsu Hatta
   Japanese Journal of Applied Physics (Vol. 45, No. 10B, 2006, p. 8398-8400)

2. Electrical Resistivities of the Diamond-Like Carbon Films Fabricated from Methane and Acetylene Using RF Plasma
   Md. Kamrul Hassan, Bimal Kumar Pramanik and Akimitsu Hatta
   New Diamond and Frontier Carbon Technology (Vol. 16, No. 4 2006, MYU Tokyo NDFCT 518, p. 211-219)

Conferences

A. International Conferences

1. Electrical Conductivity of Diamond-Like Carbon Films (Poster)
   Md. Kamrul Hasan, and Akimitsu Hatta
   The 10^{th} International Conference on New Diamond Science and Technology
   May 11-14, 2005
   AIST, Tsukuba, Japan

2. Comparative Study on Chemical Vapor Deposition of Diamond-Like Carbon Films from Methane and Acetylene Using RF Plasma (Poster**)**
   Md. Kamrul Hasan, Bimal Kumar Pramanik and Akimitsu Hatta
   6^{th} In International Conference on Reactive Plasmas and 23^{rd} Symposium on Plasma Processing
   Jan. 24-27, 2006,
   Matsushima/ Sendai, Japan

3**.** Comparison of Electrical Resistivities of Diamond-Like Carbon Films Deposited from Methane and Acetylene Using Radio Frequency Plasma (Poster)
   Md. Kamrul Hasan, Bimal Kumar Pramanik and Akimitsu Hatta
   8^{th} Asia-Pacific Conference on Plasma Science and Technology and 19th

Symposium on Plasma Science for Materials
2-5th July, 2006, Cairns, Australia

4. Effect of Argon Gas Addition on the Electrical Resistivities of Diamond-Like carbon Films Deposited from Methane Using Radio Frequency Plasma (Poster)
THIN FILMS 2006
11-15, December, 2006
Singapore

B. Domestic Conference

1. Comparison of Electrical Conductivity of Diamond-Like Carbon Films Deposited from Methane and Acetylene (Poster)
Md. Kamrul Hasan, and Akimitsu Hatta
The 19th Diamond Symposium
Japan New Diamond Forum
Nov. 24-25, 2005, Osaka, Japan